#### Thermal Effects on Peristaltic Flow of Dusty Fluids



By

Atifa Kanwal 110-FBAS/PHDMA/S19

# Department of Mathematics and Statistics Faculty of Sciences International Islamic University, Islamabad Pakistan 2025

#### Thermal Effects on Peristaltic Flow of Dusty Fluids



by

Atifa Kanwal 110-FBAS/PHDMA/S19

Supervised by Dr. Ambreen Afsar Khan

Department of Mathematics and Statistics
Faculty of Sciences
International Islamic University, Islamabad
Pakistan
2025

### Thermal Effects on Peristaltic Flow of Dusty Fluids

By

#### **Atifa Kanwal**

#### **A Thesis**

Submitted in the Partial Fulfilment of the

Requirements for the degree of

**DOCTOR OF PHILOSOPHY** 

IN

**MATHEMATICS** 

Supervised by

Dr. Ambreen Afsar Khan

Department of Mathematics and Statistics
Faculty of Sciences
International Islamic University, Islamabad
2025

#### **Declaration**

I hereby declare that this thesis is my work which has been done after admission for the degree of Ph.D. I confirm that I have developed this document on my efforts under the supervision of my supervisor. This dissertation, as a whole or as a part has not been copied or submitted by others in this or any other university or institute for the completion of the degree.

Signature:
Atifa Kanwal

PhD Scholar (Mathematis)

#### Dedication

I dedicate this thesis to

My Father (Muhammad Akram)

My Mother (Naseem Akhtar)

My Husband (Asif Masood)

And

My Kids (Aayan, Hareem, Aymen & Hasaan)

#### Acknowledgment

In the name of Allah, the Most Gracious, the Most Merciful, I extend my deepest gratitude to **Allah Almighty**, the source of all blessings and wisdom. He has granted me strength, patience, and guidance to complete this degree.

I would like to express my sincere gratitude to my supervisor, **Dr. Ambreen Afsar Khan**, for her invaluable guidance, support, and encouragement throughout this journey. Her insightful advice, patience, and attention have been instrumental in helping me overcome challenges and achieve my goals. I am deeply thankful for the time and energy she has invested in mentoring me, providing constructive feedback, and fostering an environment that encouraged growth and learning.

I am thanks to my family, whose love, patience, and unwavering support have been a constant source of strength and inspiration throughout this journey. I am thankful to my husband, **Asif Masood**, for giving me space and time to focus on my research. The love and smiles of my kids lifted me up and motivated me to keep moving forward.

The endless love and prayers of my parents made this dream comes true. I pay heartiest appreciation to my parents for their prayers, moral support, and encouragement. I am also thankful to my brother for their support and encouragement.

I extend my sincere gratitude to all the faculty members specially **Dr. Khadija Maqbool, Dr. Sajida Kausar** and **Dr. Maliha Rashid** for their valuable feedback, constructive criticism and their assistance, which enriched the quality of this work.

I would like to extend my gratitude to my Head of Department for facilitating and supporting through this journey. I want to express my appreciation to my colleagues for their sincere advice, support, and motivation.

May Allah accept this endeavor and guide us all to the path of righteousness.

#### **Preface**

The dusty fluids moving through channels having peristaltic walls extensively occur in almost all fields of life. The discussion of heat transfer effects on peristaltic dusty fluids is crucial especially in physiology, engineering and industry. In biology, the study of heat transfer is requisite for hyperthermia therapy to target cancer cells effectively, an efficient process of dialysis without damaging tissues, treating respiratory diseases. In industry, heat transfer analysis is helpful for the efficient flow of slurries and chemicals without harming the machinery due to overheating. Viscosity of various fluids also varies at different temperature. In automobiles, lubricants are used as coating agents. Effective results of such fluids at different temperature can only be assessed by thermal analysis of these fluids. In engineering, the thermal study of fluids is a key factor in designing mechanical systems for optimum output. In this thesis, thermal analysis of various nature of dusty fluids is performed. The passages considered are asymmetric or curved in nature, exhibiting peristaltic movement along the walls. The temperature profile is studied under various conditions like thermal slip, convective boundaries, and variable physical properties. The dusty fluids are examined with effects of MHD, porosity, radiation, and inhomogeneous distribution of dust particles. The ruling equations constructed for the issues are coupled and nonlinear and solved using regular perturbation technique. The effects of various eminent factors on fluid and temperature are illustrated through graphical presentation of the mathematical results.

Chapter one is based on a description of basic concepts, fundamental equations to model the problem, and important non-dimensional quantities along with physical significance. A detailed discussion of the background of the study is also included in this chapter.

Walter's B dusty fluid with peristalsis is considered through an asymmetric channel in Chapter two. The effects of radiation, velocity slip, and thermal slip are discussed. Regular perturbation technique is used to solve coupled differential equations and effects of radiation, velocity, and thermal slip are deliberated graphically. The study has applications in biology and engineering. The article is published in **Alexandria Engineering journal (2024) 106:2024.** 

Chapter three is based on discussion of peristaltic Jeffrey dusty fluid travelling through a curved channel. Mathematical model comprises of coupled differential equations. Stream functions are involved, and perturbation technique is employed using small wave number approximation. Results for stream functions, and velocity are illustrated graphically. The significance of retardation and relaxation time on stream functions and velocity profile is elaborated through graphs. The findings of the study are published in **Advances in Mechanical Engineering** (2021) 13: 6.

Heat transfer analysis of MHD peristaltic dusty fluid passing through a curved channel is presented in Chapter four. The non-uniform distribution of dust particles and variable thermal conductivity are considered. Problem is solved by taking Reynolds number small and wavelength large, and numerical solutions are portrayed graphically using NDSolve command in Mathematica. Graphical discussion is performed to study the effects of curvature of the channel, thermal conductivity, and MHD. The results are helpful in various biological treatments and optimum performance of energy storage devices. The results of the analysis are published in **International Journal of Numerical Methods for Heat & Fluid Flow (2024) 34: 4.** 

Chapter five focuses on entropy generation analysis on dusty fluid flow with slip conditions. The channel of the flow has a curved nature with peristaltic walls. Analytic solutions are obtained using

perturbation technique. The flow behavior and temperature distribution are analyzed under the impact of various significant parameters. Entropy generation rate is also debated for various parameters. The study finds its application in biomedical sciences and engineering models. The issue is accepted for publication in **Fractals** (2024).

The emphasis of Chapter six is on a dusty second grade fluid propelling peristaltically through a porous asymmetric channel. Thermal effects with slip conditions are studied. Theoretical results of the problem are obtained through perturbation technique, taking wave number as a small parameter. Graphs showing the effects of porosity, MHD, and thermal slip are plotted. Due to the non-Newtonian nature of the fluid, the analysis has a wide role in understanding the behavior of many fluids occurring in biology, engineering, and industry. The results of research are submitted in **Journal of Fluids and Structures**.

Chapter seven deals with viscous dusty fluid peristaltically flowing through curved conduit with variable properties. Thermal conductivity and fluid viscosity depend upon temperature. Convective boundary conditions are incorporated. The graphical results are obtained using NDSolve command in Mathematica to understand the impact of curvature, varying viscosity, and thermal conductivity. The issue is submitted in **Advances in Mechanical Engineering** for possible publication.

In Chapter eight, concluding remarks of the thesis are included with the significance of results in various fields of life. Some aspects of future study are also presented in this chapter.

#### Nomenclature

#### List of symbol

X,Y	Rectangular coordinates in horizontal and vertical direction in fixed frame
R, X	Radial and axial coordinates in fixed frame
$H_1, H_2$	Upper and lower walls of the channel in dimensional form
С	Speed of peristaltic wave
$a_{1}, a_{2}$	Amplitudes of peristaltic waves along upper and lower walls respectively
$d_1 + d_2$	Width of asymmetric channel
$V, V_s$	Fluid and dust particles velocity profiles
U,V	Horizontal and verticle components of fluid velocity
$U_s$ , $V_s$	Horizontal and verticle components of dust particles velocity
u, v	Non-dimensionalized fluid velocity components
$u_s, v_s$	Non-dimensionalized dust particles velocity components
$T$ , $T_s$	Fluid and dust particles temperature
Z	Heat transfer rate
F, E	Non-dimensionalized flow rate for fluid and dust particles
$Q$ , $Q_s$	Non-dimensionalized flow rate for fluid and dust particles in fixed frame
P	Pressure

Thermal conductivity of the fluid
Specific heat of the fluid
Specific heat of dust particles
Mass of solid particles
Mass of dust particles per unit volume
Curvature of the channel
Stokes resistance coefficient
Temperature relaxation time
Velocity relaxation time
Reynolds number
Brinkman number
Prandtl number
Bejan number
Eckert number
Radiation parameter
Hartmann number
Induced magnetic field
Heat Transfer rate
Porosity parameter.

#### **Greek Letters**

λ	Length of peristaltic wave
φ	Phase difference
φ	Stream function for dust particles
ψ	Stream function for fluid
Ф	Viscous dissipation term
δ	Wave number
μ	Fluid viscosity
ρ	Fluid density
β	Velocity slip parameter
3	Thermal slip parametr
$\beta_1, \beta_2$	Biot numbers
η	Variable thermal conductivity coefficient
$\Theta$ , $\Theta_s$	Non-dimensional fluid and dust particles temperature
α	Walter's B fluid parameter
$\alpha_1$	Second grade fluid parameter
ω	Variable density of dust particles parameter
ζ	Variable viscosity coefficient
$\lambda_2$	Relaxation time of Jeffrey fluid
$\alpha_0$	Retardation time of Jeffrey fluid

#### **Table of Contents**

Chapter 120	
Introduction	20
1.1 Peristalsis	20
1.2 Dusty Fluids	20
1.3 Magnetohydrodynamics (MHD)	21
1.4 Fundamental Equations	21
1.4.1 For Fluid Flow	21
1.4.2 For Particle Flow	22
1.5 Non-dimensional Numbers	22
1.5.1 Reynolds Number	22
1.5.2 Eckert Number	23
1.5.3 Prandtl Number	23
1.5.4 Brinkman Number	23
1.5.5 Bejan number	24
1.6 Methodology	24
1.7 Literature Review	24
Chanter 2	30

## Influence of Radiation and Thermal Slip on Electrically Conductive Dusty Walter's B Fluid moving Peristaltically through an

Asymmetr	ric Channel	30
2.1 Problem	Formulation	30
2.2 Method	of Solution	35
2.2.1 Zero	th Order System	36
2.2.2 First	Order System	37
2.3 Graphica	ıl Analysis	38
2.3.1 Fluid	l Flow Analysis	39
2.3.2 Solid	Particle Flow Analysis	39
2.3.3 Tem	perature Distribution Analysis	40
2.3.4 Valid	lation of Present Study	40
2.4 Conclusi	o <b>n</b>	49
Chapter 3	•••••••	50
Effect of F	Relaxation and Retardation Times on Dusty J	effrey Fluid
in a Curve	ed Channel with Peristalsis	50
3.1 Problem	Formulation	50
3.2 Method	of Solution	54
3.2.1	Zeroth Order System	55
222 1	Finat Ondon Evators	55

3.3 Graphical Analysis	56
3.3.1 Analysis of Stream Lines	57
3.3.2 Fluid Flow Analysis	57
3.3.3 Particle Flow Analysis	57
3.3.4 Pressure Gradient	58
3.4 Conclusion	67
Chapter 4	68
Heat Transfer Analysis of Magnetohydrodynamics P	eristaltic Fluid
with Inhomogeneous Solid Particles and Variable Th	ermal
Conductivity through Curved Passageway	68
4.1 Problem Formulation	69
4.1.1 For Fluid Flow:	69
4.1.2 For Solid Particles:	70
4.2 Method of Solution	72
4.3 Graphical analysis	74
4.3.1 Fluid Flow Analysis	74
4.3.2 Solid Particle Flow Analysis	75
4.3.3 Temperature Distribution Analysis	75
4.3.4 Heat Transfer Coefficient	76
4.4 Conclusion	Q.1

Chapter 5	86
Entropy Generation Analysis of Dusty Fluid with Peris	talsis in
Asymmetric Channel with Slip Effects	86
5.1 Problem Formulation	86
5.2 Method of Solution:	90
5.2.1 Zeroth Order System:	91
5.2.2 First Order System:	92
5.3 Entropy:	93
5.4 Graphical Analysis:	93
5.4.1 Fluid Flow Analysis	94
5.4.2 Solid Particle Flow Analysis	94
5.4.3 Temperature Distribution Analysis	94
5.4.4 Entropy Generation	95
5.4.5 Bejan Number	95
5.4.6 Validation of Present Study	96
5.5 Conclusion	104
Chapter 6	105
Thermal and Magnetic Effects on Second Grade Dusty	Liquid with
Peristaltic Propagation in Porous Medium	105
6.1 Problem Formulation	105

6.2 Method of Solution	110
6.2.1 Zeroth Order System	110
6.2.2 First Order System	111
6.3 Graphical Analysis	113
6.3.1 Fluid Flow Analysis	113
6.3.2 Solid Particle Flow Analysis	114
6.3.3 Pressure Gradient Graphs	114
6.3.4 Temperature Distribution Analysis	114
6.4 Conclusion	123
Theoretical Analysis of Peristaltic Dusty Fluid u Varying Thermal Conductivity and Viscosity Pa	•
Varying Thermal Conductivity and Viscosity Pa	assing Through
Varying Thermal Conductivity and Viscosity Pa	assing Through124
Varying Thermal Conductivity and Viscosity Pacture Geometry	assing Through124
Varying Thermal Conductivity and Viscosity Pa	assing Through124
Varying Thermal Conductivity and Viscosity Pacture Geometry	assing Through124
Varying Thermal Conductivity and Viscosity Pactured Geometry	124
Varying Thermal Conductivity and Viscosity Pactured Geometry	124
Varying Thermal Conductivity and Viscosity Pactured Geometry  7.1 Problem Formulation  7.2 Method of Solution  7.3 Graphical Analysis  7.3.1 Fluid Flow Analysis	124 
Varying Thermal Conductivity and Viscosity Particle Flow  7.1 Problem Formulation  7.2 Method of Solution  7.3 Graphical Analysis  7.3.1 Fluid Flow Analysis  7.3.2 Solid Particle Flow	124

Conclusions	137
Appendix	140
References	142

#### Chapter 1

#### Introduction

#### 1.1 Peristalsis

The word peristalsis, evolved from the Greek letter "peristaltikos", is dedicated to represent the successive contraction and expansion movements of walls of channels, tubes, muscles, and vessels. This phenomenon is responsible for transportation of almost all fluids in the human body. The food, we eat, is transferred to stomach due to wavy movement of esophagus. The chyme moves toward small intestine due to peristaltic waves. Urine is transported from kidneys to bladder by peristaltic propulsion. The movement of sperms through fallopian tubes is caused by peristalsis. Medical devices like heart-lung machine, dialysis machines, and pumps to infuse medicine are based on the peristaltic mechanism. In engineering, peristalsis is widely used in designing systems to transport materials and dealing with the liquids flow in chemical reactors.

#### 1.2 Dusty Fluids

The fluids (gas or liquid) that contain a distribution of solid particles, are called dusty fluids. Dusty fluid flows have vast applications in physiological systems and industry. Various examples include chyme in small intestine, urine with infection, wastewater treatment, environmental pollution, discharge of sewage from industries, glittered paints, juices with pulp etc.

#### 1.3 Magnetohydrodynamics (MHD)

The study of electrically conductive fluids is known as Magnetohydrodynamics (MHD). Liquid metals, salt water, and plasma are few examples of such fluids. The mathematical equations describing MHD are known as Maxwell's equations of electromagnetism given as

$$\nabla \cdot \boldsymbol{E} = \frac{\rho_{v}}{\epsilon_{0}},$$

$$\nabla \times \mathbf{E} = -\frac{\partial \mathbf{B}}{\partial t},$$

$$\nabla \cdot \boldsymbol{B} = 0$$
,

$$\nabla \times \mathbf{B} = \mu_0 \mathbf{J} + \mu_0 \epsilon_0 \frac{\partial E}{\partial t},$$

where  ${\pmb E}$  and  ${\pmb B}$  are electric field and magnetic field,  ${\pmb J}$  and  $\rho_v$  are current and charge density,  $\epsilon_0$  and  $\mu_0$  are permeability of fixed and free space.

#### 1.4 Fundamental Equations

#### 1.4.1 For Fluid Flow

The flow behavior of fluid is described by the following equations.

Continuity equation for incompressible fluid is

$$\nabla \cdot \mathbf{V} = 0. \tag{1.1}$$

Momentum equation for incompressible fluid is

$$\rho \frac{d\mathbf{V}}{dt} = -\nabla P + \nabla \cdot \mathbf{\tau} + \rho \mathbf{f} + kN(\mathbf{V}_s - \mathbf{V}). \tag{1.2}$$

The energy equation is

$$\rho C_p \left( \frac{dT}{dt} \right) = K \nabla^2 T + \Phi + \frac{N C_p}{\tau_T} \left( T_S - T \right) + \frac{N}{\tau_U} (U_S - U)^2, \tag{1.3}$$

where  $\Phi$  is viscous dissipation.

#### 1.4.2 For Particle Flow

The flow behavior of solid particles is described by the following equations.

Continuity equation for solid particles is

$$\nabla \cdot V_s = 0. \tag{1.4}$$

Momentum equation for solid particles is

$$mN\frac{dV_s}{dt} = mNf + kN(V - V_s). \tag{1.5}$$

The energy equation is

$$\frac{dT_s}{dt} = -\frac{C_P}{C_m}(T - T_s). \tag{1.6}$$

#### 1.5 Non-dimensional Numbers

Dimensionless numbers are key factor in understanding the dynamics of the fluid. They are defined as correlation between parameters or forces and thus helpful to illustrate flow properties of the fluid.

#### 1.5.1 Reynolds Number

The ratio of inertial forces to viscous forces is termed as Reynolds number. It is denoted by Re.

$$Re = \frac{\text{Inertial Forces}}{\text{Viscous Forces}} = \frac{\rho u L}{\mu}$$
,

where  $\rho$  is density,  $\boldsymbol{u}$  is fluid velocity, L is characteristic length and  $\mu$  is fluid viscosity.

Reynolds number described the flow pattern of a fluid.

#### 1.5.2 Eckert Number

Eckert number is the relation between kinetic energy of the flow and enthalpy difference due to temperature change in the system. It is denoted by *Ec* and

$$Ec = \frac{u^2}{C_n \Delta T},$$

where u is fluid velocity,  $C_p$  is specific heat and  $\Delta T$  is temperature difference. High Eckert number depicts that viscous dissipation has dominant role on temperature profile of the fluid otherwise viscous dissipation effects are negligible and heat transfer occurs due to conduction or convection.

#### 1.5.3 Prandtl Number

Prandtl number (Pr), named after German physicist Ludwig Prandtl, is ratio of momentum diffusivity to thermal diffusivity, i.e.,

$$Pr = \frac{C_p \mu}{k},$$

where  $\mu$  and k are viscosity and thermal conductivity of the fluid.

#### 1.5.4 Brinkman Number

The Brinkman number is dimensionless number introduced by Dutch mathematician and physicist Henri Brinkman. Brinkman number is denoted by Br and defined as

$$Br = \frac{\mu \mathbf{u}^2}{k(T_w - T_0)},$$

where  $\mu$  is the dynamic viscosity,  $\boldsymbol{u}$  is the flow velocity, k is the thermal conductivity,  $T_0$  is the bulk fluid temperature,  $T_w$  is the wall temperature.

#### 1.5.5 Bejan number

Bejan number is dimensionless number introduced by Adrian Bejan. In fluid dynamics, Bejan number denoted by (*Be*) is defined as the ratio of heat transfer irreversibility and total irreversibility due to heat transfer and viscous dissipation i.e.,

$$Be = \frac{\text{Heat Transfer Irreversibility}}{\text{Total Irreversibility(heat transfer + fluid friction)}}$$

The study of Bejan number is important to improve the systems by reducing energy loss due to both heat transfer and fluid viscosity.

#### 1.6 Methodology

The mathematical models are developed by using Navier-Stokes equations. For dusty fluid, model consists of coupled equations which are non-linear. The introduction of stream functions reduces number of linearly independent solutions but non-linear terms still retain. Therefore, regular perturbation technique is applied by taking wave number as small parameter. Resulting zeroth order and first order systems are solved using DSolver built-in command in Mathematica. For numerical analysis of the problems, NDSolver command in Mathematica is employed.

#### 1.7 Literature Review

Peristaltic propulsion of fluids abundantly occurs in physiology like blood movement through vessels, transport of chyme through small intestine, and urine flow through the kidney. In industry, peristaltic pumps are used to transport sensitive fluids. The study of peristalsis is crucial due to its

remarkable effect on flow behavior of fluids. Latham [1] primarily carried out both theoretical and experimental investigations of peristaltic pumping. Fung and Yih [2] analyzed peristaltic flow through flexible cylindrical tubes. Shapiro et al. [3] presented theoretical results of propulsion of peristaltic waves by using a low Reynolds number and long wavelength assumption. Weinberg et al. [4] performed experimental analysis of peristaltic pumping and compared experimental results with the theoretical study by Shapiro et al. [3]. Numerical technique was applied by Takabatake et al. [5] to study effects of Reynolds number, wavelength, and amplitude on axisymmetric peristaltic flow. Some other studies on peristaltic flow with different assumptions are [6-9]. Siddiqui and Schwarz [10] studied second grade fluid propelling peristaltically through axisymmetric tubes. Mekheimer [11] studied magnetohydrodynamic effects on blood flowing peristaltically through two-dimensional channel. Tsui et al. [12] investigated the flow behavior of peristaltic fluid in a finite tube. Nadeem and Akram [13] considered Williamson fluid model flowing through peristaltic asymmetric channel. Javid et al. [14] studied effects of porous media on biological fluid travelling through wavy channel. Rani et al. [15] carried out heat and mass transfer analysis of Walter's B fluid moving sinusoidally through a symmetric channel with MHD and slip effects. MHD and partial slip impacts on Jeffery fluid propulsion under peristalsis through rectangular channel have been presented by Ellahi and Hussain [16]. Jagadesh et al. [17] worked on peristaltic propulsion of MHD Casson fluid with free convection through an inclined porous channel. Gafel [18] conducted the study for the effects of inclined magnetohydrodynamics and source/sink on peristaltic flow of blood in the presence of thermal radiation. Elmhedy et al. [19] focused on Robinowitsch fluid model with peristaltic transport through an inclined channel and studied effects of MHD and heat transfer. Some other studies are [20-24].

Fluids having a distribution of solid particles occur abundantly in physiology and industry. Some instances include blood, chyme in the small intestine, urine, air containing dust particles, juices with pulp, paints with glitter, and crude oil. Saffman [25] primarily described the problem of laminar flow of gas containing tiny dust particles. The unsteady flow of incompressible gas with dust particle suspension is discussed by Gupta and Gupta [26]. Some other related studies are [27-29]. The unsteady case of electrically conductive dusty fluid between two parallel plates with heat transfer effects has been investigated by Makinde and Chinyoka [30]. They also considered variable fluid viscosity and constant pressure gradient. The analysis of MHD dusty fluid travelling through a rectangular channel with porous medium under volume fraction effects has been provided by Madhura and Swetha [31]. Sivaraj and Kumar [32] analyzed unsteady Couette flow of Walter's B fluid in an irregular configuration with MHD effects. Ali et al. [33] dealt with the study of unsteady flow of dusty fluid with elastic properties, MHD, and free convection. The discussion of dusty fluid through the channel exhibiting peristaltic movement is an emerging issue due to its immense application in medical science, engineering, chemical, and food industry. Mekheimer et al. [34] studied the dusty fluid passing through a wavy symmetric channel. Srinivasacharya et al. [35] conducted the investigation of liquid with particle suspension propelling through peristaltic channel with flexible walls. Eldesoky et al. [36] deliberated the influence of MHD and wall slip conditions on fluid-particle flow through flexible channel. Ramesh et al. [37] performed analysis of particle suspended fluid moving through asymmetric microchannel under peristalsis. They studied MHD and wall slip effects on Jeffrey fluid model. The impact of porosity and wall properties on dusty fluid flowing through uniform passage with wavy walls has been studied by Parthasarathy et al. [38]. While Tariq and Khan [39] reported the effects of porosity on MHD dusty fluid through an endoscope with peristalsis. Further, Tariq and Khan [40] considered

the dispersion of solid particles in the fluid inhomogeneous and studied the peristaltic propulsion through an asymmetric channel. Few contributions addressing different conditions are [41- 43].

Vessels and arteries in living organisms also involve curved geometries that influence the flow behavior as well as temperature transference of the fluid. The flow behavior of fluid in curved passage was primarily discussed by Dean [44]. Peristaltic flow through a curved configuration was addressed by Sato et al. [45] by neglecting inertial forces and assuming very large wavelength. Non-Newtonian fluid travelling through curved channel with peristalsis was studied by Ali et al. [46]. Javid et al. [47] focused on the numerical study of peristaltic effects on Jeffrey fluid driven through curved geometry. Flow is subject to an applied magnetic field. Ramanamurthy et al. [48] described the mathematical model of the unsteady problem of peristaltic flow in curved passage and carried out analysis for flow behavior and thermal effects. Abbasi et al. [49] conducted the analysis of MHD viscoelastic fluid with wavy propulsion through duct of curved nature with ciliated walls. The shear-thinning and shear-thickening fluid with rhythmic sinusoidal movement through curved channel was considered by Hina et al. [50]. The study highlights the impact of wall properties and heat and mass transfer on fluid flow. Jeffrey fluid with convective boundary conditions transported through curved path was dealt with Hayat et al. [51]. Simulations are used to highlight the effects of retardation and relaxation time parameters. The issue of peristaltic dusty fluid under mass transfer driven through curved conduit with elastic walls was explored by Khan [52]. Rashed and Ahmed [53] analyzed the dynamic of dusty nanofluid with peristaltic mechanism. Few other articles in this context are [54-56].

The study of temperature distribution through the peristaltic fluid and solid particles is a salient factor in the fields of medicine, engineering, and chemicals. Javed et al. [57] performed thermal analysis for dusty peristaltic fluid. They also studied the impact of magnetohydrodynamic and

flexible wall properties. Walter's B dusty fluid progression through vertical wavy channel under convective boundary conditions and mass transfer has been investigated by Sivaraj and Kumar [58]. Bhatti et al. [59] modeled the problem of electrically conductive dusty fluid with elastic properties and peristaltic pumping and studied the impact of nonlinear thermal radiation, MHD, and porosity of the channel. Kalpana and Saleem [60] investigated the temperature profile of particulate fluid progressing through porous inclined channel with wavy walls under MHD. The focus of the article by Elmhedy et al. [61] was to discuss heat transfer and MHD effects on Rabinowitsch fluid with solid particle distribution. The passage of the fluid is inclined with peristaltic walls. Zeeshan et al. [62] conducted a study for heat and mass transfer effects on asymmetric flow of dusty fluid in peristaltic curved channel. Riaz et al. [63] considered porous medium of curved duct and partial slip while conducting thermal analysis of second grade dusty fluid under peristaltic propulsion. Tariq et al. [64] studied thermal and MHD effects on Walter's B dusty fluid moving peristaltically. A study to illustrate Dufour and Soret effects on peristaltically travelling Jeffrey fluid is performed by Hayat et al. [65]. They considered channel of curved nature with convective conditions at the walls.

The study of fluids under variable viscosity and thermal conductivity is a crucial factor in food processing, cosmetics production, automobile industry, cooling systems, and medicines. Sinha et al. [66] addressed the significance of variable viscosity and velocity slip on the peristaltic liquid flowing under MHD in an asymmetric channel. Hayat and Ali [67] deliberated the effects of temperature varying viscosity on viscous peristaltic fluid moving in an asymmetric channel. The effects of variable viscosity and velocity slip on non-Newtonian fluid through a wavy porous channel are illustrated through graphical results by Khan et al. [68]. Akbar and Abbasi et al. [69] presented the results to illustrate the impact of temperature dependent viscosity on a viscous fluid

with entropy generation transported peristaltically. Tanveer et al. [70] provided analysis of peristaltic fluid flow under the impact of temperature dependent viscosity in a curved configuration. They also carried out entropy analysis. Abbasi et al. [71] explored the peristaltic motion of Carreau-Yasuda fluid in the presence of velocity slip and by considering variable thermal conductivity and convective boundary conditions. The temperature varying thermal conductivity effects along with mass transfer on an MHD peristaltic fluid flow through porous medium with complaint walls have been examined by Vaidya et al. [72]. The article presented by Mekheimer and Abd Elmaboud [73] was based on the analysis of peristaltic fluid flow under the impact of both variable viscosity and thermal conductivity. Manjunatha et al. [74] aimed to discuss the flow behavior of Jeffrey fluid with variable nature of viscosity and thermal conductivity. The fluid flow was peristaltic with a non-uniform porous channel. The effect of varying aspect of thermal conductivity and viscosity on nanofluid following Carreau fluid model with MHD and peristalsis was discussed by Khan et al. [75]. The focus of the analysis provided by Bibi et al. [76] was to study wavy Sisko fluid with variable thermal conductivity and viscosity. They also discussed entropy generation in Sisko fluid. Bhatti and Zeeshan [77] carried out analysis for heat transfer and variable viscosity effects on dusty peristaltic fluid. Swetha and Madhura [78] performed the heat transfer analysis to study temperature varying viscosity on Jeffrey dusty fluid with sinusoidal movement. Kalpana and Madhura [79] formulated the problem of dusty fluid flowing through an inclined channel with porous medium and performed numerical analysis to study effects of MHD, variable viscosity, and pressure. Some other articles are [80-87].

#### Chapter 2

## Influence of Radiation and Thermal Slip on Electrically Conductive Dusty Walter's B Fluid moving Peristaltically through an Asymmetric

#### Channel

This chapter presents the study of dusty Walter's B fluid travelling peristaltically through an asymmetric channel with wall slip. A discussion is also presented to examine heat transfer effects with thermal radiation and slip at the wall. The regular perturbation technique is employed to evaluate the mathematical model of the problem, which is first simplified by using stream functions. Mathematical results are plotted to illustrate flow characteristics of fluid and solid particles in salient quantities. Also, graphs of temperature distribution of fluid and dust particles have been discussed to study the impacts of various parameters.

#### 2.1 Problem Formulation

An incompressible dusty fluid obeying Walter's B model is moving through an asymmetric channel having width  $d_1 + d_2$  and walls exhibiting sinusoidal wavy motion. A uniform distribution of spherical particles is assumed in the fluid, with a magnetic field acting in a transverse direction. Wall geometry is given as:

$$H_1(X,t) = d_1 + a_1 \sin\left[\frac{2\pi}{\lambda}(X - ct)\right],$$
 (2.1a)

$$H_2(X,t) = -d_2 - a_2 \sin\left[\frac{2\pi}{\lambda}(X - ct) + \phi\right].$$
 (2.1b)

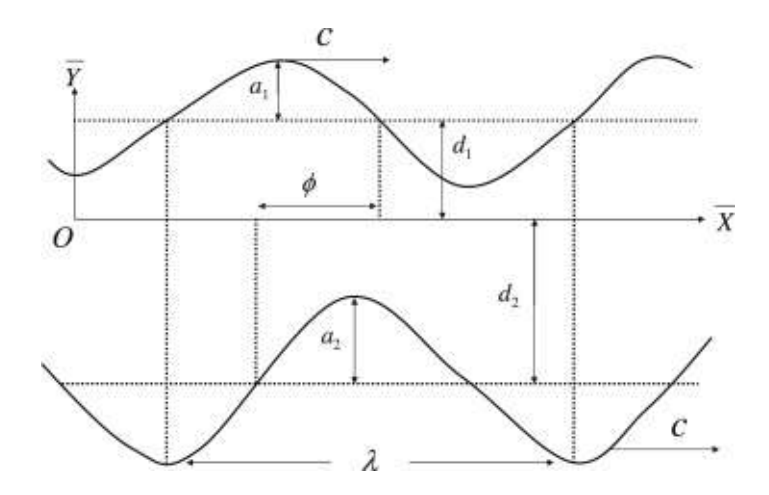


Fig 2.1: Geometry of the channel

The shear stress tensor for Walter's B fluid model referred from [64] is

$$\tau = 2\mu_0 e - 2\sigma_0 \frac{\delta e}{\delta t},\tag{2.2}$$

$$\frac{\delta e}{\delta t} = \frac{\partial e}{\partial t} + V \cdot \nabla e - e \nabla V - (\nabla V)^T e, \tag{2.3}$$

where e is rate of stress tensor and  $\mu_0$  (limiting viscosity of shear stress) and  $\sigma_0$  (short memory coefficient) are

$$\mu_0 = \int_0^\infty O(t_0) dt_0, \tag{2.4}$$

$$\sigma_0 = \int_0^\infty t_0 O(t_0) dt_0, \tag{2.5}$$

where  $t_0$  and  $\mathcal{O}(t_0)$  are relaxation time and distribution function respectively.

$$\int_0^\infty (t_0)^n O(t_0) dt_0 \, , n \ge 2. \tag{2.6}$$

Momentum and energy equations describing fluid flow in fixed frame are

$$\frac{\partial U}{\partial x} + \frac{\partial V}{\partial y} = 0, (2.7)$$

$$\rho \frac{dU}{dt} = -\frac{\partial P}{\partial X} + \frac{\partial \tau_{XX}}{\partial X} + \frac{\partial \tau_{XY}}{\partial Y} + kN(U_S - U) - \sigma B_0^2 U, \tag{2.8}$$

$$\rho \frac{dV}{dt} = -\frac{\partial P}{\partial Y} + \frac{\partial \tau_{XY}}{\partial X} + \frac{\partial \tau_{YY}}{\partial Y} + kN(V_S - V), \tag{2.9}$$

$$\rho C_p \left( \frac{dT}{dt} \right) = k^* \nabla^2 T + \Phi + \frac{\partial q_r}{\partial Y} + \frac{N C_p}{\tau_T} \left( T_S - T \right) + \frac{N}{\tau_U} (U_S - U)^2. \tag{2.10}$$

Momentum and energy equations for solid particles in fixed frame are

$$\frac{\partial U_S}{\partial x} + \frac{\partial V_S}{\partial y} = 0, (2.11)$$

$$\frac{dU_S}{dt} = \frac{k}{m}(U - U_S),\tag{2.12}$$

$$\frac{dV_S}{dt} = \frac{k}{m}(V - V_S),\tag{2.13}$$

$$\frac{dT_s}{dt} = -\frac{C_P}{C_{rr}}(T - T_s). \tag{2.14}$$

Fixed frame coordinates (X, Y) are related to moving frame coordinates (x, y) by

$$x = X - ct, y = Y, v = V, u = U - c, u_s = U_s - c, v_s = V_s, p(x) = P(X, t).$$
 (2.15)

Introducing the dimensionless quantities and stream functions

$$x' = \frac{x}{\lambda}, y' = \frac{y}{d_1}, \ \delta = \frac{d_1}{\lambda}, h_{1,2} = \frac{H_{1,2}}{d_1}, u = \frac{\partial \psi}{\partial y}, \ v = -\delta \frac{\partial \psi}{\partial x}, \ u_S = \frac{\partial \varphi}{\partial y}, \ v_S = -\delta \frac{\partial \varphi}{\partial x}, u_S = \frac{\partial \psi}{\partial x}, u_S =$$

$$\Theta = \frac{T - T_0}{T_1 - T_0}, \quad \Phi' = \frac{d_1^2 \Phi}{\mu_0 c^2}, \quad M^2 = \frac{\sigma d_1 B_0^2}{\mu_0}, \\ Re = \frac{\rho c d_1}{\mu_0}, \\ Ec = \frac{c^2}{c_p (T_1 - T_0)}, \quad Pr = \frac{\mu_0 C_p}{k^*}, \quad \alpha = \frac{\sigma_0 c}{\mu_0 d_1}, \\ Re = \frac{\rho c d_1}{\mu_0}, \\ Re =$$

$$A = \frac{kNd_1^2}{\mu_0}, \ B = \frac{kd_1}{mc}, \ A_1 = \frac{Nd_1^2}{\mu_0\tau_T}, \ B_1 = \frac{Nd_1^2}{\mu_0\tau_U}, \ C = \frac{d_1C_P}{cC_m}. \tag{2.16}$$

where A, B, C,  $A_1$ , and  $B_1$  are non-dimensional quantities.

Shear stress components for Walter's B fluid in nondimensionalized form are

$$\tau_{xx} = 4\delta \frac{\partial^2 \psi}{\partial x \partial y} - \alpha \left[ 4\delta^2 \left( \frac{\partial^2 \psi}{\partial x^2} \right) \left( \frac{\partial^2 \psi}{\partial y^2} \right) + 4\delta^2 \frac{\partial \psi}{\partial y} \frac{\partial^3 \psi}{\partial x^2 \partial y} - 8\delta^2 \left( \frac{\partial^2 \psi}{\partial x \partial y} \right)^2 - 4\delta^4 \left( \frac{\partial^2 \psi}{\partial x^2} \right)^2 - 4\delta^2 \frac{\partial^3 \psi}{\partial y^2 \partial x} \right], \tag{2.17}$$

$$\tau_{xy} = 2 \left[ \frac{\partial^2 \psi}{\partial y^2} - \delta^2 \frac{\partial^2 \psi}{\partial x^2} \right] - \alpha \left[ 2\delta \frac{\partial \psi}{\partial y} \frac{\partial^3 \psi}{\partial y^2 \partial x} + 2\delta^3 \frac{\partial \psi}{\partial x} \frac{\partial^3 \psi}{\partial x^2 \partial y} - 2\delta \frac{\partial^3 \psi}{\partial y^3} \frac{\partial \psi}{\partial x} - 4\delta \frac{\partial^2 \psi}{\partial x \partial y} \frac{\partial^2 \psi}{\partial y^2} - 4\delta^3 \frac{\partial^2 \psi}{\partial x^2} \frac{\partial^2 \psi}{\partial x^2} - 2\delta^3 \frac{\partial^3 \psi}{\partial x^3} \frac{\partial \psi}{\partial y} \right], \tag{2.18}$$

$$\tau_{yy} = -4\delta \frac{\partial^2 \psi}{\partial x \partial y} - \alpha \left[ 4\delta^2 \frac{\partial \psi}{\partial x} \frac{\partial^3 \psi}{\partial y^2 \partial x} + 4\delta^2 \frac{\partial^2 \psi}{\partial x^2} \frac{\partial^2 \psi}{\partial y^2} - 4\delta^2 \frac{\partial \psi}{\partial y} \frac{\partial^3 \psi}{\partial x^2 \partial y} - 8\delta^2 \left( \frac{\partial^2 \psi}{\partial x \partial y} \right)^2 - 4 \left( \frac{\partial^2 \psi}{\partial y^2} \right)^2 \right]. \tag{2.19}$$

For fluid and solid particles, compatibility equations are obtained as

$$\delta Re \left[ \frac{\partial \psi}{\partial y} \frac{\partial}{\partial x} (\nabla_1^2 \psi) - \frac{\partial \psi}{\partial x} \frac{\partial}{\partial y} (\nabla_1^2 \psi) \right] = \left( \frac{\partial^2}{\partial y^2} - \delta^2 \frac{\partial^2}{\partial x^2} \right) \tau_{xy} + \delta \left( \frac{\partial^2}{\partial x \partial y} \left\{ \tau_{xx} - \tau_{yy} \right\} \right) - M^2 \frac{\partial^2 \psi}{\partial y^2} + A \left( \frac{\partial^2 \psi}{\partial y^2} - \frac{\partial^2 \psi}{\partial y^2} \right), \tag{2.20}$$

$$\delta \left[ \frac{\partial \varphi}{\partial y} \frac{\partial}{\partial x} (\nabla_1^2 \varphi) - \frac{\partial \varphi}{\partial x} \frac{\partial}{\partial y} (\nabla_1^2 \varphi) \right] = B(\nabla_1^2 \psi - \nabla_1^2 \varphi). \tag{2.21}$$

Energy equations for fluid and dust particles are nondimensionalized as

$$Re\delta\left(\frac{\partial\psi}{\partial y}\frac{\partial\Theta}{\partial x} - \frac{\partial\psi}{\partial x}\frac{\partial\Theta}{\partial y}\right) = \frac{1}{Pr}\left(\delta^2\frac{\partial^2\Theta}{\partial x^2} + \frac{\partial^2\Theta}{\partial y^2}\right) + A_1(\Theta_S - \Theta) + B_1Ec\left(\frac{\partial\varphi}{\partial y} - \frac{\partial\psi}{\partial y}\right)^2 + \frac{Rd}{Pr}\frac{\partial^2\Theta}{\partial y^2} + Ec\Phi,$$
(2.22)

$$\delta\left(\frac{\partial\varphi}{\partial y}\frac{\partial\Theta_S}{\partial x} - \frac{\partial\varphi}{\partial x}\frac{\partial\Theta_S}{\partial y}\right) = C(\Theta_S - \Theta). \tag{2.23}$$

The nondimensionalized expression of viscous dissipation term is

$$\Phi = 2\left(\frac{\partial^2 \psi}{\partial y^2}\right)^2 + 4\delta^2 \left(\frac{\partial^2 \psi}{\partial x \partial y}\right)^2 + 4\alpha\delta^3 \frac{\partial^3 \psi}{\partial y^2 \partial x} \frac{\partial^2 \psi}{\partial x \partial y} \frac{\partial \psi}{\partial x} - 4\alpha\delta^2 \frac{\partial^2 \psi}{\partial x \partial y} \frac{\partial^3 \psi}{\partial x^2 \partial y} + 8\alpha\delta^3 \left(\frac{\partial^2 \psi}{\partial x \partial y}\right)^3 - 2\delta^2 \psi^2 + 2\delta^2 \psi^2 +$$

$$12\alpha\delta^{3}\frac{\partial^{2}\psi}{\partial x\partial y}\frac{\partial^{2}\psi}{\partial x^{2}}\frac{\partial^{2}\psi}{\partial y^{2}}+6\alpha\delta^{5}\left(\frac{\partial^{2}\psi}{\partial x^{2}}\right)^{2}\frac{\partial^{2}\psi}{\partial x\partial y}-4\delta^{2}\frac{\partial^{2}\psi}{\partial x^{2}}\frac{\partial^{2}\psi}{\partial y^{2}}-2\alpha\delta\frac{\partial^{2}\psi}{\partial y^{2}}\frac{\partial\psi}{\partial y}\frac{\partial^{3}\psi}{\partial y^{2}\partial x}+2\alpha\delta^{3}\frac{\partial^{2}\psi}{\partial y^{2}}\frac{\partial\psi}{\partial y}\frac{\partial^{3}\psi}{\partial x^{3}}+$$

$$2\alpha\delta\frac{\partial\psi}{\partial x}\frac{\partial^2\psi}{\partial y^2}\frac{\partial^3\psi}{\partial y^3} - 2\alpha\delta^3\frac{\partial\psi}{\partial x}\frac{\partial^2\psi}{\partial y^2}\frac{\partial^3\psi}{\partial x^2\partial y} + 6\alpha\delta\left(\frac{\partial^2\psi}{\partial y^2}\right)^2\frac{\partial^2\psi}{\partial x\partial y} - 6\alpha\delta\frac{\partial^2\psi}{\partial y^2}\frac{\partial^2\psi}{\partial x\partial y} + 2\delta^4\left(\frac{\partial^2\psi}{\partial x^2}\right)^2 + 2\delta^4\left(\frac{\partial^2\psi}{\partial x^2}\right)^2\frac{\partial^2\psi}{\partial x\partial y} + 2\delta^4\left(\frac{\partial^2\psi}{\partial x\partial y}\right)^2\frac{\partial^2\psi}{\partial x\partial y} + 2\delta^2\left(\frac{\partial^2\psi}{\partial x\partial$$

$$2\alpha\delta^3\frac{\partial\psi}{\partial y}\frac{\partial^2\psi}{\partial x^2}\frac{\partial^3\psi}{\partial y^2\partial x}-2\alpha\delta^5\frac{\partial\psi}{\partial y}\frac{\partial^2\psi}{\partial x^2}\frac{\partial^3\psi}{\partial x^3}-2\alpha\delta^3\frac{\partial\psi}{\partial x}\frac{\partial^2\psi}{\partial x^2}\frac{\partial^3\psi}{\partial y^3}+2\alpha\delta^5\frac{\partial\psi}{\partial x}\frac{\partial^2\psi}{\partial x^2}\frac{\partial^3\psi}{\partial x^2}\frac{\partial^3\psi}{\partial x^2\partial y}+$$

$$6\alpha\delta^4\frac{\partial^2\psi}{\partial x^2}\frac{\partial^2\psi}{\partial x\partial y}+4\delta^2\left(\frac{\partial^2\psi}{\partial x\partial y}\right)^2-4\alpha\delta^3\frac{\partial^2\psi}{\partial x\partial y}\frac{\partial\psi}{\partial y}\frac{\partial^3\psi}{\partial x^2\partial y}+2\alpha\delta^3\frac{\partial^2\psi}{\partial x\partial y}\frac{\partial\psi}{\partial x}\frac{\partial^3\psi}{\partial y^2\partial x}-8\alpha\delta^3\left(\frac{\partial^2\psi}{\partial x\partial y}\right)^3+$$

$$2\alpha\delta^3 \frac{\partial^2\psi}{\partial x^2} \frac{\partial^2\psi}{\partial y^2} \frac{\partial^2\psi}{\partial x\partial y}.$$
 (2.24)

The walls exhibiting peristaltic movement are described in dimensionless form as

$$h_1(x) = 1 + a\sin(2\pi x),$$
 (2.25a)

$$h_2(x) = -d - b\sin(2\pi x + \phi),$$
 (2.25b)

having boundary conditions

$$\psi = \frac{F}{2}, \frac{\partial \psi}{\partial y} + 2\beta \frac{\partial^2 \psi}{\partial y^2} = -1, \varphi = \frac{E}{2} \quad at \quad y = h_1(x), \tag{2.26a}$$

$$\psi = -\frac{F}{2}, \frac{\partial \psi}{\partial y} - 2\beta \frac{\partial^2 \psi}{\partial y^2} = -1, \varphi = -\frac{E}{2} \quad at \quad y = h_2(x), \tag{2.26b}$$

$$\Theta - \varepsilon \frac{\partial \Theta}{\partial y} = 0$$
 at  $y = h_1(x)$ , (2.26c)

$$\Theta + \varepsilon \frac{\partial \Theta}{\partial y} = 1$$
 at  $y = h_2(x)$ . (2.26d)

$$\Theta_s - \varepsilon \frac{\partial \Theta_s}{\partial y} = 0$$
 at  $y = h_1(x)$ , (2.26e)

$$\Theta_s + \varepsilon \frac{\partial \Theta_s}{\partial y} = 1$$
 at  $y = h_2(x)$ , (2.26f)

The dimensionless time mean flow rate is denoted by F

$$Q = F + 1 + d, (2.27a)$$

where

$$F = \int_{h_2(x)}^{h_1(x)} \frac{\partial \psi}{\partial y} dy. \tag{2.27b}$$

The dimensionless time flow rate of solid particles is

$$Q_s = E + 1 + d, (2.28a)$$

where

$$E = \int_{h_2(x)}^{h_1(x)} \frac{\partial \varphi}{\partial y} dy. \tag{2.28b}$$

The heat transfer coefficient in non-dimensionalized form is described as

$$z = \frac{\partial \Theta}{\partial y} \frac{\partial h_1}{\partial x}.$$

#### 2.2 Method of Solution

Mathematical formulation of the problem consists of coupled nonlinear differential equations. Regular perturbation technique is applied to solve the system. We use  $\delta$  as perturbation parameter to describe fluid and particle stream functions  $\psi$  and  $\varphi$ , fluid and particle temperature  $\Theta$  and  $\Theta_s$ , time flow rates of fluid and particles F and E and pressure P as

$$\psi = \psi_0 + \delta \psi_1 + O(\delta^2), \tag{2.29}$$

$$\varphi = \varphi_0 + \delta \,\varphi_1 + O(\delta^2),\tag{2.30}$$

$$\Theta = \Theta_0 + \delta\Theta_1 + O(\delta^2), \tag{2.31}$$

$$\Theta_s = \Theta_{0s} + \delta\Theta_{1s} + O(\delta^2), \tag{2.32}$$

$$F = F_0 + \delta F_1 + O(\delta^2), \tag{2.33}$$

$$E = E_0 + \delta E_1 + O(\delta^2), \tag{2.34}$$

$$p = p_0 + \delta p_1 + O(\delta^2). \tag{2.35}$$

#### 2.2.1 Zeroth Order System

$$2\frac{\partial^4 \psi_0}{\partial v^4} - M^2 \frac{\partial^2 \psi_0}{\partial v^2} + A \left( \frac{\partial^2 \varphi_0}{\partial v^2} - \frac{\partial^2 \psi_0}{\partial v^2} \right) = 0, \tag{2.36}$$

$$B\left(\frac{\partial^2 \psi_0}{\partial v^2} - \frac{\partial^2 \varphi_0}{\partial v^2}\right) = 0,\tag{2.37}$$

$$(1 + Rd)\frac{\partial^2 \Theta_0}{\partial y^2} + A_1 \Pr(\Theta_{0s} - \Theta_0) + B_1 Br \left(\frac{\partial \varphi_0}{\partial y} - \frac{\partial \psi_0}{\partial y}\right)^2 + 2Br \left(\frac{\partial^2 \psi_0}{\partial y^2}\right)^2 = 0, \tag{2.38}$$

$$\Theta_{0s} - \Theta_0 = 0, \tag{2.39}$$

with boundary conditions

$$\psi_0 = \frac{F_0}{2}, \frac{\partial \psi_0}{\partial y} + 2\beta \frac{\partial^2 \psi_0}{\partial y^2} = -1, \varphi_0 = \frac{E_0}{2} \quad at \quad y = h_1(x),$$
 (2.40a)

$$\psi_0 = -\frac{F_0}{2}, \frac{\partial \psi_0}{\partial y} - 2\beta \frac{\partial^2 \psi_0}{\partial y^2} = -1, \varphi_0 = -\frac{E_0}{2} \quad at \quad y = h_2(x),$$
 (2.40b)

$$\Theta_0 - \varepsilon \frac{\partial \Theta_0}{\partial y} = 0$$
 at  $y = h_1(x)$ , (2.40c)

$$\Theta_0 + \varepsilon \frac{\partial \Theta_0}{\partial y} = 1$$
 at  $y = h_2(x)$ . (2.40d)

$$\Theta_{0s} - \varepsilon \frac{\partial \Theta_{0s}}{\partial y} = 0$$
 at  $y = h_1(x)$ , (2.40e)

$$\Theta_{0s} + \varepsilon \frac{\partial \Theta_{0s}}{\partial y} = 1$$
 at  $y = h_2(x)$ . (2.40f)

Using DSolver command in Mathematica, the solution of zeroth order system is as follows:

$$\psi_0(y) = A1 + A2y + A3 \cosh\left(\frac{M}{\sqrt{2}}y\right) + A4 \sinh\left(\frac{M}{\sqrt{2}}y\right),\tag{2.41}$$

$$\varphi_0(y) = A5 + yA6 + \frac{M}{\sqrt{2}} \left( \frac{\sqrt{2}A3\cosh\left(\frac{M}{\sqrt{2}}y\right)}{M} + \frac{\sqrt{2}A4\sinh\left(\frac{M}{\sqrt{2}}y\right)}{M} \right). \tag{2.42}$$

#### 2.2.2 First Order System

$$Re\left(\frac{\partial\psi_0}{\partial y}\frac{\partial^3\psi_0}{\partial x\partial y^2} - \frac{\partial\psi_0}{\partial x}\frac{\partial^3\psi_0}{\partial y^3}\right) = \frac{\partial^2}{\partial x\partial y}\left(\tau_{0xx} - \tau_{0yy}\right) + \frac{\partial^2\tau_{1xy}}{\partial y^2} + A\left(\frac{\partial^2\varphi_1}{\partial y^2} - \frac{\partial^2\psi_1}{\partial y^2}\right) - M^2\frac{\partial^2\psi_1}{\partial y^2}, \quad (2.43)$$

$$\frac{\partial \varphi_0}{\partial y} \frac{\partial^3 \varphi_0}{\partial x \partial y^2} - \frac{\partial \varphi_0}{\partial x} \frac{\partial^3 \varphi_0}{\partial y^3} = B \left( \frac{\partial^2 \psi_1}{\partial y^2} - \frac{\partial^2 \varphi_1}{\partial y^2} \right), \tag{2.44}$$

$$Re\left[\frac{\partial\Theta_0}{\partial x}\frac{\partial\psi_0}{\partial y} - \frac{\partial\Theta_0}{\partial y}\frac{\partial\psi_0}{\partial x}\right] = (1+Rd)\frac{\partial^2\Theta_1}{\partial y^2} + A_1(\Theta_{1s} - \Theta_1) + 2B_1Br\left(\frac{\partial\varphi_0}{\partial y} - \frac{\partial\psi_0}{\partial y}\right)\left(\frac{\partial\varphi_1}{\partial y} - \frac{\partial\psi_1}{\partial y}\right) + \frac{\partial^2\Theta_1}{\partial y^2} + \frac{\partial^2\Theta$$

$$Ec\Phi_1,$$
 (2.45)

$$\frac{\partial \varphi_0}{\partial y} \frac{\partial \Theta_{0s}}{\partial x} - \frac{\partial \varphi_0}{\partial x} \frac{\partial \Theta_{0s}}{\partial y} = -C(\Theta_{1s} - \Theta_1), \tag{2.46}$$

where

$$\tau_{0xx} = 0, \tag{2.47}$$

$$\tau_{0yy} = 4\alpha \left(\frac{\partial^2 \psi_0}{\partial y^2}\right)^2,\tag{2.48}$$

$$\tau_{1xy} = 2\frac{\partial^2 \psi_1}{\partial y^2} - \alpha \left( 2\frac{\partial \psi_0}{\partial y} \frac{\partial^3 \psi_0}{\partial x \partial y^2} - 2\frac{\partial \psi_0}{\partial x} \frac{\partial^3 \psi_0}{\partial y^3} - 4\frac{\partial^2 \psi_0}{\partial y^2} \frac{\partial^2 \psi_0}{\partial x \partial y} \right), \tag{2.49}$$

$$\Phi_{1} = 4 \frac{\partial^{2} \psi_{0}}{\partial y^{2}} \left( \frac{\partial^{2} \psi_{1}}{\partial y^{2}} \right)^{2} + 2\alpha \left( 3 \frac{\partial^{2} \psi_{0}}{\partial x \partial y} \left( \frac{\partial^{2} \psi_{0}}{\partial y^{2}} \right)^{2} - \frac{\partial \psi_{0}}{\partial y} \frac{\partial^{2} \psi_{0}}{\partial y^{2}} \frac{\partial^{3} \psi_{0}}{\partial x \partial y^{2}} + \frac{\partial \psi_{0}}{\partial x} \frac{\partial^{2} \psi_{0}}{\partial y^{2}} \frac{\partial^{3} \psi_{0}}{\partial y^{3}} - 3 \frac{\partial^{2} \psi_{0}}{\partial y^{2}} \frac{\partial^{2} \psi_{0}}{\partial x \partial y} \right). \tag{2.50}$$

with boundary conditions

$$\psi_1 = \frac{F_1}{2}, \frac{\partial \psi_1}{\partial y} + 2\beta \frac{\partial^2 \psi_1}{\partial y^2} = 0, \quad \varphi_1 = \frac{E_1}{2} \quad at \quad y = h_1(x), \tag{2.51a}$$

$$\psi_1 = -\frac{F_1}{2}, \frac{\partial \psi_1}{\partial y} - 2\beta \frac{\partial^2 \psi_1}{\partial y^2} = 0, \varphi_1 = -\frac{E_1}{2} \quad at \quad y = h_2(x),$$
 (2.51b)

$$\Theta_1 - \varepsilon \frac{\partial \Theta_1}{\partial y} = 0$$
 at  $y = h_1(x)$ , (2.51c)

$$\Theta_1 + \varepsilon \frac{\partial \Theta_1}{\partial y} = 0$$
 at  $y = h_2(x)$ . (2.51d)

$$\Theta_{1s} - \varepsilon \frac{\partial \Theta_{1s}}{\partial y} = 0$$
 at  $y = h_1(x)$ , (2.51e)

$$\Theta_{1s} + \varepsilon \frac{\partial \Theta_{1s}}{\partial y} = 0$$
 at  $y = h_2(x)$ . (2.51f)

Above system of differential equations has been solved by applying DSolver command in Mathematica. Since  $\delta$  is small parameter therefore the terms of  $O(\delta^2)$  have negligible contribution and thus they have been neglected.

## 2.3 Graphical Analysis

This section aims to present a comprehensive analysis of the effects of various significant factors on the velocity and temperature profiles of fluid flow and solid particles. Graphs of fluid velocity are plotted for Walter's B fluid parameter  $\alpha$ , slip parameter  $\beta$ , wave number  $\delta$ , MHD parameter M, and Reynolds number Re. The effects of Prandtl number Pr, Brickman number Br, thermal

slip parameter  $\varepsilon$ , and radiation parameter Rd on temperature distribution are delineated graphically.

#### 2.3.1 Fluid Flow Analysis

The analysis of fluid flow for Walter's B fluid parameter  $\alpha$ , wave number  $\delta$ , slip parameter  $\beta$ , MHD parameter M, and Reynolds number Re is represented in Figs. 2.2-2.6. Fluid velocity exhibits parabolic behavior. Fig. 2.2 deliberates the fluid flow behavior as Walter's B fluid parameter  $\alpha$  changes. As  $\alpha$  increases, velocity of the fluid reduces. The effect of the slip parameter  $\beta$  is shown in Fig. 2.3. A rise in  $\beta$  values increases resistive force, which results in a significant decrease in fluid speed. It is observed from Fig. 2.4 that an increase in wave number  $\delta$  enhances fluid velocity. A considerable reduction in fluid velocity occurs with increasing Hartmann number M as Fig. 2.5 illustrates. Due to a magnetic field, a Lorentz force is generated that opposes fluid flow direction, and consequently, fluid motion slows down. The high Reynolds number indicates that inertial forces are dominant which implies an enhancement of fluid speed, as presented in Fig. 2.6.

### 2.3.2 Solid Particle Flow Analysis

The solid particle velocity is discussed for Walter's B fluid parameter  $\alpha$ , slip parameter  $\beta$ , MHD parameter M, wave number  $\delta$ , and Reynolds number Re, which are represented in Figs. 2.7-2.11 via graphs. Fig. 2.7 elaborates the effect of viscoelastic parameter  $\alpha$  on velocity of solid particles. As viscosity increases, movement of solid particles becomes slightly slower. In Fig. 2.8, particle velocity graph is demonstrated for slip parameter  $\beta$ . High values of  $\beta$  generates resistance and hence solid particle velocity declines. Fig. 2.9 is representation of particle velocity under the impact of wave number  $\delta$ . As wave number  $\delta$  increases, contraction and expansion of boundaries

becomes frequent and hence particles move faster. Fig. 2.10 exhibits Hartmann number M effect on particle speed. An increase in Hartmann number remarkably slows down the movement of solid particles. Reynolds number Re has a minimal effect on the velocity of solid granules. Fig. 2.11 shows that particle velocity increases with a rise in Reynolds number Re because viscous forces become ineffective.

#### 2.3.3 Temperature Distribution Analysis

The transfer of heat through the fluid and particles is deliberated for Brinkman number Br, radiation parameter Rd, and thermal slip parameter  $\varepsilon$  in Figs. 2.12-2.15. Fig. 2.12 shows the fluid temperature profile for Brinkman number Br. High values of Brinkman number Br indicate that viscous effects are assertive that enhances heat conduction and hence the temperature rises. As radiation parameter Rd is enlarged, fast heat transfer is observed through the fluid as shown in Fig. 2.13. Slow heat transfer through the fluid is noticed in Fig. 2.14 as slip parameter  $\varepsilon$  is assigned higher values. As the slip intensifies the connection of fluid molecules and boundary becomes weak therefore heat transfer of the fluid becomes slow. Fig. 2.15 is drawn for temperature distribution of solid particles to study effects of Brinkman number Br. It is revealed that the temperature of solid particles also rises as Brinkman number Br is enhanced, as in the case of fluid temperature profile.

### 2.3.4 Validation of Present Study

The graph of shear stress has been compared with the graph presented in the article by Mehmood et. al. [89]. Fig. 2.16 shows that shear stress graph obtained in recent work exactly matches with the graph obtained by Mehmood et. al. [89].

Table 2.1 represents the comparison of recent study with the work of Srinivas and Kothandapani [88]. The data for viscous fluid presented by Srinivas and Kothandapani [88] has been reproduced.

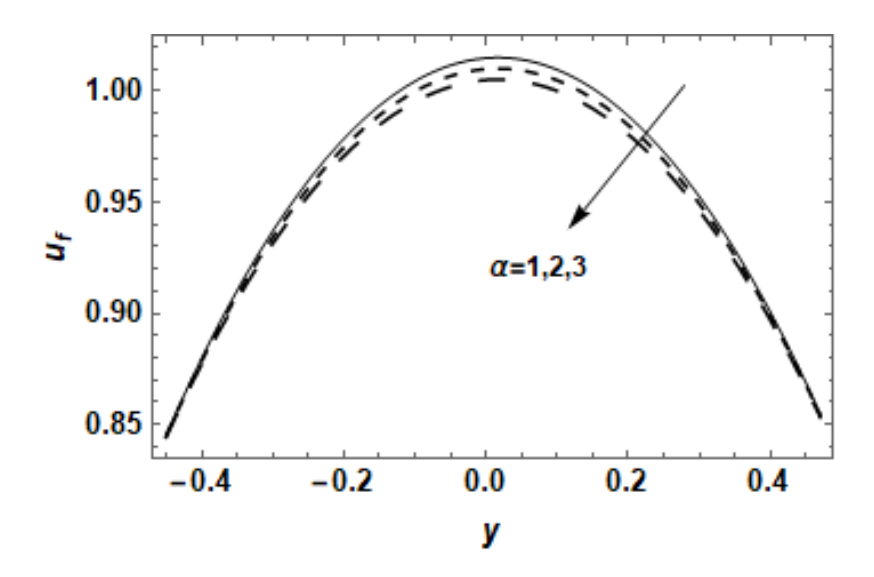


**Fig. 2.2:** The fluid flow behavior with Re = 10,  $\delta = 0.01$ ,  $\beta = 0.4$ , M = 0.2, A = 0.2, B = 0.6, a = 0.2, d = 0.3, b = 0.77,  $\phi = \frac{\pi}{3}$ .

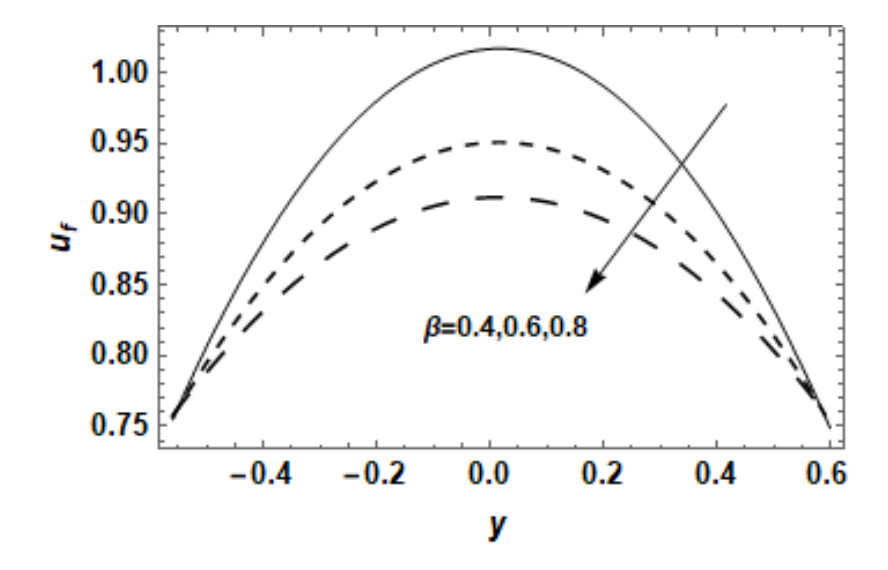


**Fig. 2.3:** The fluid flow behavior with Re = 10,  $\delta = 0.01$ ,  $\alpha = 0.6$ , M = 0.2, A = 0.2, B = 0.6, a = 0.2, d = 0.3, b = 0.77,  $\phi = \frac{\pi}{3}$ .

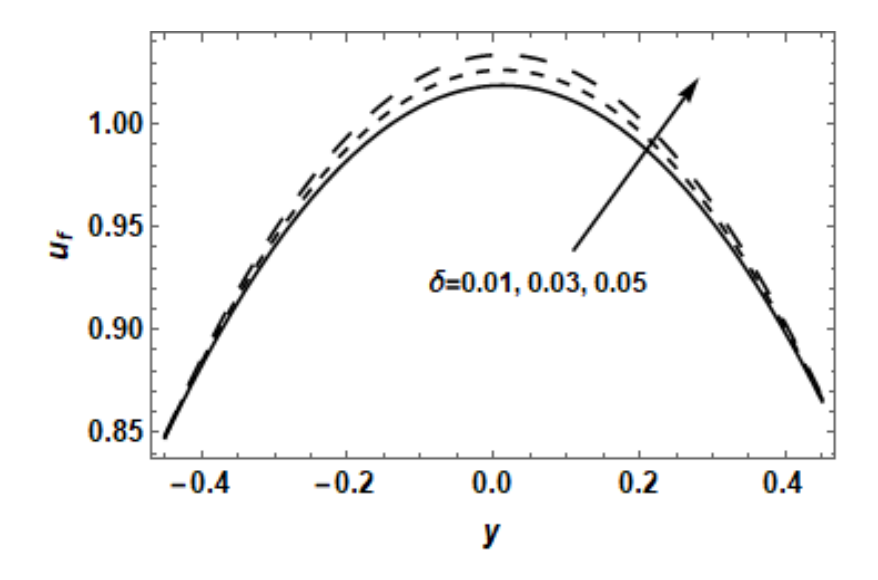


**Fig. 2.4:** The fluid flow behavior with Re = 30,  $\alpha = 0.3$ ,  $\beta = 0.4$ , M = 0.2, A = 0.2, B = 0.6, a = 0.2, d = 0.3, b = 0.78,  $\phi = \frac{\pi}{3}$ .

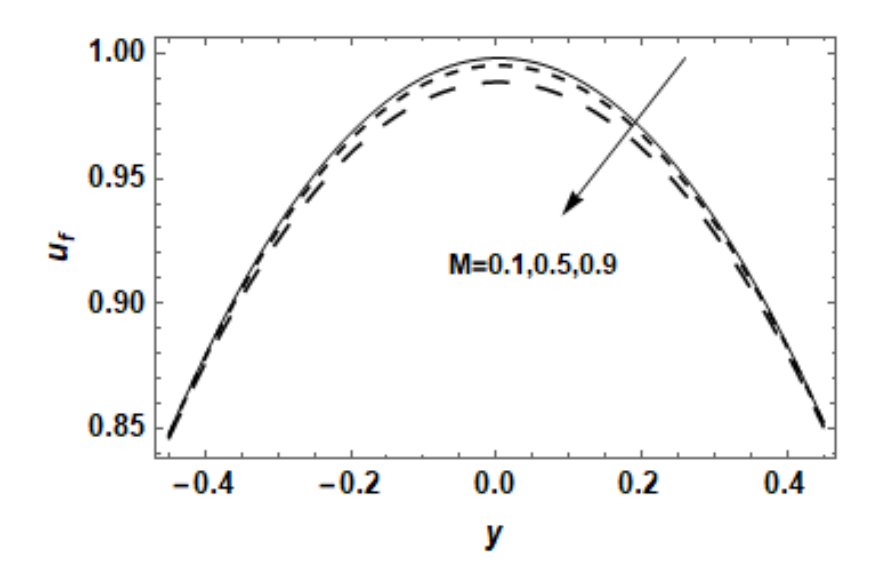
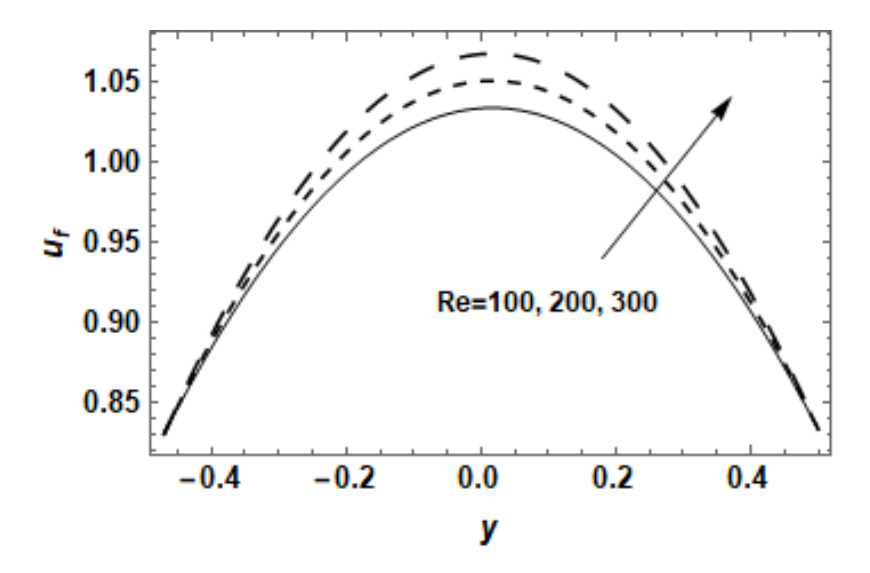
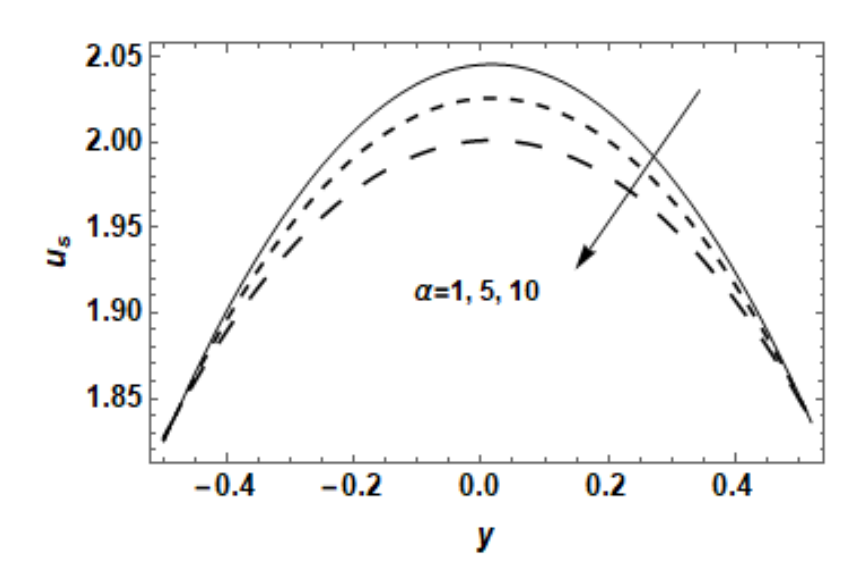


Fig. 2.5: The fluid flow behavior with Re = 5,  $\delta = 0.01$ ,  $\alpha = 3$ ,  $\beta = 0.4$ , A = 0.6, B = 0.4,  $\alpha = 0.1$ , d = 0.3, b = 0.8,  $\phi = \frac{\pi}{3}$ .



**Fig. 2.6:** The fluid flow behavior with  $\delta = 0.01$ ,  $\alpha = 0.3$ ,  $\beta = 0.4$ , M = 0.2, A = 0.2, B = 0.6, a = 0.2, d = 0.3, b = 0.77,  $\phi = \frac{\pi}{3}$ .



**Fig. 2.7:** The particle velocity with Re = 20,  $\delta = 0.01$ ,  $\beta = 0.4$ , M = 0.3, A = 0.2, B = 0.6, a = 0.2, d = 0.3, b = 0.77,  $\phi = \frac{\pi}{3}$ .

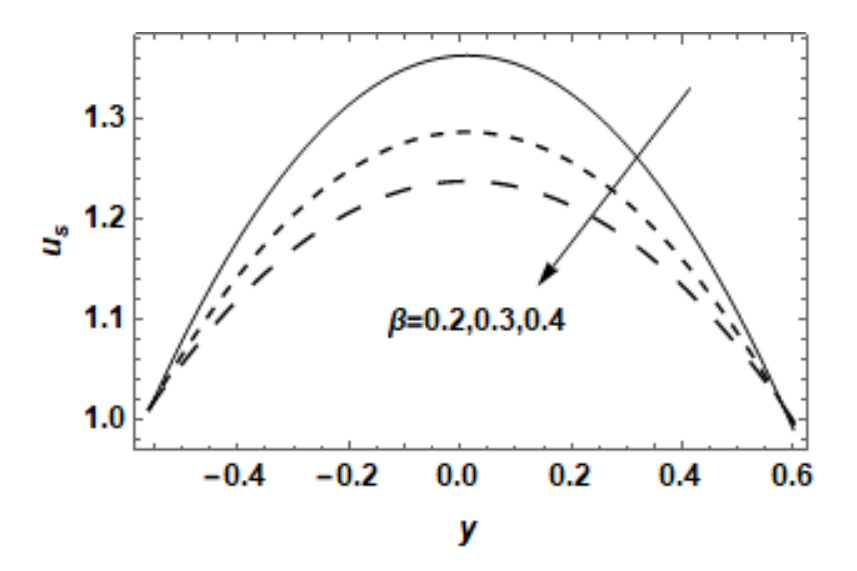


**Fig. 2.8:** The particle velocity with Re = 20,  $\delta = 0.01$ ,  $\alpha = 0.3$ , M = 0.3, A = 0.2, B = 0.6,  $\alpha = 0.1$ , d = 0.3, b = 0.78,  $\phi = \frac{\pi}{3}$ .

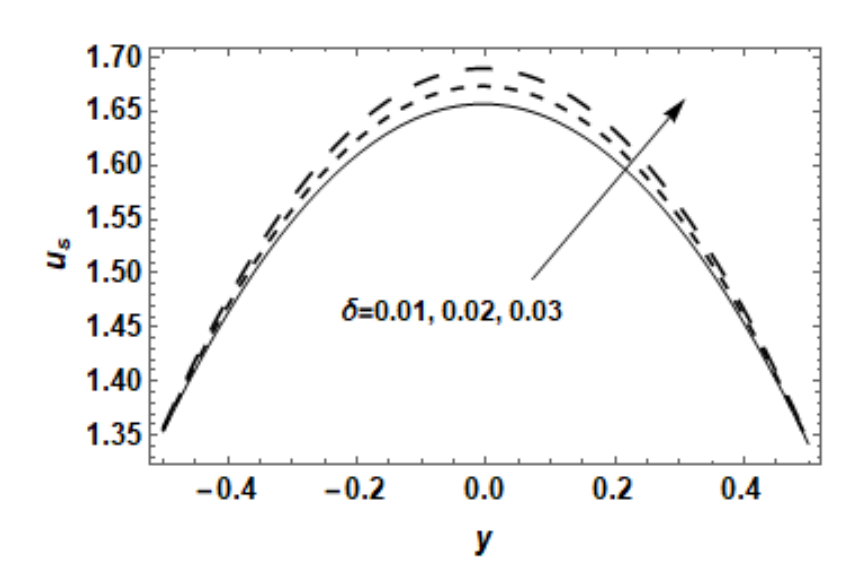


**Fig. 2.9:** The particle velocity with  $Re = 20, \beta = 0.2, \alpha = 0.3, M = 0.3, A = 0.2, B = 0.6, \alpha = 0.1, d = 0.36, b = 0.75, <math>\phi = \frac{\pi}{3}$ .

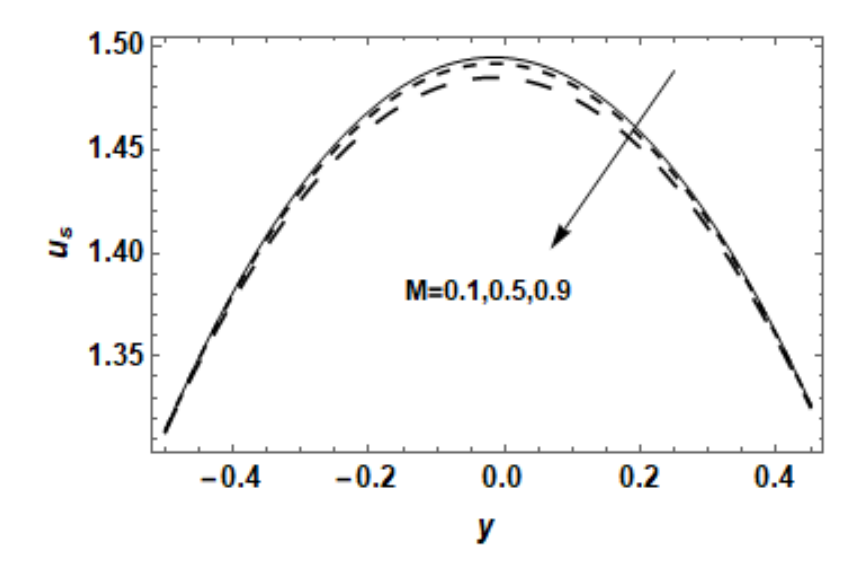


**Fig. 2.10:** The particle velocity with Re = 0.5,  $\beta = 0.4$ ,  $\alpha = 0.3$ ,  $\delta = 0.01$ , A = 0.2, B = 0.6,  $\alpha = 0.1$ , d = 0.34, b = 0.8,  $\phi = \frac{\pi}{3}$ .

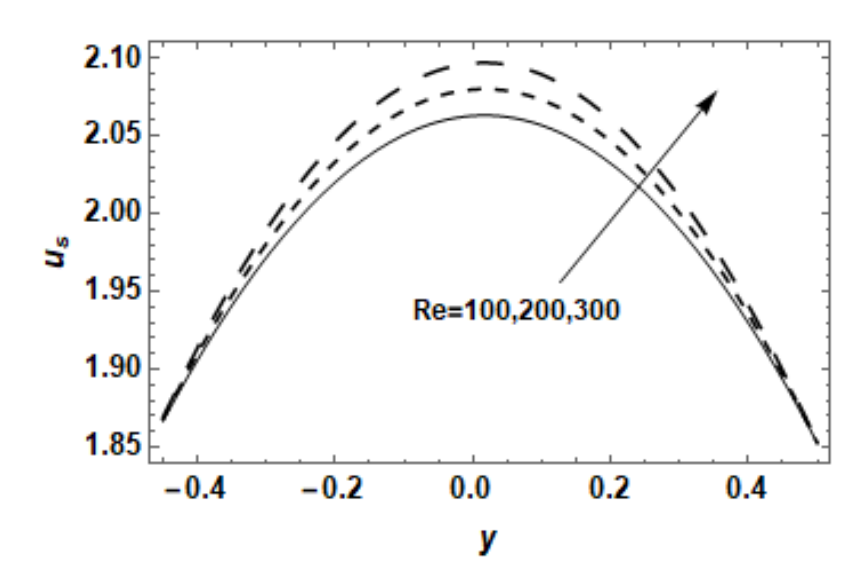


**Fig. 2.11:** The particle velocity with  $\beta = 0.4$ ,  $\alpha = 0.3$ ,  $\delta = 0.01$ , M = 0.2, A = 0.2, B = 0.6, a = 0.2, d = 0.3, b = 0.77,  $\phi = \frac{\pi}{3}$ .

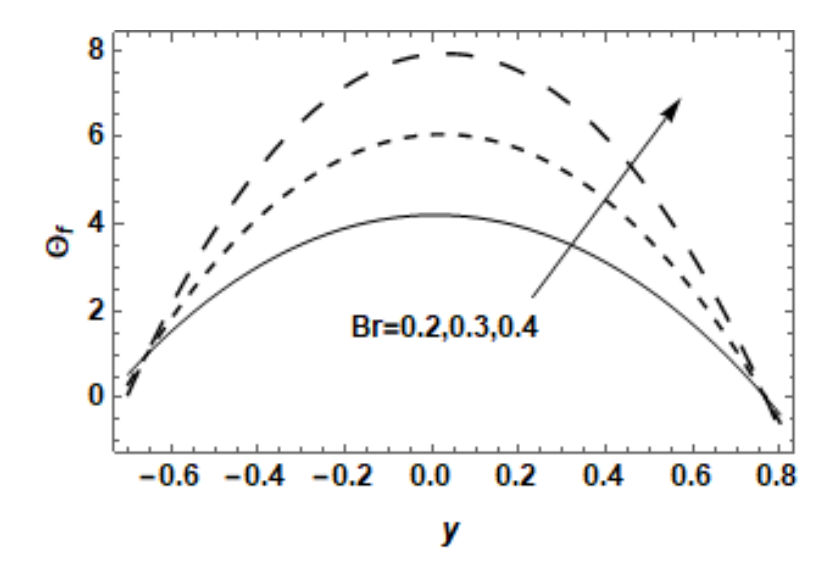


**Fig. 2.12:** The fluid temperature profile with Re = 0.3, Rd = 3, Pr = 1.5,  $\varepsilon = 0.2$ ,  $\beta = 0.4$ ,  $\alpha = 0.5$ ,  $\delta = 0.01$ , M = 0.5,  $B_1 = 0.7$ ,  $A_1 = 0.2$ ,  $A_2 = 0.1$ ,  $A_3 = 0.4$ ,  $A_4 = 0.4$ ,  $A_5 = 0.4$ ,  $A_6 = 0.4$ ,  $A_7 = 0.4$ ,  $A_8 = 0.4$ ,  $A_8 = 0.4$ ,  $A_8 = 0.4$ ,  $A_8 = 0.4$ ,  $A_9 = 0.$ 

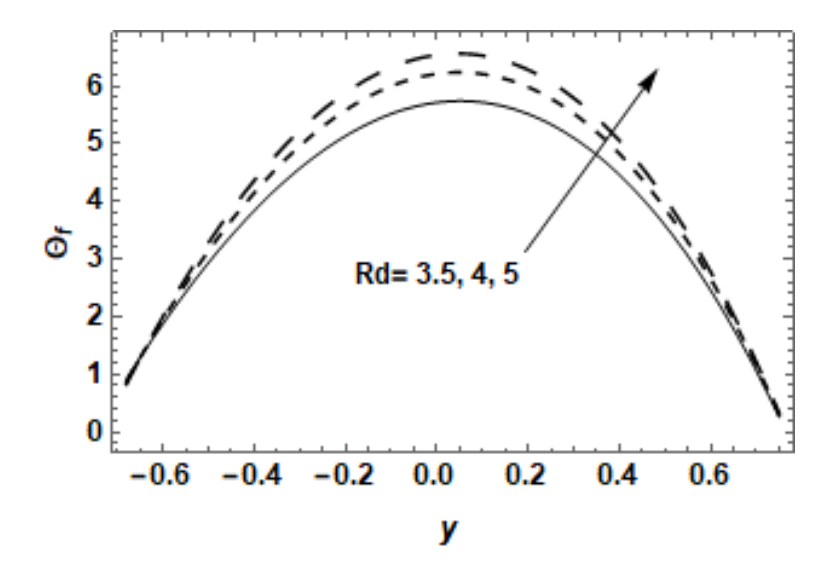


**Fig. 2.13:** The fluid temperature profile with Re = 0.3, Br = 0.5, Pr = 0.2,  $\varepsilon = 0.2$ ,  $\beta = 0.4$ ,  $\alpha = 0.6$ ,  $\delta = 0.01$ , M = 0.4,  $B_1 = 0.7$ ,  $A_1 = 0.55$ , A = 0.1, B = 0.6, C = 0.4,  $A_2 = 0.35$ ,  $A_3 = 0.2$ ,  $A_4 = 0.4$ ,  $A_5 = 0.4$ ,  $A_5 = 0.4$ ,  $A_6 = 0.4$ ,  $A_7 = 0.4$ ,  $A_8 = 0.4$ ,  $A_8 = 0.4$ ,  $A_8 = 0.4$ ,  $A_9 = 0.4$ 

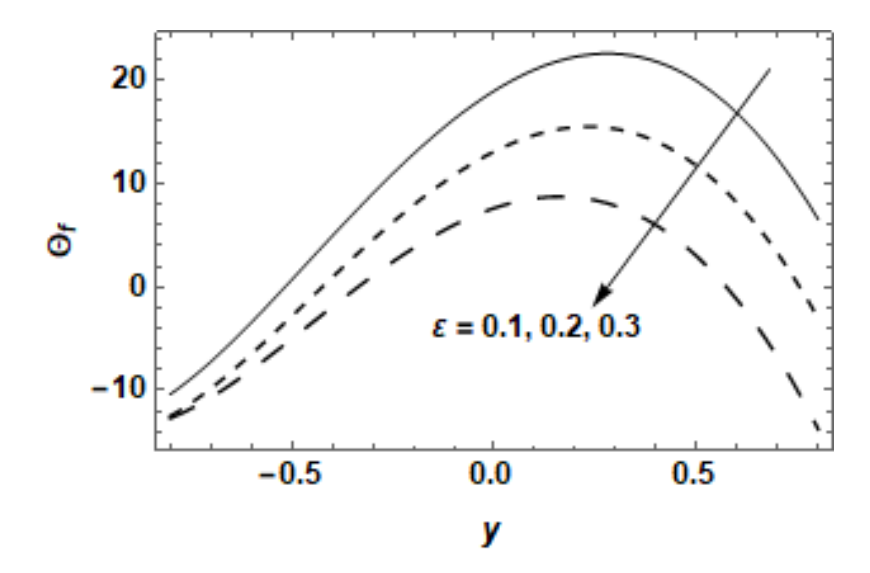


**Fig. 2.14:** The fluid temperature profile with Re = 0.3, Br = 0.5, Pr = 0.8, Rd = 3,  $\beta = 0.4$ ,  $\alpha = 0.5$ ,  $\delta = 0.01$ , M = 0.4,  $B_1 = 0.6$ ,  $A_1 = 0.2$ , A = 0.1, B = 0.6, C = 0.6, C = 0.6, C = 0.2, C = 0.78, C = 0.78,

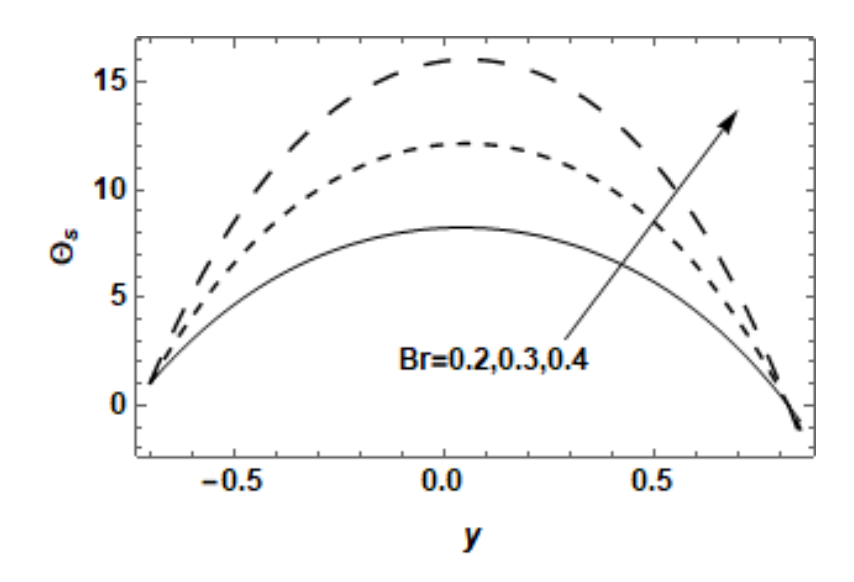


**Fig. 2.15:** The particle temperature profile with Re = 0.3, Pr = 1.5, Rd = 3,  $\varepsilon = 0.2$ ,  $\beta = 0.4$ ,  $\alpha = 0.5$ ,  $\delta = 0.01$ , M = 0.5,  $B_1 = 0.7$ ,  $A_1 = 0.2$ , A = 0.1, B = 0.6, C = 0.8, A = 0.4, A = 0.2, A = 0.8, A = 0.8

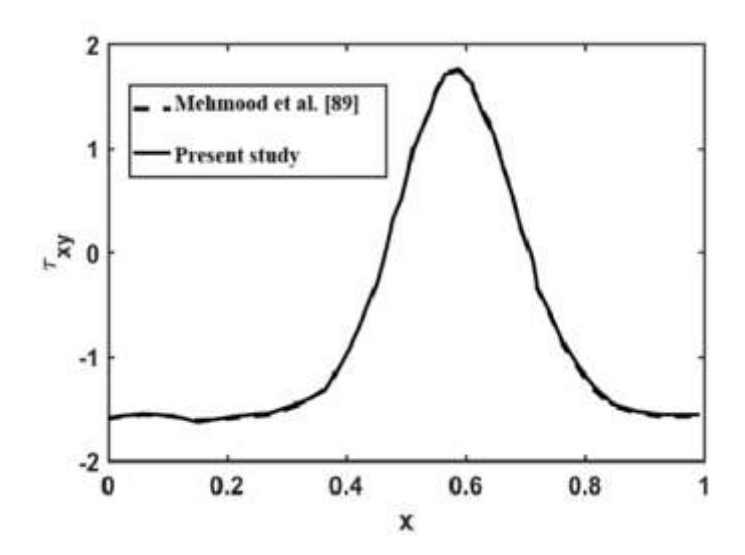


**Fig. 2.16:** Comparison of shear stress graph for  $\alpha = 0.5$ ,  $\beta = Re = M = A = B = E = 0$  with the graph of Mehmood et. al. [89].

**Table 2.1**: Comparison of recent work with results of Srinivas and Kothandapani [88] for heat transfer coefficient.

$a = 0.5, b = 0.6, d = 1.5, Pr = 1, \phi = \frac{\pi}{4}, F_0 = -2, Re = 0, Rd = 0, \varepsilon = 0, \alpha = 0, \delta = 0, \beta = 0$				
$0, B_1 = 0, A_1 = 0, C = 0, A = 0, B = 0, E = 0$				
x	M			
	0	2	3	4
0.1	1.8449	1.9440	2.1353	2.3848
0.2	1.8352	1.8582	1.912	1.9920
0.3	1.9378	1.9789	1.9932	2.0182

## 2.4 Conclusion

In this chapter, analysis of heat transfer in Walter'B fluid is presented, with dust particles distributed uniformly through the fluid and sinusoidal waves propelling along the walls of asymmetric channels. The results of velocity and temperature profiles are graphically analyzed for several influential parameters. Significant findings are listed as follows:

- As Walter's B fluid parameter, Hartmann number, and slip parameter grow, fluid and dust particles both move slowly.
- Fluid and particle movement is accelerated by increasing Reynolds number and wave number  $\delta$ . High wavenumber means frequency of waves per unit length is increased that implies contraction and expansion is occurring more frequently along the length of blood vessel and consequently movement of blood is accelerated. As Reynolds number is increased velocity of blood flow in the vessels is greater than the viscosity of blood. Therefore, blood moves faster that results in efficient transport of nutrients and oxygen from blood to organs and tissues.
- Heat transfer becomes slower when thermal slip parameter increases.
- High values of Brinkman number are responsible for fast heat conduction through the fluid and solid granules.

# **Chapter 3**

## Effect of Relaxation and Retardation Times on

## **Dusty Jeffrey Fluid in a Curved Channel with**

## **Peristalsis**

In this chapter, the Jeffrey liquid with uniform dust particles in a symmetric channel is studied. Moving sinusoidal wave is executed on the walls of the channel, which generates peristaltic transport in the fluid. The governing equations for fluid and dust particles have been formulated using stream functions. Perturbation method is used to get analytic solution of the problem by using small wave number. Graphical analysis has been carried out for stream function and velocity of fluid and dust particles. Effects of different parameters such as curvature k, relaxation time  $\lambda_2$ , wave number  $\delta$ , and retardation time  $\lambda_1$  are debated through graphs for both dust particles and fluid.

## 3.1 Problem Formulation

We consider flow of an incompressible Jeffrey fluid having uniform dust particles, whose number density N is considered as a constant. A two-dimensional curved channel of width 2a is taken. The radial velocities of fluid and dust particles are  $\overline{V}$  and  $\overline{V}_s$  while  $\overline{U}$  and  $\overline{U}_s$  are axial velocities, respectively. The walls are geometrically described by

$$\overline{H}(\overline{X}, \overline{t}) = a + b \sin\left[\frac{2\pi}{\lambda}(\overline{X} - c\overline{t})\right], \text{ Upper Wall}$$
 (3.1)

$$\overline{H}(\overline{X}, \overline{t}) = -a - b \sin\left[\frac{2\pi}{\lambda}(\overline{X} - c\overline{t})\right], \text{Lower Wall}$$
(3.2)

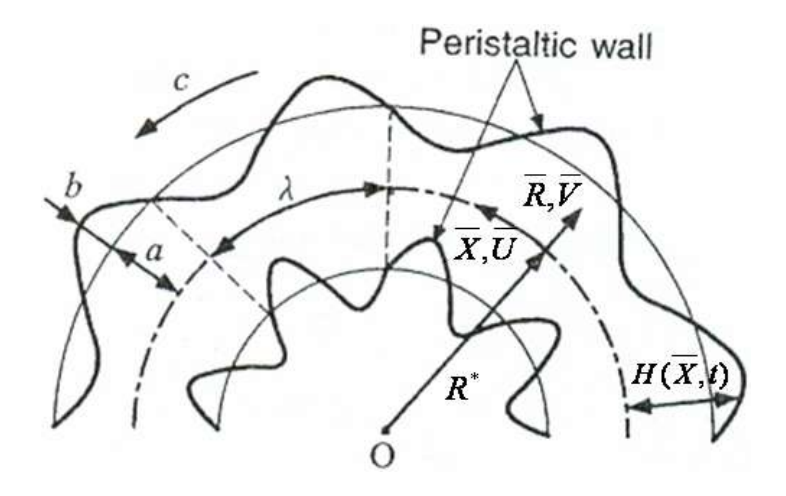


Figure 3.1. Geometry of the channel

The stress tensor of Jeffrey fluid is given as [65]

$$\boldsymbol{\tau} = \frac{\mu}{1+\lambda_2} \left[ \boldsymbol{A}_1 + \lambda_1 \left( \frac{\partial \boldsymbol{A}_1}{\partial t} + (\overline{\boldsymbol{V}} \cdot \nabla) \boldsymbol{A}_1 \right) \right], \tag{3.3}$$

where

$$\mathbf{A_1} = (\nabla \overline{\mathbf{V}}) + (\nabla \overline{\mathbf{V}})^T. \tag{3.4}$$

The flow problem is explained by the following equations:

The equations of fluid flow are defined as [65]

$$\frac{\partial}{\partial \bar{R}}(\bar{R} + R^*)\bar{V} + R^*\frac{\partial \bar{U}}{\partial \bar{X}} = 0, \tag{3.5}$$

$$\rho\left(\frac{\partial \overline{V}}{\partial t} + (\overline{V}.\nabla)\overline{V} - \frac{\overline{U}^{2}}{\overline{R} + R^{*}}\right) = -\frac{\partial P}{\partial \overline{R}} + \frac{1}{R^{*} + \overline{R}}\frac{\partial}{\partial \overline{R}}\left[(\overline{R} + R^{*})\tau_{rr}\right] + \frac{R^{*}}{R^{*} + \overline{R}}\frac{\partial \tau_{rx}}{\partial \overline{X}} - \frac{1}{\overline{R} + R^{*}}\tau_{xx} + sN(\overline{V}_{S} - \overline{V}),$$
(3.6)

$$\rho\left(\frac{\partial \overline{U}}{\partial t} + (\overline{V}.\nabla)\overline{U} + \frac{\overline{U}\overline{V}}{\overline{R} + R^*}\right) = -\frac{R^*}{\overline{R} + R^*}\frac{\partial P}{\partial \overline{X}} + \frac{1}{(R^* + \overline{R})^2}\frac{\partial}{\partial \overline{R}}\left[(\overline{R} + R^*)^2\tau_{rx}\right] + \frac{R^*}{\overline{R} + R^*}\frac{\partial \tau_{xx}}{\partial \overline{X}} + sN(\overline{U}_S - \overline{U}).$$
(3.7)

The equations of solid particles are defined as [52]

$$\frac{\partial}{\partial \bar{R}}(\bar{R} + R^*)\bar{V}_S + R^*\frac{\partial \bar{U}_S}{\partial \bar{X}} = 0, \tag{3.8}$$

$$\frac{\partial \overline{U}_S}{\partial t} + \overline{V}_S \frac{\partial \overline{U}_S}{\partial \overline{R}} - \frac{\overline{U}_S}{\overline{R}} \frac{\partial}{\partial \overline{X}} \left( (\overline{R} + R^*) \overline{V}_S \right) + \frac{\overline{U}_S \overline{V}_S}{\overline{R} + R^*} = \frac{k}{m} (\overline{U} - \overline{U}_S), \tag{3.9}$$

$$\frac{\partial \overline{V}_S}{\partial t} + \overline{V}_S \frac{\partial \overline{V}_S}{\partial \overline{R}} + \frac{R^* \overline{U}_S}{\overline{R} + R^*} \frac{\partial \overline{V}_S}{\partial \overline{X}} - \frac{\overline{U}_S^2}{\overline{R} + R^*} = \frac{k}{m} (\overline{V} - \overline{V}_S), \tag{3.10}$$

The laboratory frame  $(\bar{R}, \bar{X})$  and the wave frame  $(\bar{r}, \bar{x})$  coordinates are associated by the following transformation.

$$\bar{u} = \bar{U} - c$$
,  $\bar{u}_s = \bar{U}_s - c$ ,  $\bar{v} = \bar{V}$ ,  $\bar{v}_s = \bar{V}_s$ ,  $\bar{y} = \bar{Y}$ ,  $\bar{x} = \bar{X} - ct$ ,  $\bar{r} = \bar{R}$ . (3.11)

Introducing the following stream functions and dimensionless quantities

$$x = \frac{\bar{x}}{\lambda} , L = \frac{R^*}{a}, p = \frac{Pa^2}{\lambda\mu c}, Re = \frac{\rho ca}{\mu}, r = \frac{\bar{r}}{a}, \tau^* = \frac{\tau c}{\mu a}, v = \frac{\bar{v}}{\delta c}, \delta = \frac{a}{\lambda}, A = \frac{kNa^2}{\mu}, u = \frac{\bar{u}}{c}, \delta = \frac{\bar{u}}{\lambda}$$

$$B = \frac{ka}{mc}, \quad \alpha_0 = \frac{\lambda_1 c}{a}, \quad u = -\frac{\partial \psi}{\partial r}, \quad v = \frac{k}{r+k} \frac{\partial \psi}{\partial x}, \quad v_s = \frac{k}{r+k} \frac{\partial \varphi}{\partial x}, \quad u_s = -\frac{\partial \varphi}{\partial r}. \tag{3.12}$$

where A and B are non-dimensional parameters.

After using above quantities, the governing equations thus become as:

For fluid flow

$$Re \, \delta \left[ -\frac{\partial^{2}\psi}{\partial r\partial x} + \frac{L}{r+L} \left( 1 - \frac{\partial\psi}{\partial r} \right) \frac{\partial^{2}\psi}{\partial x\partial r} - \frac{L}{r+L} \frac{\partial\psi}{\partial x} \frac{\partial^{2}\psi}{\partial r^{2}} - \frac{L}{(r+L)^{2}} \frac{\partial\psi}{\partial x} \left( 1 - \frac{\partial\psi}{\partial r} \right) \right] = -\frac{L}{r+L} \frac{\partial p}{\partial x} + \frac{\partial\tau^{*}_{xr}}{\partial x} + \frac{2\tau^{*}_{xr}}{r+L} + \frac{\delta L}{r+L} \frac{\partial\tau^{*}_{xx}}{\partial x} + A \left( \frac{\partial\psi}{\partial r} - \frac{\partial\varphi}{\partial r} \right), \tag{3.13}$$

$$Re \, \delta \begin{bmatrix} -\delta^{2} \frac{L}{r+L} \frac{\partial^{2} \psi}{\partial x^{2}} + \delta^{2} \left( \frac{L}{r+L} \right)^{2} \frac{\partial \psi}{\partial x} \frac{\partial^{2} \psi}{\partial r \partial x} \\ +\delta^{2} \left( \frac{L}{r+L} \right)^{2} \left( 1 - \frac{\partial \psi}{\partial r} \right) \frac{\partial^{2} \psi}{\partial x^{2}} - \left( 1 - \frac{\partial \psi}{\partial r} \right)^{2} \frac{1}{r+L} \end{bmatrix} = -\delta \frac{\partial p}{\partial r} + \frac{\delta^{2} L}{r+L} \frac{\partial^{2} \tau^{*}_{xr}}{\partial x^{2}} + \frac{\partial \tau^{*}_{rr}}{\partial r} + \frac{\tau^{*}_{rr}}{r+L} + \frac{\tau^{*}_{rr}}{r+L} + \frac{L\delta}{r+L} \frac{\partial \tau^{*}_{xx}}{\partial x} - \frac{\tau^{*}_{xx}}{r+L} + A \left[ \frac{\delta L}{r+L} \left( \frac{\partial \varphi}{\partial x} - \frac{\partial \psi}{\partial x} \right) \right].$$

$$(3.14)$$

For solid particles

$$\delta\left[-\frac{L}{r+L}\frac{\partial\varphi}{\partial x}\frac{\partial^{2}\varphi}{\partial r^{2}} + \frac{\delta L}{r(r+L)}\frac{\partial^{2}\varphi}{\partial x^{2}}\left(1 - \frac{\partial\varphi}{\partial r}\right) + \frac{L}{(r+L)^{2}}\left(1 - \frac{\partial\varphi}{\partial r}\right)\frac{\partial\varphi}{\partial x}\right] = B\left[\frac{\partial\varphi}{\partial r} - \frac{\partial\psi}{\partial r}\right],\tag{3.15}$$

$$\delta \left[ \frac{\delta^2 L}{r + L} \frac{\partial \varphi}{\partial x} \frac{\partial^2 \varphi}{\partial r \partial x} + L \delta^2 \left( 1 - \frac{\partial \varphi}{\partial r} \right) \frac{\partial^2 \varphi}{\partial x^2} - \frac{1}{L} \left( 1 - \frac{\partial \varphi}{\partial r} \right)^2 \right] = B \left( \frac{\partial \psi}{\partial x} - \frac{\partial \varphi}{\partial x} \right). \tag{3.16}$$

The compatibility equations for solid particles and fluid are

$$Re\delta \begin{bmatrix} \frac{1}{L}\frac{\partial^{2}\psi}{\partial r\partial x} - \frac{1}{r+L}\frac{\partial\psi}{\partial x}\frac{\partial^{2}\psi}{\partial r^{2}} + \frac{1}{(r+L)^{2}}\left(1 - \frac{\partial\psi}{\partial r}\right)\frac{\partial\psi}{\partial x} - \frac{1}{r+L}\left(1 - \frac{\partial\psi}{\partial r}\right)\frac{\partial^{2}\psi}{\partial r\partial x} \\ + \frac{L+r}{L}\frac{\partial^{3}\psi}{\partial r^{2}\partial x} - \frac{\partial\psi}{\partial x}\frac{\partial^{3}\psi}{\partial r^{3}} - \frac{r+L}{L}\left(1 - \frac{\partial\psi}{\partial r}\right)\frac{\partial^{2}}{\partial r^{2}}\left(\frac{L}{L+r}\frac{\partial\psi}{\partial x}\right) \\ + \frac{\delta^{2}L}{r+L}\frac{\partial^{3}\psi}{\partial r^{3}} + \frac{2\delta^{2}L^{2}}{(r+L)^{3}}\frac{\partial\psi}{\partial x}\frac{\partial^{2}\psi}{\partial x^{2}} - \delta^{2}\left(\frac{L}{r+L}\right)^{2}\frac{\partial\psi}{\partial x}\frac{\partial^{3}\psi}{\partial r\partial x^{2}} \\ - \delta^{2}\left(1 - \frac{\partial\psi}{\partial r}\right)\left(\frac{L}{r+L}\right)^{2}\frac{\partial^{3}\psi}{\partial x^{3}} + \frac{2}{r+L}\left(1 - \frac{\partial\psi}{\partial r}\right)\frac{\partial^{2}\psi}{\partial r\partial x} \end{bmatrix} = \left(\delta\frac{\partial^{2}}{\partial r\partial x} + \frac{\delta}{r+L}\frac{\partial}{\partial x}\right)\tau_{xx}^{*} + \frac{\delta}{r+L}\frac{\partial}{\partial x}$$

$$\left[\frac{\partial}{\partial r}\left(\frac{1}{(L+r)L}\frac{\partial}{\partial r}(r+L)^2\right) - \frac{\delta^2L}{r+L}\frac{\partial^2}{\partial x^2}\right]\tau_{xr}^* - \frac{\delta}{L+r}\frac{\partial^2}{\partial r\partial x}\left[(r+L)\tau_{rr}^*\right] + \frac{\delta^2L}{r^2}\left[(r+L)\tau_{rr}^*\right] + \frac{\delta^2L}{r^2}\left[(r+L)\tau_{rr}^*\right]$$

$$A \begin{bmatrix} \left( \left( \frac{L+r}{L} \right) \frac{\partial^2}{\partial r^2} + \frac{1}{L} \frac{\partial}{\partial r} + \delta^2 \frac{\partial^2}{\partial x^2} \right) \psi \\ - \left( \left( \frac{r+L}{L} \right) \frac{\partial^2}{\partial r^2} + \frac{1}{L} \frac{\partial}{\partial r} + \delta^2 \frac{\partial^2}{\partial x^2} \right) \varphi \end{bmatrix}, \tag{3.17}$$

$$\delta \begin{bmatrix} \frac{1}{L} \frac{\partial^2 \varphi}{\partial r \partial x} - \frac{1}{r + L} \frac{\partial \varphi}{\partial x} \frac{\partial^2 \varphi}{\partial r^2} + \frac{1}{(r + L)^2} \left( 1 - \frac{\partial \varphi}{\partial r} \right) \frac{\partial \varphi}{\partial x} - \frac{1}{r + L} \left( 1 - \frac{\partial \varphi}{\partial r} \right) \frac{\partial^2 \varphi}{\partial r \partial x} \\ + \left( \frac{r + L}{L} \right) \frac{\partial^3 \varphi}{\partial r^2 \partial x} - \frac{\partial \varphi}{\partial x} \frac{\partial^3 \varphi}{\partial r^3} - \left( \frac{r + L}{L} \right) \left( 1 - \frac{\partial \varphi}{\partial r} \right) \frac{\partial}{\partial r} \left( - \frac{L}{(r + L)^2} \frac{\partial \varphi}{\partial x} + \frac{L}{r + L} \frac{\partial^2 \varphi}{\partial r \partial x} \right) \\ + \delta^2 \frac{\partial^3 \varphi}{\partial x^3} + \frac{\delta^2}{r + L} \frac{\partial^2 \varphi}{\partial x^2} - \delta^2 \frac{\partial^3 \varphi}{\partial x^2 \partial r} - \frac{\delta^2 L}{r + L} \left( 1 - \frac{\partial \varphi}{\partial r} \right) \frac{\partial^3 \varphi}{\partial x^3} - \frac{2}{L} \left( 1 - \frac{\partial \varphi}{\partial r} \right) \frac{\partial^2 \varphi}{\partial r \partial x} \end{bmatrix} =$$

$$B \begin{bmatrix} \left(\frac{1}{L}\frac{\partial}{\partial r} + \frac{r+L}{L}\frac{\partial^{2}}{\partial r^{2}} + \delta^{2}\frac{\partial^{2}}{\partial x^{2}}\right)\varphi \\ -\left(\frac{1}{L}\frac{\partial}{\partial r} + \frac{r+L}{L}\frac{\partial^{2}}{\partial r^{2}} + \delta^{2}\frac{\partial^{2}}{\partial x^{2}}\right)\psi \end{bmatrix}, \tag{3.18}$$

where

$$\tau_{rr}^{*} = \frac{\delta}{(1+\lambda_{2})} \left[ +2\alpha_{0}\delta \left( \frac{2L^{2}}{(r+L)^{4}} \left( \frac{\partial \psi}{\partial x} \right)^{2} + \left( \frac{L}{r+L} \right)^{2} \frac{\partial \psi}{\partial x} \frac{\partial^{3}\psi}{\partial r^{2}\partial x} - \frac{2L^{2}}{(r+L)^{3}} \frac{\partial \psi}{\partial x} \frac{\partial^{2}\psi}{\partial r\partial x} \right) \right],$$

$$+2\alpha_{0}\delta \left( 1 - \frac{\partial \psi}{\partial r} \right) \left( -\frac{L^{2}}{(r+L)^{3}} \frac{\partial^{2}\psi}{\partial x^{2}} + \left( \frac{L}{r+L} \right)^{2} \frac{\partial^{3}\psi}{\partial r\partial x^{2}} \right)$$

$$(3.19)$$

$$\tau_{rx}^{*} = \frac{1}{(1+\lambda_{2})} \begin{bmatrix} \frac{\delta^{2}k^{2}}{(r+L)^{2}} \frac{\partial^{2}\psi}{\partial x^{2}} - \frac{1}{r+L} \left(1 - \frac{\partial\psi}{\partial r}\right) - \frac{\partial^{2}\psi}{\partial r^{2}} - \frac{2\delta^{3}L^{3}\alpha_{0}}{(r+L)^{4}} \frac{\partial\psi}{\partial x} \frac{\partial^{2}\psi}{\partial x^{2}} \\ + \frac{\delta^{3}L^{3}\alpha_{0}}{(r+L)^{3}} \frac{\partial\psi}{\partial x} \frac{\partial^{3}\psi}{\partial r\partial x^{2}} + \frac{\delta^{3}L^{3}\alpha_{0}}{(r+L)^{3}} \left(1 - \frac{\partial\psi}{\partial r}\right) \frac{\partial^{3}\psi}{\partial x^{3}} + \frac{\delta L\alpha_{0}}{(r+L)^{2}} \frac{\partial\psi}{\partial x} \frac{\partial^{2}\psi}{\partial x^{2}} \\ + \frac{\delta k\alpha_{0}}{(r+L)^{3}} \frac{\partial\psi}{\partial x} \left(1 - \frac{\partial\psi}{\partial r}\right) + \frac{\delta L\alpha_{0}}{(r+L)^{2}} \frac{\partial^{2}\psi}{\partial r\partial x} \left(1 - \frac{\partial\psi}{\partial r}\right) \\ - \frac{\delta L\alpha_{0}}{r+L} \frac{\partial\psi}{\partial x} \frac{\partial^{3}\psi}{\partial r^{3}} - \frac{\delta L\alpha_{0}}{r+L} \left(1 - \frac{\partial\psi}{\partial r}\right) \frac{\partial^{3}\psi}{\partial x^{2}\partial r} \end{bmatrix},$$

$$(3.20)$$

$$\tau_{xx}^* = \frac{\delta}{(1+\lambda_2)} \left[ -2\alpha_0 \delta \left( \frac{2L^2}{(r+L)^4} \left( \frac{\partial \psi}{\partial x} \right)^2 - \frac{2L^2}{(r+L)^3} \frac{\partial \psi}{\partial x} \frac{\partial^2 \psi}{\partial r \partial x} + \left( \frac{L}{r+L} \right)^2 \frac{\partial \psi}{\partial x} \frac{\partial^3 \psi}{\partial r^2 \partial x} \right) \right].$$

$$-2\alpha_0 \delta^2 \left( 1 - \frac{\partial \psi}{\partial r} \right) \left( -\frac{L^2}{(r+L)^3} \frac{\partial^2 \psi}{\partial x^2} + \left( \frac{L}{r+L} \right)^2 \frac{\partial^3 \psi}{\partial r \partial x^2} \right)$$

$$(3.21)$$

The walls in dimensionless form are

$$r = \pm h = \pm (1 + \varphi \sin(x)),$$
 (3.22)

with boundary conditions

$$\psi = \frac{F}{2}, \quad \varphi = \frac{E}{2}, \quad \frac{\partial \psi}{\partial r} = 1, \quad \text{at } r = h,$$
 (3.23)

$$\psi = -\frac{F}{2}$$
,  $\varphi = -\frac{E}{2}$ ,  $\frac{\partial \psi}{\partial r} = 1$ , at  $r = -h$ . (3.24)

### 3.2 Method of Solution

For low Reynolds number and small wave number, the momentum equation (3.17) for fluid particles becomes

$$\left(\delta \frac{\partial^2}{\partial r \partial x} + \frac{\delta}{r+L} \frac{\partial}{\partial x}\right) \tau_{xx}^* + \left[\frac{\partial}{\partial r} \left(\frac{1}{L(L+r)} \frac{\partial}{\partial r} (r+L)^2\right) - \frac{\delta^2 L}{r+L} \frac{\partial^2}{\partial x^2}\right] \tau_{xr}^*$$

$$-\frac{\delta}{r+L}\frac{\partial^{2}}{\partial r\partial x}\left[(L+r)\tau_{rr}^{*}\right] + A\begin{bmatrix} \left(\frac{r+L}{L}\frac{\partial^{2}}{\partial r^{2}} + \frac{1}{L}\frac{\partial}{\partial r} + \delta^{2}\frac{\partial^{2}}{\partial x^{2}}\right)\psi\\ -\left(\frac{r+L}{L}\frac{\partial^{2}}{\partial r^{2}} + \frac{1}{L}\frac{\partial}{\partial r} + \delta^{2}\frac{\partial^{2}}{\partial x^{2}}\right)\varphi \end{bmatrix} = 0.$$
(3.25)

Perturbation method has been utilized to find the solution of the problem. The stream functions  $\psi$  and  $\varphi$ , E and F are expanded in terms of  $\delta$  as

$$\psi = \psi_0 + \delta \psi_1 + O(\delta^2), \tag{3.26}$$

$$\varphi = \varphi_0 + \delta \varphi_1 + O(\delta^2), \tag{3.27}$$

$$F = F_0 + \delta F_1 + O(\delta^2), \quad E = E_0 + \delta E_1 + O(\delta^2). \tag{3.28}$$

#### 3.2.1 Zeroth Order System

$$\left[\frac{\partial}{\partial r} \left(\frac{1}{(r+L)L} \frac{\partial}{\partial r} (r+L)^2\right)\right] \tau_{0xr}^* + A \begin{bmatrix} \left(\frac{r+L}{L} \frac{\partial^2}{\partial r^2} + \frac{1}{L} \frac{\partial}{\partial r}\right) \psi_0 \\ -\left(\frac{r+L}{L} \frac{\partial^2}{\partial r^2} + \frac{1}{L} \frac{\partial}{\partial r}\right) \varphi_0 \end{bmatrix} = 0, \tag{3.29}$$

$$B\left[\frac{1}{L}\left(\frac{\partial\varphi_0}{\partial r} - \frac{\partial\psi_0}{\partial r}\right) + \frac{r+L}{L}\left(\frac{\partial^2\varphi_0}{\partial r^2} - \frac{\partial^2\psi_0}{\partial r^2}\right)\right] = 0,$$
(3.30)

where

$$\tau_{0xr}^* = \frac{1}{(1+\lambda_2)} \left[ -\frac{1}{r+L} \left( 1 - \frac{\partial \psi_0}{\partial r} \right) - \frac{\partial^2 \psi_0}{\partial r^2} \right],\tag{3.31}$$

along with the boundary conditions

$$\psi_0 = -\frac{F_0}{2}, \quad \varphi_0 = -\frac{E_0}{2}, \quad \frac{\partial \psi_0}{\partial r} = 1 \quad \text{at } r = -h,$$
 (3.32)

$$\psi_0 = \frac{F_0}{2}, \quad \varphi_0 = \frac{E_0}{2}, \quad \frac{\partial \psi_0}{\partial r} = 1 \quad \text{at } r = h. \tag{3.33}$$

#### 3.2.2 First Order System

$$\left(\frac{\partial^2}{\partial r \partial x} + \frac{1}{r+L}\frac{\partial}{\partial x}\right)\tau_{0xx}^* + \left[\frac{\partial}{\partial r}\left(\frac{1}{(r+L)L}\frac{\partial}{\partial r}(r+L)^2\right)\right]\tau_{1xr}^*$$

$$-\frac{1}{r+k}\frac{\partial^{2}}{\partial r\partial x}\left[(L+r)\tau_{0rr}^{*}\right] + A\begin{bmatrix} \left(\frac{r+L}{L}\frac{\partial^{2}}{\partial r^{2}} + \frac{1}{L}\frac{\partial}{\partial r}\right)\psi_{1} \\ -\left(\frac{r+L}{L}\frac{\partial^{2}}{\partial r^{2}} + \frac{1}{L}\frac{\partial}{\partial r}\right)\varphi_{1} \end{bmatrix} = 0, \tag{3.34}$$

$$\begin{bmatrix} \frac{1}{L}\frac{\partial^{2}\varphi_{0}}{\partial r\partial x} - \frac{1}{r+L}\frac{\partial\varphi_{0}}{\partial x}\frac{\partial^{2}\varphi_{0}}{\partial r^{2}} + \frac{1}{(r+L)^{2}}\left(1 - \frac{\partial\varphi_{0}}{\partial r}\right)\frac{\partial\varphi_{0}}{\partial x} - \frac{1}{L+r}\left(1 - \frac{\partial\varphi_{0}}{\partial r}\right)\frac{\partial^{2}\varphi_{0}}{\partial r\partial x} \\ + \frac{L+r}{L}\frac{\partial^{3}\varphi_{0}}{\partial r^{2}\partial x} - \frac{\partial\varphi_{0}}{\partial x}\frac{\partial^{3}\varphi_{0}}{\partial r^{3}} - \frac{L+r}{L}\left(1 - \frac{\partial\varphi_{0}}{\partial r}\right)\frac{\partial}{\partial r}\left(-\frac{L}{(r+L)^{2}}\frac{\partial\varphi_{0}}{\partial x} + \frac{L}{r+L}\frac{\partial^{2}\varphi_{0}}{\partial r\partial x}\right) \\ - \frac{2}{L}\left(1 - \frac{\partial\varphi_{0}}{\partial r}\right)\frac{\partial^{2}\varphi_{0}}{\partial r\partial x} \end{bmatrix} =$$

$$B \begin{bmatrix} \left(\frac{r+L}{L}\frac{\partial^2}{\partial r^2} + \frac{1}{L}\frac{\partial}{\partial r}\right)\varphi_1 \\ -\left(\frac{r+L}{L}\frac{\partial^2}{\partial r^2} + \frac{1}{L}\frac{\partial}{\partial r}\right)\psi_1 \end{bmatrix}, \tag{3.35}$$

where

$$\tau_{0xx}^* = 0, \quad \tau_{0rr}^* = 0,$$

$$\tau_{1xr}^* = \frac{1}{(1+\lambda_2)} \left[ -\frac{1}{r+L} \left( 1 - \frac{\partial \psi_1}{\partial r} \right) - \frac{\partial^2 \psi_1}{\partial r^2} + \frac{L\alpha_0}{(r+L)^2} \frac{\partial \psi_0}{\partial x} \frac{\partial^2 \psi_0}{\partial x^2} + \frac{L\alpha_0}{(r+L)^3} \frac{\partial \psi_0}{\partial x} \left( 1 - \frac{\partial \psi_0}{\partial r} \right) + \frac{L\alpha_0}{(r+L)^2} \frac{\partial^2 \psi_0}{\partial r \partial x} \left( 1 - \frac{\partial \psi_0}{\partial r} \right) - \frac{L\alpha_0}{r+L} \frac{\partial \psi_0}{\partial x} \frac{\partial^3 \psi_0}{\partial r^3} - \frac{L\alpha_0}{r+L} \left( 1 - \frac{\partial \psi_0}{\partial r} \right) \frac{\partial^3 \psi_0}{\partial x^2 \partial r} \right],$$
(3.36)

along with the boundary conditions

$$\psi_1 = -\frac{F_1}{2}, \quad \varphi_1 = -\frac{E_1}{2}, \quad \frac{\partial \psi_1}{\partial r} = 0 \quad \text{at } r = -h,$$
 (3.37)

$$\psi_1 = \frac{F_1}{2}, \, \varphi_1 = \frac{E_1}{2}, \, \frac{\partial \psi_1}{\partial r} = 0 \quad \text{at } r = h.$$
 (3.38)

The solution of above system of equations are calculated by applying DSolver in Mathematica.

### 3.3 Graphical Analysis

Graphical demonstration of various parameters on velocity profile and stream functions will be discussed in this section. The establishment of an internally circulating bolus of fluid by closed stream lines is called trapping and this is pushed along with the peristaltic wave.

#### 3.3.1 Analysis of Stream Lines

In the Figs. 3.2 to 3.4 streamline graphs have been drawn for different values of curvature L, retardation time  $\alpha_0$ , and wave number  $\delta$  and behavior of bolus has been discussed. In Fig. 3.2, streamline graphs are drawn for different values of L. This figure indicates that bolus moves towards left by increasing curvature L of the channel. Fig. 3.3 shows that size of bolus increases as wave number increases. Effect of retardation time can be seen in Fig. 3.4. It shows that significant increase in retardation time moves bolus towards left.

#### 3.3.2 Fluid Flow Analysis

Impact of curvature L, relaxation time  $\lambda_2$ , retardation time  $\alpha_0$ , and wavenumber  $\delta$  on fluid velocity can be seen in Figs. 3.5 to 3.8. In Fig. 3.5, velocity profile is plotted for different values of retardation time  $\alpha_0$ . It is depicted that velocity increases by increasing  $\alpha_0$ . In Fig. 3.6, fluid velocity graph is plotted for different values of relaxation time  $\lambda_2$ . It is observed that by increasing relaxation time  $\lambda_2$ , fluid velocity decreases. This specifies more time is required by the fluid particles to derive back to the equilibrium condition from perturbed condition. In Fig. 3.7, velocity graph is presented for varying values of wave number  $\delta$ . It portrays the enhanced behavior of velocity by increasing  $\delta$ . In Fig. 3.8, velocity graph is drawn for variation of curvature L. It indicates that fluid velocity is decayed by increasing curvature of channel. Velocity rises for straight channel in contrast with curved channel.

## 3.3.3 Particle Flow Analysis

Impact of curvature L, relaxation time  $\lambda_2$ , and retardation time  $\alpha_0$  on particle velocity can be observed in Figs. 3.9 to 3.11. In Fig. 3.9, dust particle velocity graph is plotted for different values

of retardation time  $\alpha$ . It is observed that by increasing  $\alpha_0$ , particle velocity decreases. In Fig. 3.10, velocity graph is presented for varying values of curvature L. It portrays the decreasing behavior of velocity by increasing curvature of the channel. In Fig. 3.11, velocity profile for dust particles is drawn for variation of relaxation time  $\lambda_2$ . It depicts that velocity declines by increasing  $\lambda_2$ .

#### 3.3.4 Pressure Gradient

Graphs of pressure gradient versus x are shown in Figs. 3.12-3.14 for different values of wave number  $\delta$ , relaxation time  $\lambda_2$ , and retardation time  $\alpha_0$ . In Fig. 3.12, pressure gradient graphs are drawn for different values of wave number  $\delta$ . Graphs of pressure gradient are plotted for various values of retardation time  $\alpha_0$  in Fig. 3.13. Influence of relaxation time  $\lambda_2$  on pressure gradient is graphically demonstrated in Fig. 3.14. The pressure gradient increases as relaxation time increases. The pressure gradient as produced by the peristaltic motion of the walls is closely associated to the azimuthal normal stress and shear stress which are both controlled by fluid's elasticity (see Eq. 3.13).

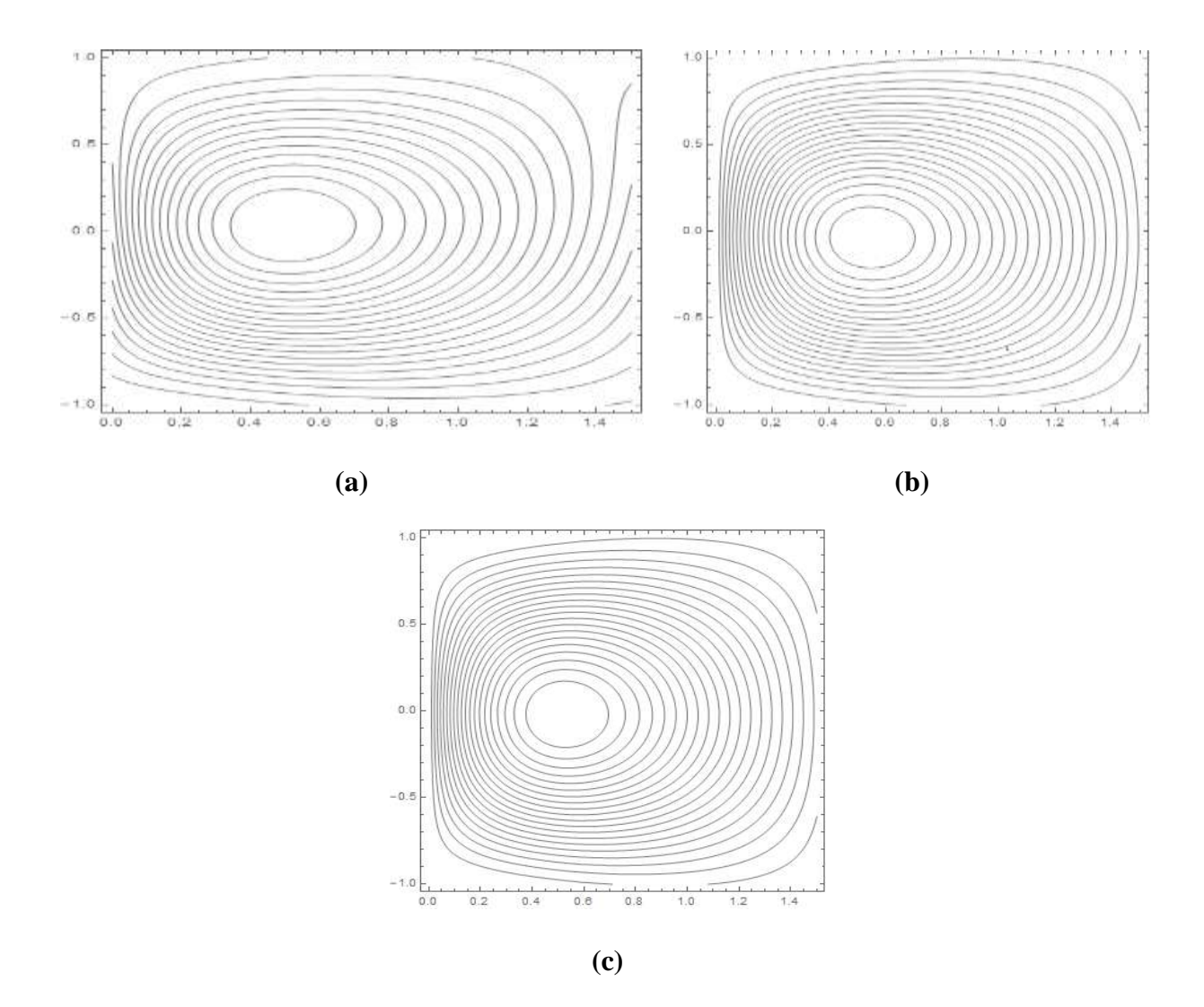


**Fig. 3.2:** Streamline presentation for fluid for (a) L = 4 (b) L = 10 (c) L = 20 with  $\mu = 0.1$ ,  $\alpha = 0.2$ , C = 0.3,  $\alpha_0 = 0.6$ ,  $\delta = 0.01$ ,  $\phi = 0.2$ , A = 0.2, B = 0.1,  $\lambda_2 = 0.4$ .

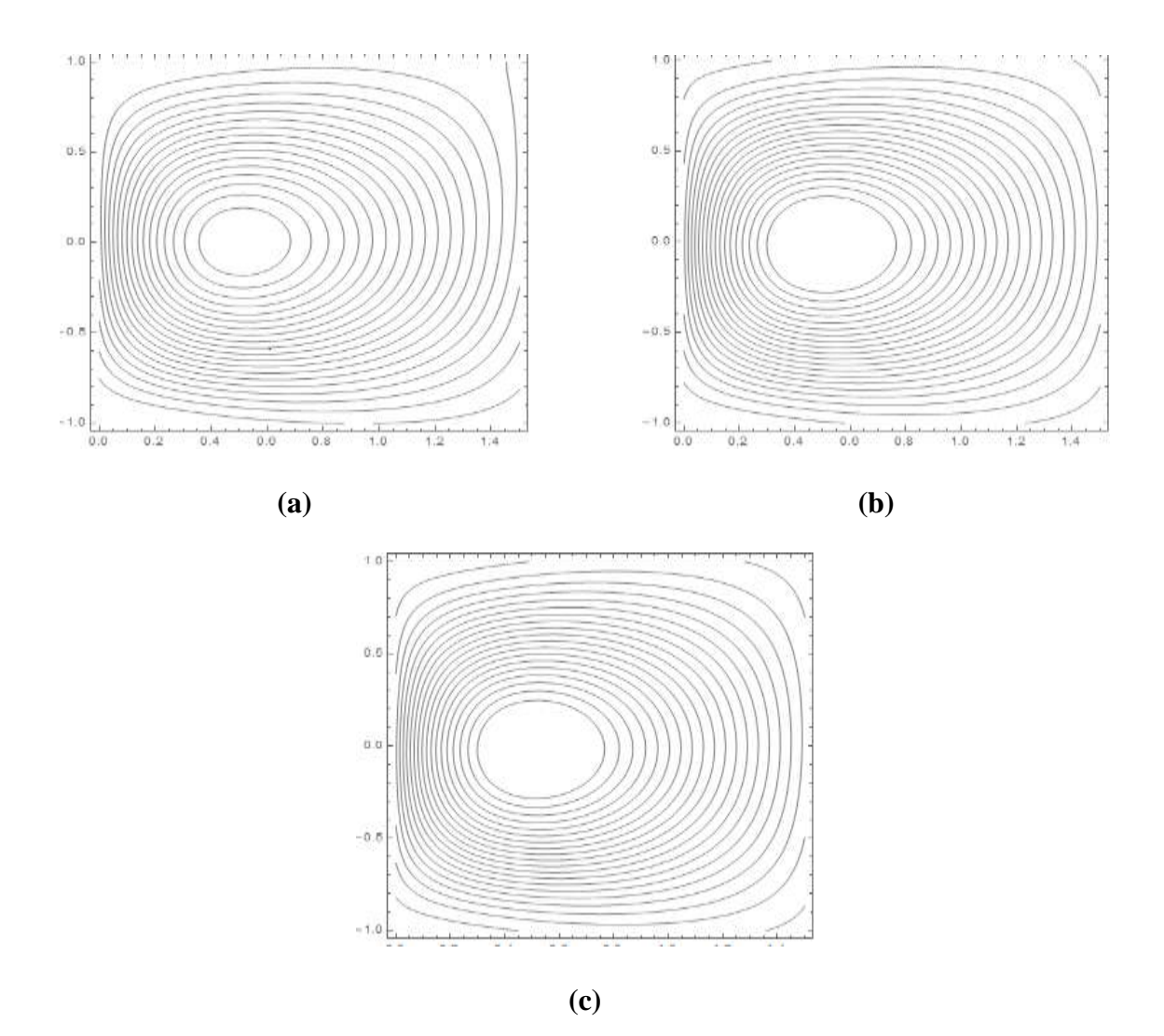


**Fig. 3.3:** Streamline presentation for fluid for (a)  $\delta = 0.02$  (b)  $\delta = 0.06$  (c)  $\delta = 0.09$  with  $L = 4, \mu = 0.1, \alpha = 0.2, C = 0.3, \alpha_0 = 0.6, \phi = 0.2, A = 0.2, B = 0.1, \lambda_2 = 0.4.$ 

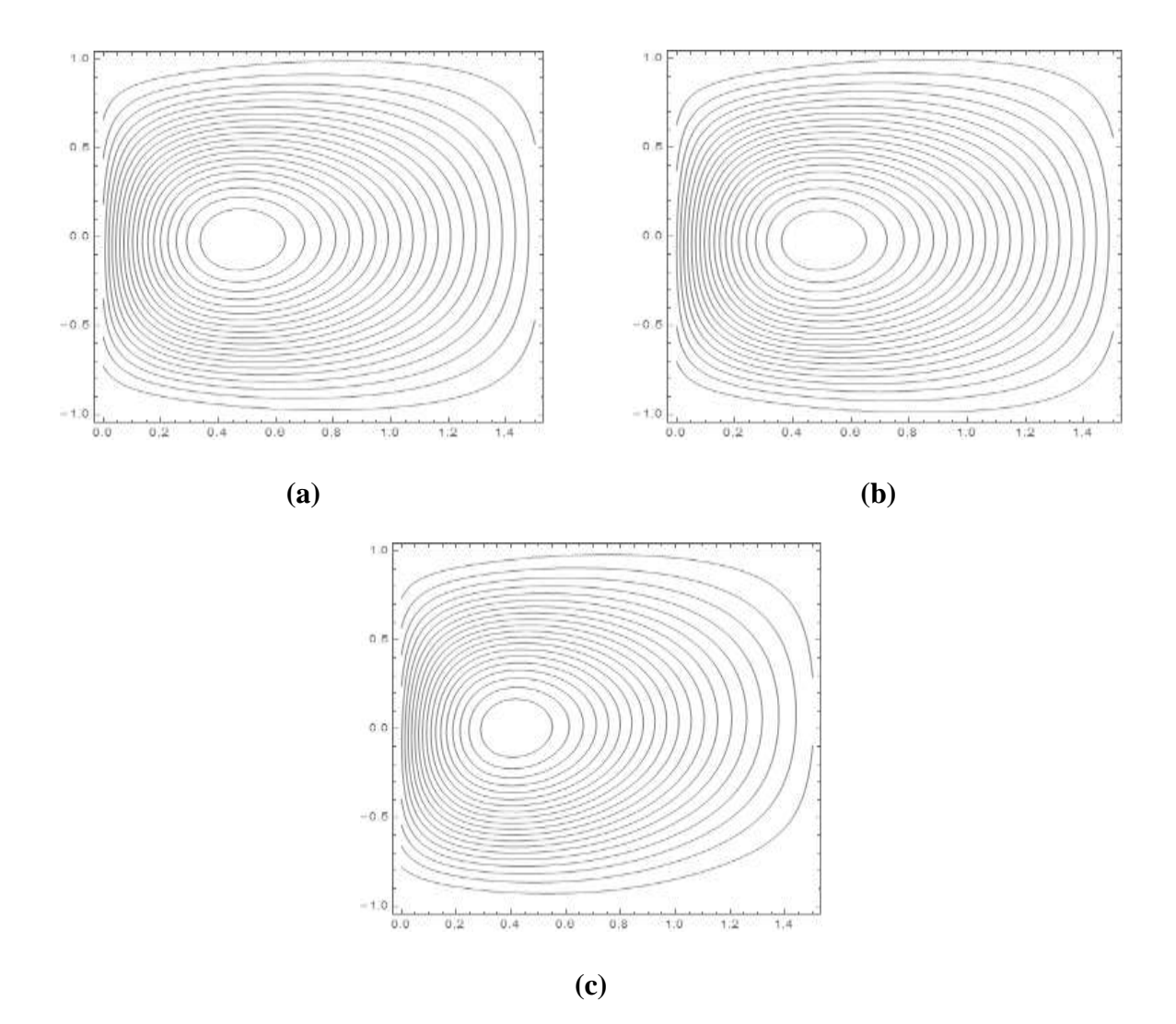


**Fig. 3.4:** Streamline presentation for fluid for (a)  $\alpha_0 = 60$  (b)  $\alpha_0 = 160$  (c)  $\alpha_0 = 360$  with  $\delta = 0.09$ , L = 4,  $\mu = 0.1$ ,  $\alpha = 0.2$ , C = 0.3,  $\phi = 0.2$ , A = 0.2, B = 0.1,  $\lambda_2 = 0.4$ .

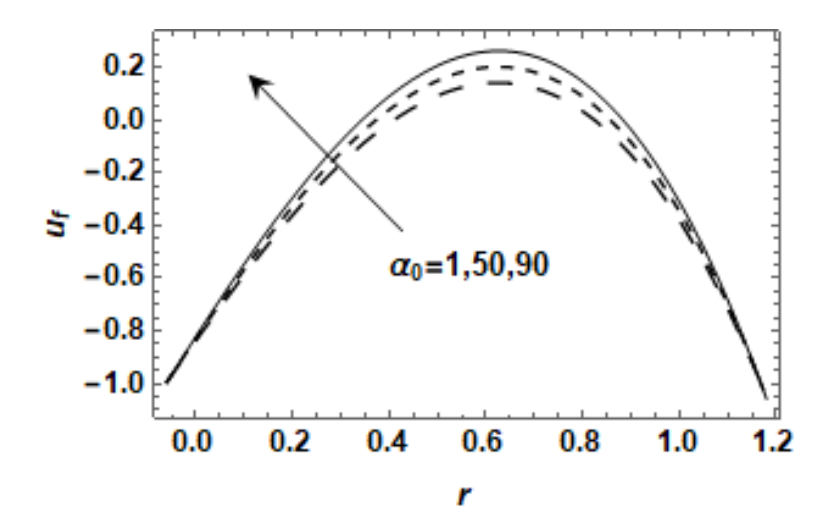


**Fig. 3.5:** The fluid velocity with  $\mu = 0.1$ ,  $\lambda_2 = 0.7$ , L = 4, a = 0.2, C = 0.3,  $\delta = 0.01$ ,  $\phi = 0.2$ , A = 0.2, B = 0.1.

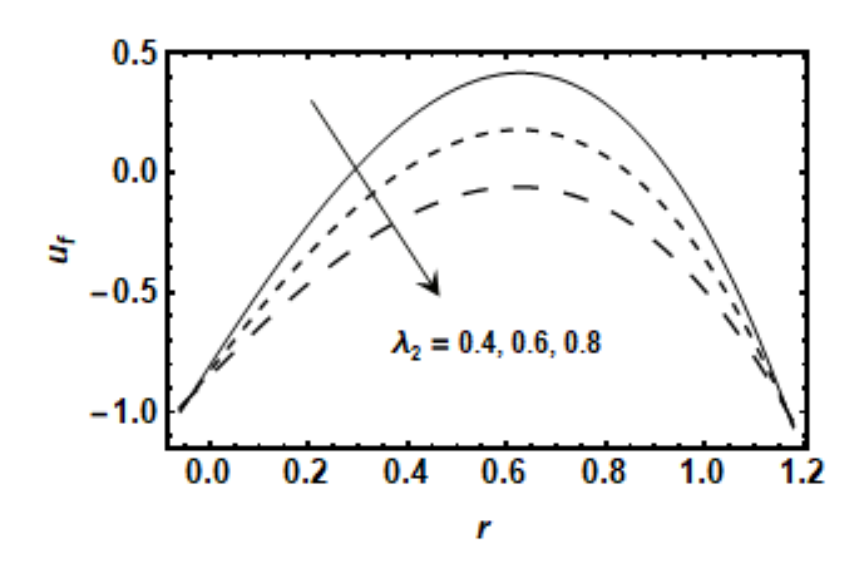


**Fig. 3.6:** The fluid velocity with  $\mu = 0.1$ , L = 4,  $\alpha = 0.2$ , C = 0.3,  $\alpha_0 = 0.2$ ,  $\delta = 0.01$ ,  $\phi = 0.2$ , A = 0.2, B = 0.1.

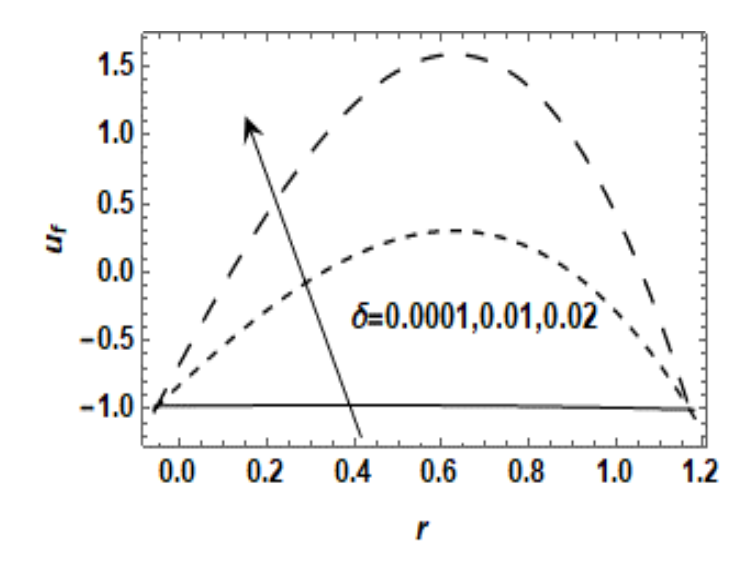


**Fig. 3.7:** The fluid velocity with  $\mu = 0.1$ ,  $\lambda_2 = 0.7$ ,  $\alpha = 0.2$ , C = 0.3,  $\alpha_0 = 0.2$ , L = 4,  $\phi = 0.2$ , A = 0.2, B = 0.1.

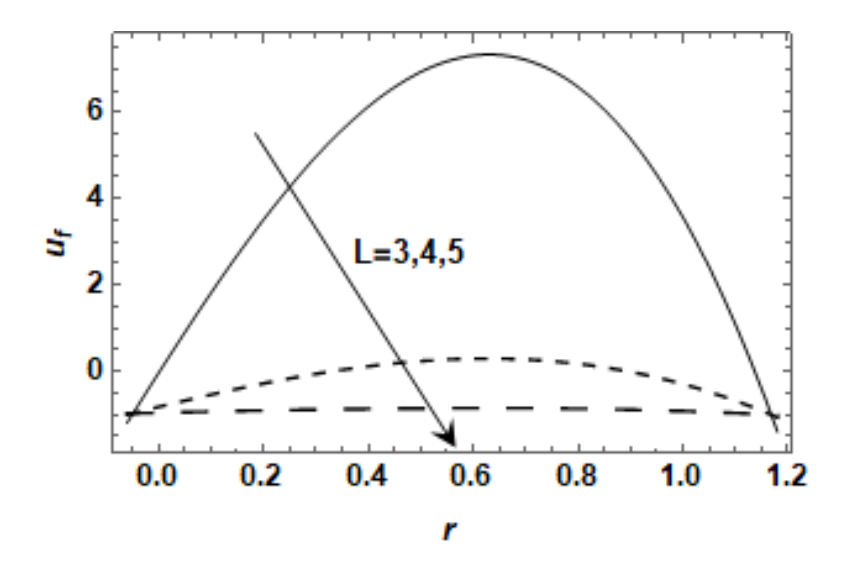


**Fig. 3.8:** The fluid velocity with  $\mu = 0.1$ ,  $\lambda_2 = 0.7$ ,  $\alpha_0 = 0.2$ , C = 0.3,  $\alpha = 0.2$ ,  $\delta = 0.01$ ,  $\phi = 0.2$ , A = 0.2, B = 0.1.

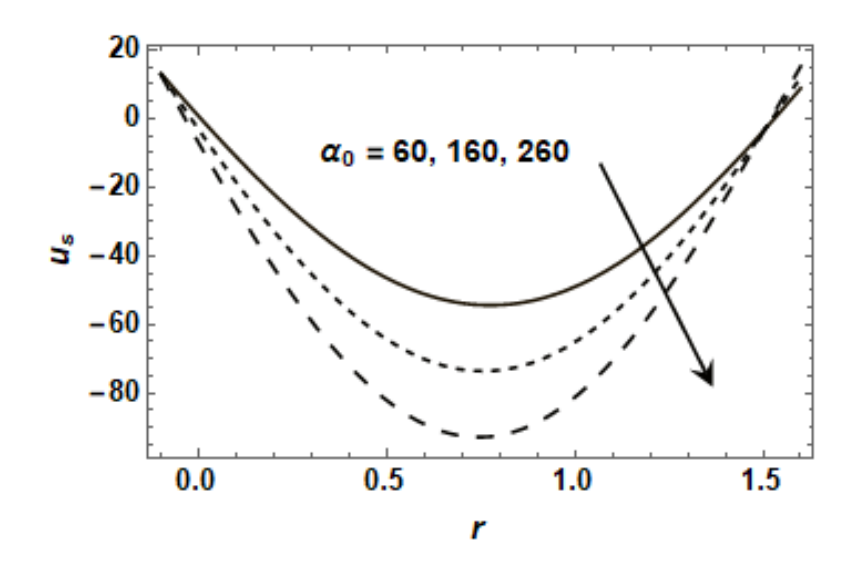


**Fig. 3.9:** The particle velocity with  $\mu = 0.1$ ,  $\lambda_2 = 0.3$ , L = 4, a = 0.2, C = 0.3,  $\delta = 0.05$ ,  $\phi = 0.6$ , A = 0.2, B = 0.4.

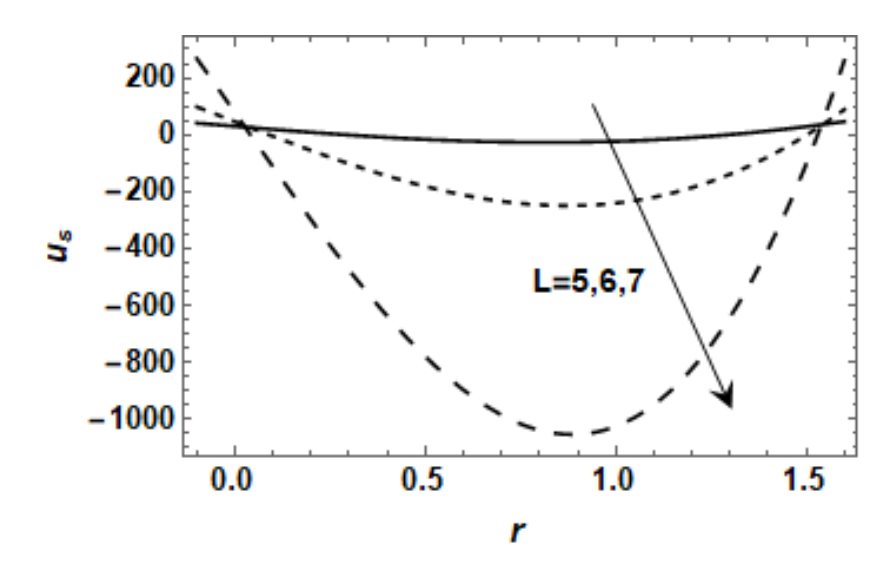


**Fig. 3.10:** The particle velocity with  $\mu = 0.1$ ,  $\lambda_2 = 0.3$ ,  $\alpha = 0.2$ , C = 0.3,  $\alpha_0 = 0.5$ ,  $\delta = 0.01$ ,  $\phi = 0.6$ , A = 0.2, B = 0.4.

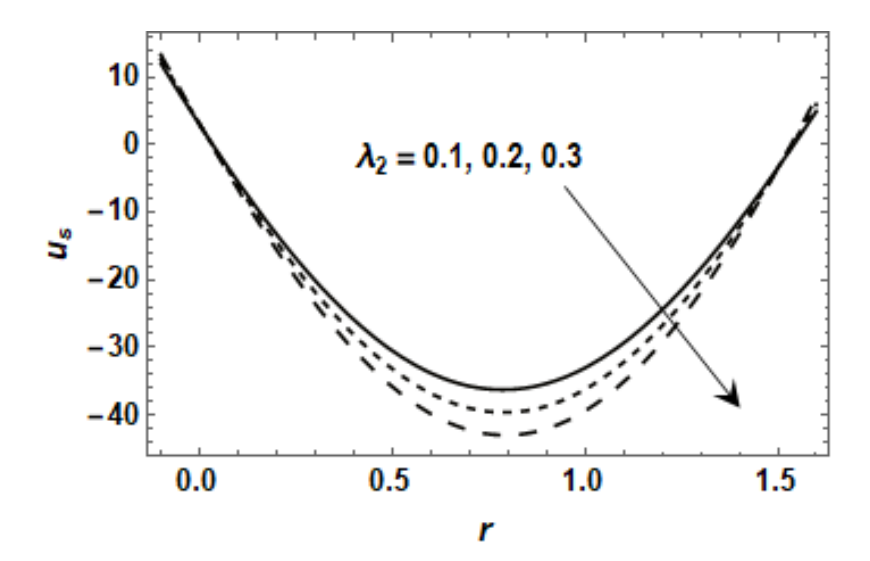


**Fig. 3.11:** The particle velocity with  $\mu = 0.1$ ,  $\alpha_0 = 0.5$ , L = 4, a = 0.2, C = 0.3,  $\delta = 0.05$ ,  $\phi = 0.6$ , A = 0.2, B = 0.4.

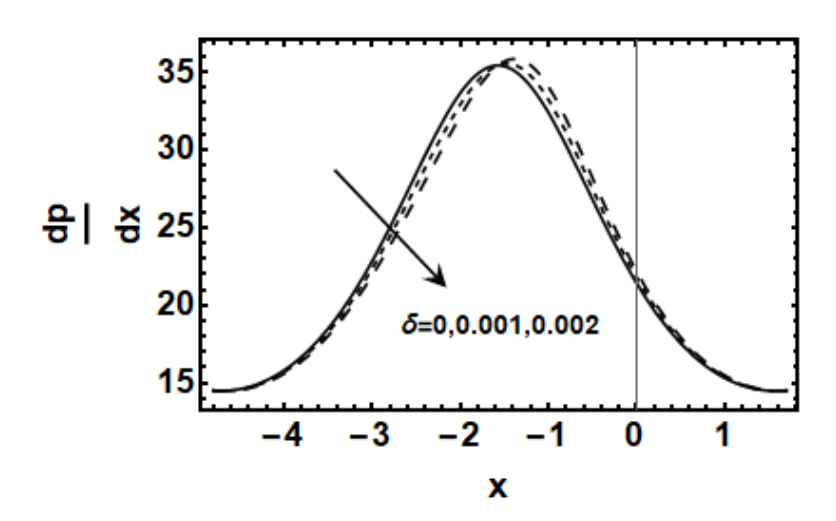


**Fig. 3.12:** Pressure gradient with  $\mu = 0.1$ , Re = 6,  $\lambda_2 = 0.1$ ,  $\alpha = 0.2$ , C = 0.8,  $\alpha_0 = 0.2$ , L = 2,  $\phi = 0.2$ , A = 0.2, B = 1.2, C = 0.2, D = 0

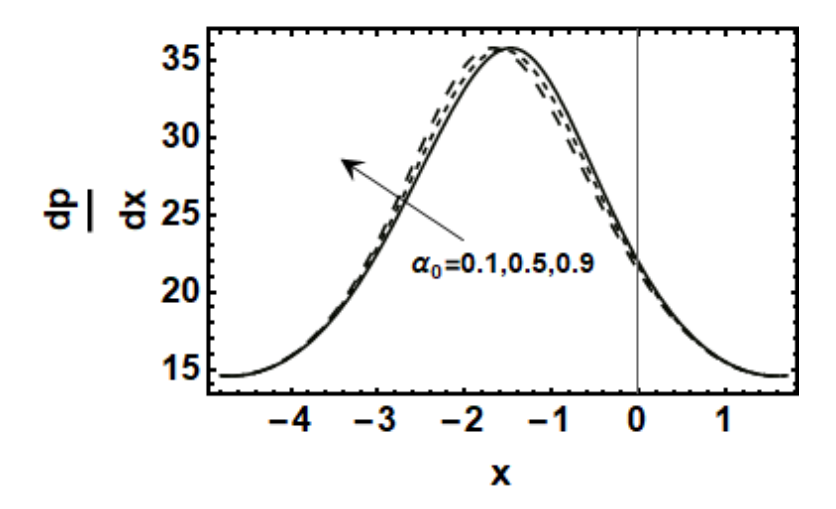
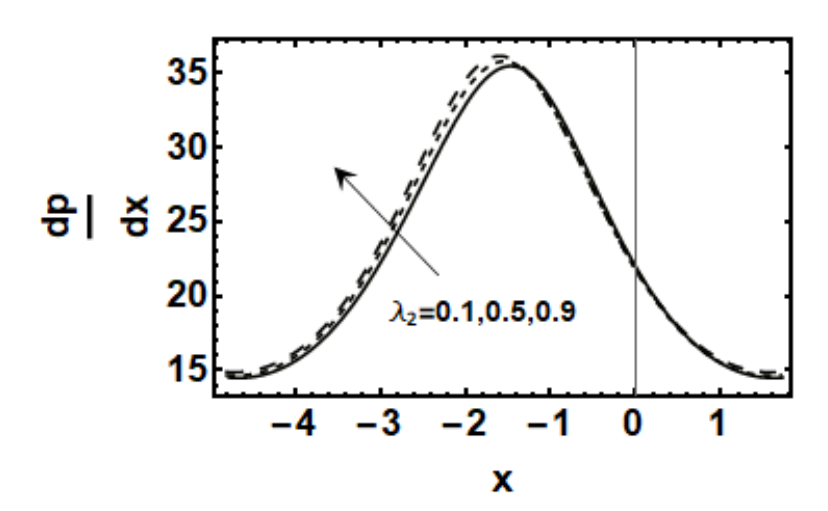


Fig. 3.13: Pressure gradient with  $\mu = 0.1$ , Re = 6,  $\lambda_2 = 0.3$ , a = 0.2, C = 0.8, L = 2,  $\delta = 0.001$ ,  $\phi = 0.2$ , A = 0.2, B = 1.2, C = 0.8, C = 0.8



**Fig. 3.14:** Pressure gradient with  $\mu = 0.1$ , Re = 6,  $\alpha_0 = 0.3$ ,  $\alpha = 0.2$ , C = 0.8, L = 2,  $\delta = 0.001$ ,  $\phi = 0.2$ , A = 0.2, B = 1.2, r = 2, Q = 1.

## 3.4 Conclusion

This chapter presents the analysis of peristaltic motion of dusty fluid following Jeffrey fluid model with curved boundary walls. Impacts of various parameters on stream function, fluid velocity, and particle velocity has been discussed graphically. Significant features of current analysis are:

- Size of bolus increases by increasing wave number.
- Significant increase in retardation time moves bolus towards left.
- Bolus moves toward left by increasing curvature.
- Fluid velocity decays by increasing curvature parameter, relaxation time.
- Particle velocity decays as retardation time, relaxation time and curvature increase.
- Pressure gradient enhances by increasing relaxation time.

# **Chapter 4**

# **Heat Transfer Analysis of**

Magnetohydrodynamics Peristaltic Fluid with

**Inhomogeneous Solid Particles and Variable** 

# **Thermal Conductivity through Curved**

# **Passageway**

In this chapter inhomogeneous dispersion of solid particles in Newtonian dusty fluid is considered. The fluid flows through wavy curved passage under applied magnetic field. Heat transfer is discussed with variable thermal conductivity. The mathematical model of the problem consists of coupled differential equations which are simplified using stream functions. The results of time flow rate for fluid and solid granules have been derived numerically. The fluid and dust particle velocity profiles are being presented graphically to analyze the effects of density of solid particles, magnetohydrodynamics, curvature, and slip parameters. Heat transfer analysis is also performed for magnetic parameter, density of dust particles, variable thermal conductivity, slip parameter, and curvature.

### 4.1 Problem Formulation

Consider the dusty viscous fluid flowing through a curved channel as shown in Fig. 3.1. The walls of channel undergo peristaltic movement. Solid particles are considered to be spherical in shape and their distribution in the fluid is not homogeneous. Thermal conductivity depends on temperature and applied magnetic field is considered in radial direction. The density of solid particles  $N(\bar{R})$  depends on  $\bar{R}$ . The passage is curled into a circle having center O and radius  $R^*$ . The sinusoidal wave is propelling along the walls with speed c and wavelength  $\lambda$ . The width of the curved channel is 2a and wave amplitude is b. The description of walls is expressed in Eqns. (3.1) and (3.2).

Fluid flow is described by the following equations.

#### 4.1.1 For Fluid Flow:

$$R^* \frac{\partial \overline{U}}{\partial \overline{X}} + \frac{\overline{V}}{(\overline{R} + R)} + (\overline{R} + R^*) \frac{\partial \overline{V}}{\partial \overline{R}} = 0, \tag{4.1}$$

$$\rho\left(\frac{\partial \overline{V}}{\partial t} + \overline{V}\frac{\partial \overline{V}}{\partial \bar{R}} + \frac{R^*}{\bar{R} + R^*}\overline{U}\frac{\partial \overline{V}}{\partial \bar{X}} - \frac{\overline{U}^2}{\bar{R} + R^*}\right) = -\frac{\partial \bar{P}}{\partial \bar{R}} + \mu\left(\frac{1}{\bar{R} + R^*}\frac{\partial}{\partial \bar{R}}\left[(\bar{R} + R^*)\frac{\partial \bar{V}}{\partial \bar{R}}\right] + \left(\frac{R^*}{\bar{R} + R^*}\right)^2\frac{\partial^2 \overline{V}}{\partial \bar{X}^2} - \frac{\overline{V}}{(\bar{R} + R^*)^2} - \frac{\bar{V}^2}{\bar{R} + R^*}\right)$$

$$2\frac{R}{(\bar{R}+R^*)^2}\frac{\partial \bar{U}}{\partial \bar{X}} + kN(\bar{R})(\bar{V}_S - \bar{V}), \tag{4.2}$$

$$\rho\left(\frac{\partial \overline{U}}{\partial t} + \overline{V}\frac{\partial \overline{U}}{\partial \overline{R}} + \frac{R^*}{\overline{R} + R^*}\overline{U}\frac{\partial \overline{U}}{\partial \overline{X}} + \frac{\overline{U}\overline{V}}{\overline{R} + R^*}\right) = -\frac{R^*}{\overline{R} + R^*}\frac{\partial \overline{P}}{\partial \overline{X}} + \mu\left(\frac{1}{\overline{R} + R^*}\frac{\partial}{\partial \overline{R}}\right]\left((\overline{R} + R^*)\frac{\partial \overline{U}}{\partial \overline{R}}\right) + \left(\frac{R^*}{\overline{R} + R^*}\right)^2\frac{\partial^2 \overline{U}}{\partial \overline{X}^2} - \frac{1}{\overline{R} + R^*}\frac{\partial \overline{U}}{\partial \overline{X}} + \frac{1}{\overline{R}$$

$$\frac{\overline{U}}{(\overline{R}+R^*)^2} - 2\frac{R^*}{(\overline{R}+R^*)^2}\frac{\partial \overline{V}}{\partial \overline{X}} + kN(\overline{R})(\overline{U}_S - \overline{U}) - \sigma B_0^2 \left(\frac{R^*}{\overline{R}+R^*}\right)^2 \overline{U}, \tag{4.3}$$

$$\rho C_{P} \left( \frac{\partial \overline{T}}{\partial t} + \overline{V} \frac{\partial \overline{T}}{\partial \overline{R}} + \frac{R^{*}}{\overline{R} + R^{*}} \overline{U} \frac{\partial \overline{T}}{\partial \overline{X}} \right) = -\nabla \cdot \left( -K(\overline{T}) \nabla \overline{T} \right) + \mu \left[ 2 \left( \frac{\partial \overline{V}}{\partial \overline{R}} \right)^{2} + \left( \frac{R^{*}}{\overline{R} + R^{*}} \frac{\partial \overline{V}}{\partial \overline{X}} - \frac{\overline{U}}{\overline{R} + R^{*}} \right) \left( \frac{\partial \overline{U}}{\partial \overline{R}} - \frac{\overline{U}}{\overline{R} + R^{*}} + \frac{\overline{U}}{\overline{R} + R^{*}} \right) \right] + \frac{\partial \overline{U}}{\partial \overline{R}} \left( \frac{\partial \overline{U}}{\partial \overline{R}} + \frac{R^{*}}{\overline{R} + R^{*}} \frac{\partial \overline{V}}{\partial \overline{X}} - \frac{\overline{U}}{\overline{R} + R^{*}} \right) + 2 \left( \frac{R^{*}}{\overline{R} + R^{*}} \frac{\partial \overline{U}}{\partial \overline{X}} + \frac{\overline{V}}{\overline{R} + R^{*}} \right)^{2} + \frac{NC_{P}}{\tau_{T}} (\overline{T}_{S} - \overline{T}) + \frac{N}{\tau_{V}} (\overline{U}_{S} - \overline{U})^{2},$$

$$(4.4)$$

where  $K(\overline{T})$  is thermal conductivity that depends on temperature. Mathematically it is described by [84] as

$$K(\overline{T}) = K_0 \left( 1 + \eta(\overline{T} - T_0) \right), \tag{4.5}$$

where  $K_0$  is constant thermal conductivity.

#### **4.1.2 For Solid Particles:**

$$R^* \frac{\partial \overline{U}_S}{\partial \overline{X}} + \frac{\overline{V}_S}{(\overline{R} + R^*)} + (\overline{R} + R^*) \frac{\partial \overline{V}_S}{\partial \overline{R}} = 0, \tag{4.6}$$

$$\left(\frac{\partial \bar{V}_S}{\partial t} + \bar{V}_S \frac{\partial \bar{V}_S}{\partial \bar{R}} + \frac{R^*}{\bar{R} + R^*} \bar{U}_S \frac{\partial \bar{V}_S}{\partial \bar{X}} - \frac{\bar{U}_S^2}{\bar{R} + R^*}\right) = \frac{k}{m} (\bar{V} - \bar{V}_S), \tag{4.7}$$

$$\left(\frac{\partial \overline{U}_S}{\partial t} + \overline{V}_S \frac{\partial \overline{U}_S}{\partial \overline{R}} + \frac{R^*}{\overline{R} + R^*} \overline{U}_S \frac{\partial \overline{U}_S}{\partial \overline{X}} + \frac{\overline{U}_S \overline{V}_S}{\overline{R} + R^*}\right) = \frac{k}{m} (\overline{U} - \overline{U}_S), \tag{4.8}$$

$$\left(\frac{\partial \bar{T}_S}{\partial t} + \bar{V}_S \frac{\partial \bar{T}_S}{\partial \bar{R}} + \frac{R^*}{\bar{R} + R^*} \bar{U}_S \frac{\partial \bar{T}_S}{\partial \bar{X}}\right) = -\frac{C_P}{C_m} (\bar{T} - \bar{T}_S). \tag{4.9}$$

Fixed frame coordinates  $(\bar{R}, \bar{X})$  are related to moving frame coordinates (r, x) by

$$\overline{X} = x + ct, \overline{R} = r, \overline{U} = u + c, \overline{V} = v, \overline{U}_S = u_S + c, \overline{V}_S = v_S, \overline{T} = T, \overline{T}_S = T_S, \overline{P} = P.$$
 (4.10)

The dimensionless quantities and stream functions are given by:

$$r' = \frac{r}{a}, \quad x' = \frac{x}{\lambda}, \quad u' = \frac{u}{c}, \quad v' = \frac{v}{\delta c}, \quad u'_{S} = \frac{u_{S}}{c}, \quad v'_{S} = \frac{v_{S}}{\delta c}, \quad P = \frac{p\lambda\mu c}{a^{2}}, \quad \Theta = \frac{T-T_{0}}{T_{1}-T_{0}}, \quad \Theta_{S} = \frac{T_{S}-T_{0}}{T_{1}-T_{0}},$$

$$u = -\frac{\partial\psi}{\partial r}, \quad v = -\frac{L}{r+L}\frac{\partial\psi}{\partial x}, \quad u_{S} = -\frac{\partial\varphi}{\partial r}, \quad v_{S} = -\frac{L}{r+L}\frac{\partial\varphi}{\partial x}, \quad \delta = \frac{a}{\lambda}, \quad L = \frac{R^{*}}{a}, \quad Re = \frac{\rho ca}{u}, \quad A = \frac{kNa^{2}}{u},$$

$$B = \frac{ka}{mc'} \text{ MHD}(M^2) = \frac{\sigma B_0^2 a^2}{\mu}, Pr = \frac{\mu C_P}{K_0}, Ec = \frac{c^2}{C_P(T - T_0)}, A_1 = \frac{N_0 a^2}{\tau_T \mu}, B_1 = \frac{N_0 a^2}{\tau_u \mu}, \gamma = \frac{a C_P}{c C_m},$$

$$N(r') = \frac{N(r)}{N_0}.$$
(4.11)

where  $A, B, \alpha, \beta$  and  $\gamma$  are dimensionless quantities. To study non-uniform distribution of solid particles, density of solid particles in dimensionless form is described in [40] as

$$N(\bar{R}) = e^{-\omega r} = 1 - \omega r. \tag{4.12}$$

Using Eqs. (4.11) and (4.12), the equations of compatibility for fluid and dust particles are

$$\begin{split} Re\delta\left(\frac{1}{L}\frac{\partial^2\psi}{\partial r\partial x} + \frac{(r+L)}{L}\frac{\partial^3\psi}{\partial r^2\partial x} - \frac{\partial^2\psi}{\partial x^2}\frac{\partial^2\psi}{\partial r^2} - \frac{\partial\psi}{\partial x}\frac{\partial^3\psi}{\partial r^3} - \frac{\partial^2\psi}{\partial r^2}\frac{\partial^2\psi}{\partial r\partial x} - \frac{\partial^3\psi}{\partial r^2\partial x}\left(1 - \frac{\partial\psi}{\partial r}\right) - \frac{1}{r+L}\frac{\partial\psi}{\partial x}\frac{\partial^2\psi}{\partial r^2} + \\ \frac{1}{r+L}\frac{\partial^2\psi}{\partial x^2}\left(1 - \frac{\partial\psi}{\partial r}\right) - \frac{1}{(r+L)^2}\frac{\partial\psi}{\partial x}\left(1 - \frac{\partial\psi}{\partial r}\right) - \frac{L}{r+L}\frac{\partial^3\psi}{\partial x^3} + \frac{L}{(r+L)^2}\left(\frac{\partial^2\psi}{\partial x^2}\right)^2 - \delta^2\left(-2\frac{L^2}{(r+L)^3}\frac{\partial\psi}{\partial x}\frac{\partial^2\psi}{\partial x^2} + \frac{L^2}{(r+L)^2}\frac{\partial\psi}{\partial x}\frac{\partial^2\psi}{\partial x^2} + \frac{L^2}{(r+L)^2}\frac{\partial^3\psi}{\partial x^3}\left(1 - \frac{\partial\psi}{\partial r}\right) + \frac{2}{r+L}\left(1 - \frac{\partial\psi}{\partial r}\right)\frac{\partial^2\psi}{\partial r\partial x}\right)\right) = -\frac{1}{L}\frac{\partial^2}{\partial r^2}\left(r + L\right)\frac{\partial^2\psi}{\partial r^2}\right) + \frac{1}{(r+L)^2}\left(1 - \frac{\partial\psi}{\partial r}\right) + \frac{1}{L(r+L)}\frac{\partial^2\psi}{\partial r^2} + \delta^2\left(-\frac{L}{r+L}\frac{\partial^4\psi}{\partial r^2\partial x^2} + 3\frac{L}{(r+L)^2}\frac{\partial^3\psi}{\partial r^2\partial x} - 3\frac{L}{(r+L)^3}\frac{\partial^2\psi}{\partial x^2} + \frac{2}{r+L}\frac{\partial\psi}{\partial r}\right)\right) - \delta^4\frac{L}{r+L}\frac{\partial\psi}{\partial x} + M^2\frac{\partial}{\partial r}\left(\frac{L^2}{r+L}\frac{\partial\psi}{\partial r}\right) - \\ A\left(\frac{\partial}{\partial r}\left\{\frac{(r+L)}{L}\left(1 - \omega r\right)\left(\frac{\partial\varphi}{\partial r} - \frac{\partial\psi}{\partial r}\right)\right\} + \delta^2\left(1 - \omega r\right)\frac{L}{r+L}\frac{\partial^2}{\partial x^2}\left(\varphi - \psi\right)\right), \end{aligned} \tag{4.13}$$

$$\frac{L^2}{(r+L)^2} \left(\frac{\partial^2 \varphi}{\partial x^2}\right)^2 - \frac{L^2}{(r+L)^3} \frac{\partial \varphi}{\partial x} \frac{\partial^2 \varphi}{\partial x^2} + \left(\frac{L}{r+L}\right)^2 \frac{\partial \varphi}{\partial x} \frac{\partial^3 \varphi}{\partial r \partial x^2} - \left(\frac{L}{r+L}\right)^2 \frac{\partial^2 \varphi}{\partial r \partial x} \frac{\partial^2 \varphi}{\partial x^2} + \left(\frac{L}{r+L}\right)^2 \frac{\partial^3 \varphi}{\partial x^3} \left(1 - \frac{\partial \varphi}{\partial r}\right) + \frac{\partial^2 \varphi}{\partial x^2} \frac{\partial^2 \varphi}{\partial x^2} +$$

$$\frac{2}{r+L}\frac{\partial^{2}\varphi}{\partial r\partial x}\left(1-\frac{\partial\varphi}{\partial r}\right)\right) = B\left(\frac{(r+L)}{L}\left(\frac{\partial^{2}\varphi}{\partial r^{2}}-\frac{\partial^{2}\psi}{\partial r^{2}}\right)+\frac{1}{L}\left(\frac{\partial\varphi}{\partial r}-\frac{\partial\psi}{\partial r}\right)-\frac{L}{r+L}\delta^{2}\frac{\partial^{2}}{\partial x^{2}}\left(\psi-\varphi\right)\right). \tag{4.14}$$

The non-dimensional energy equations for fluid and solid particles are:

$$\delta\left[-\frac{\partial\Theta}{\partial x} + \frac{L}{r+L}\frac{\partial\psi}{\partial x}\frac{\partial\Theta}{\partial r} + \frac{L}{r+L}\left(1 - \frac{\partial\psi}{\partial r}\right)\frac{\partial\Theta}{\partial x}\right] = (1 + \eta\Theta)\left\{\frac{\partial^2\Theta}{\partial r^2} + \frac{1}{r+L}\frac{\partial\Theta}{\partial r}\right\} + \eta\left(\frac{\partial\Theta}{\partial r}\right)^2 + \delta^2\left(\frac{L}{r+L}\right)^2\left\{(1 + \eta\Theta)\left(\frac{\partial^2\Theta}{\partial r}\right) + \frac{1}{r+L}\frac{\partial\Theta}{\partial r}\right\}\right\}$$

$$\eta\Theta\left(\frac{\partial^{2}\Theta}{\partial x^{2}}\right) + \eta\left(\frac{\partial\Theta}{\partial x}\right)^{2} + Br\left(2\delta^{2}\left(\frac{\partial}{\partial r}\left(\frac{1}{r+L}\frac{\partial\psi}{\partial x}\right)\right)^{2} + 2\delta^{2}\left(\frac{L}{r+L}\frac{\partial^{2}\psi}{\partial r\partial x} + \frac{L}{(r+L)^{2}}\frac{\partial\psi}{\partial x}\right)^{2} + \left(\delta^{2}\left(\frac{L}{r+L}\right)^{2}\frac{\partial^{2}\psi}{\partial x^{2}} - \frac{1}{r+L}\left(1 - \frac{\partial\psi}{\partial r}\right) - \frac{\partial^{2}\psi}{\partial r^{2}}\right)^{2}\right) + A_{1}\Pr(1 - \frac{\partial\psi}{\partial r}) + A_{2}\Pr(1 - \frac{\partial\psi}{\partial r}) + A_{3}\Pr(1 - \frac{\partial\psi}{\partial r}) + A_{4}\Pr(1 - \frac{\partial\psi}{\partial r}) + A_{5}\Pr(1 - \frac{\partial\psi}{$$

$$\omega r)(\Theta_s - \Theta) + B_1 B r (1 - \omega r) \left(\frac{\partial \varphi}{\partial r} - \frac{\partial \psi}{\partial r}\right)^2, \tag{4.15}$$

$$\delta\left[-\frac{\partial\Theta_{S}}{\partial x} + \frac{L}{r+L}\frac{\partial\varphi}{\partial x}\frac{\partial\Theta_{S}}{\partial r} + \frac{L}{r+L}\left(1 - \frac{\partial\varphi}{\partial r}\right)\frac{\partial\Theta_{S}}{\partial x}\right] = -\gamma(\Theta_{S} - \Theta). \tag{4.16}$$

The non-dimensional form of boundaries of the passage are given by the Eqn. (3.22).

## 4.2 Method of Solution

Under the assumption of long wavelength and low Reynolds number, Eqns. (4.13) to (4.16) become

$$\frac{\partial^{2}}{\partial r^{2}} \left( (r+L) \frac{\partial^{2} \psi}{\partial r^{2}} \right) - \frac{1}{(r+L)^{2}} \left( 1 - \frac{\partial \psi}{\partial r} \right) - \frac{1}{(r+L)} \frac{\partial^{2} \psi}{\partial r^{2}} + A \frac{\partial}{\partial r} \left\{ (r+L)(1-\omega r) \left( \frac{\partial \varphi}{\partial r} - \frac{\partial \psi}{\partial r} \right) \right\} - M^{2} \frac{\partial}{\partial r} \left( \frac{L^{2}}{r+L} \frac{\partial \psi}{\partial r} \right) = 0,$$
(4.17)

$$(r+L)\left(\frac{\partial^2 \varphi}{\partial r^2} - \frac{\partial^2 \psi}{\partial r^2}\right) + \left(\frac{\partial \varphi}{\partial r} - \frac{\partial \psi}{\partial r}\right) = 0. \tag{4.18}$$

$$(1+\eta\Theta)\left\{\frac{\partial^2\Theta}{\partial r^2} + \frac{1}{r+L}\frac{\partial\Theta}{\partial r}\right\} + \eta\left(\frac{\partial\Theta}{\partial r}\right)^2 + Br\left(\frac{1}{r+L}\left(1-\frac{\partial\psi}{\partial r}\right) + \frac{\partial^2\psi}{\partial r^2}\right)^2 + A_1\Pr(1-\omega r)(\Theta_s-\Theta) + \frac{\partial^2\Psi}{\partial r^2}\left(\frac{\partial\Psi}{\partial r}\right)^2 + \frac{\partial\Psi}{\partial r}\left(\frac{\partial\Psi}{\partial r}\right)^2 + \frac{\partial\Psi}{\partial r}\left($$

$$B_1 Br(1 - \omega r) \left(\frac{\partial \varphi}{\partial r} - \frac{\partial \psi}{\partial r}\right)^2 = 0, \tag{4.19}$$

$$\Theta_s - \Theta = 0. (4.20)$$

Non-dimensional boundary conditions are

$$\psi = \frac{F}{2}, \quad \varphi = \frac{E}{2}, \quad \frac{\partial \psi}{\partial r} + \beta \frac{\partial^2 \psi}{\partial r^2} = -1, \quad \text{at } r = h,$$
 (4.21)

$$\psi = -\frac{F}{2}$$
,  $\varphi = -\frac{E}{2}$ ,  $\frac{\partial \psi}{\partial r} - \beta \frac{\partial^2 \psi}{\partial r^2} = -1$ , at  $r = -h$ , (4.22)

$$\Theta = 1 \quad \text{at } r = h, \tag{4.23}$$

$$\Theta = 0 \quad \text{at } r = -h, \tag{4.24}$$

$$\Theta_s = 1 \qquad \text{at } r = h, \tag{4.25}$$

$$\Theta_s = 0 \qquad \text{at } r = -h. \tag{4.26}$$

The non-dimensional form of heat transfer rate is

$$z = \frac{\partial \Theta}{\partial r} \, \frac{\partial h}{\partial x}.$$

This leads to a system of coupled differential equations (4.17) - (4.20) that are nonlinear in nature which is solved by using NDSolver command in Mathematica.

## 4.3 Graphical analysis

The velocity and temperature profiles are discussed through graphs plotted for various influential parameters. These include slip parameter  $\beta$ , curvature L, MHD M, inhomogeneous parameter  $\omega$ , and Brickman number Br.

#### 4.3.1 Fluid Flow Analysis

Figs. 4.1- 4.4 are plotted to discuss fluid velocity profile for slip parameter  $\beta$ , curvature L, MHD M, and inhomogeneous parameter  $\omega$ . Fig. 4.1 reveals the fluid velocity behavior as curvature varies. As curvature L increases velocity decreases near lower wall and increases near upper wall. This is due to the centrifugal force that moves the fluid towards the upper wall of the channel and fluid speeds up near the upper boundary and velocity of fluid declines near lower wall. Fig. 4.2 presents impact of varying density  $\omega$  of dust particles on fluid flow behavior. Below the central line of the passage fluid velocity increases while above the central line velocity of fluid decreases as value of  $\omega$  increases. The effects of magnetohydrodynamics M are depicted in Fig. 4.3. As MHD parameter M rises, the fluid velocity decrease near lower boundary and increases near upper wall of the channel. Due to resistive force generated by magnetic field, maximum velocity is reduced and symmetry of the flow is disturbed. The variation in fluid velocity due to slip on the channel walls can be seen in Fig. 4.4. It shows increase in fluid velocity near the walls by increasing values of slip parameter  $\beta$ . This is because friction force is minimized between fluid and boundary and thus allows fluid move more freely. While in the central part of channel fluid moves slowly as  $\beta$  increases. Fig. 4.5 shows the comparison of fluid velocity results obtained by NDSolver command with HPM. Both results exactly match.

#### 4.3.2 Solid Particle Flow Analysis

Figs. 4.6-4.9 are plotted to discuss particle velocity profile for slip parameter  $\beta$ , curvature L, MHD M, and inhomogeneous parameter  $\omega$ . Fig. 4.6 portrays impact of curvature L on particle velocity. By increasing curvature, particles flow becomes slower in lower half and speeds up in upper half of the passage. Fig. 4.7 exhibits effect of particle density. The behavior of particle velocity is dual. As particle density  $\omega$  enhances, particles movement speeds up near lower boundary and slows down near upper boundary. Influence of MHD on particle velocity is manifested in Fig. 4.8. Dust particles travel more quickly close to the channel's walls and more slowly in its center as the MHD parameter rises. Plots for different values of slip parameter are drawn in Fig. 4.9. Decrease in particle velocity is observed by increasing slip parameter in the middle of passage. The increased values of slip reduce drag force near the walls allowing solid particle to move freely.

## 4.3.3 Temperature Distribution Analysis

Figs. 4.10 to 4.14 are plotted to discuss fluid temperature distribution for slip parameter  $\beta$ , curvature L, variable thermal conductivity  $\eta$ , inhomogenous parameter  $\omega$ , and Brickman number Br. Fig. 4.10 is graph of temperature distribution for differing values of curvature L. Rise in temperature is observed as channel becomes more curved. In Fig. 4.11, it is found that as density parameter increases fluid temperature reduces. Fig. 4.12 shows results of fluid temperature profile as slip parameter  $\beta$  varies. High slip parameter slows down the fluid and as a result heat transfer enhances. Thermal conductivity is ability to transfer heat between molecules of fluid. High thermal conductivity results in fast heat transfer within the fluid which is illustrated in Fig. 4.13. The impact of Brinkman number Br is demonstrated in Fig. 4.14. Decline in temperature is observed with increase in Brinkman parameter.

#### 4.3.4 Heat Transfer Coefficient

Impact of slip parameter  $\beta$  and Brickman number Br on heat transfer coefficient is discussed in Figs. 4.15 and 4.16. As the movement of the channel walls is peristaltic therefore the behavior of heat transfer coefficient is oscillatory. Influence of slip parameter  $\beta$  on heat transfer coefficient is exhibited in Fig. 4.15. As slip parameter  $\beta$  increases heat transfer coefficient decreases in the interval  $-1.8 \le x \le 1.8$  and increases otherwise. Fig. 4.16 shows effect of Brickman number Br on heat transfer coefficient. With the rise in Brickman number heat transfer coefficient increases in the range  $-1.8 \le x \le 1.8$  and decreases elsewhere.

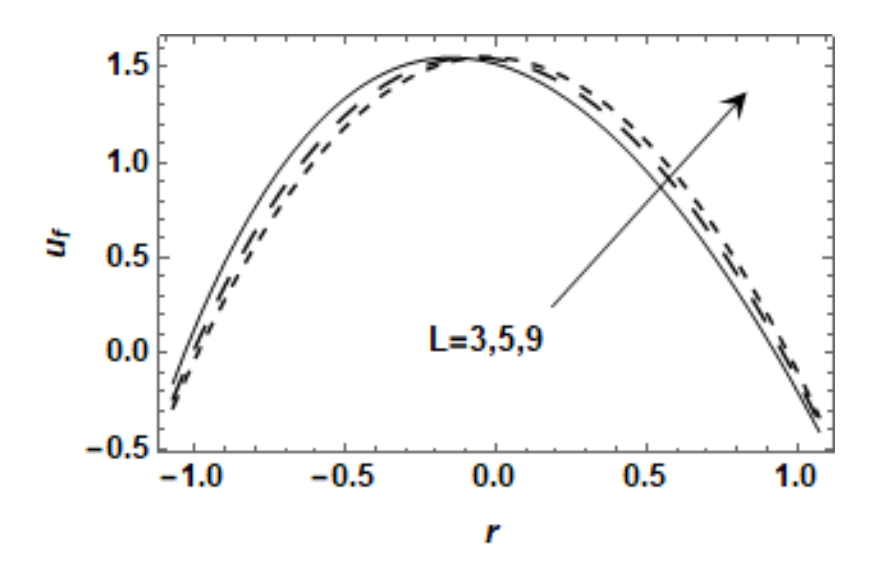


Fig 4.1: The fluid velocity profile with  $\beta = 0.2$ , M = 0.1, b = 0.8, a = 0.6, A = 0.5,  $\eta = 0.03$ , Br = 0.3, Pr = 0.02,  $\omega = 3$ ,  $\phi = \frac{\pi}{6}$ .

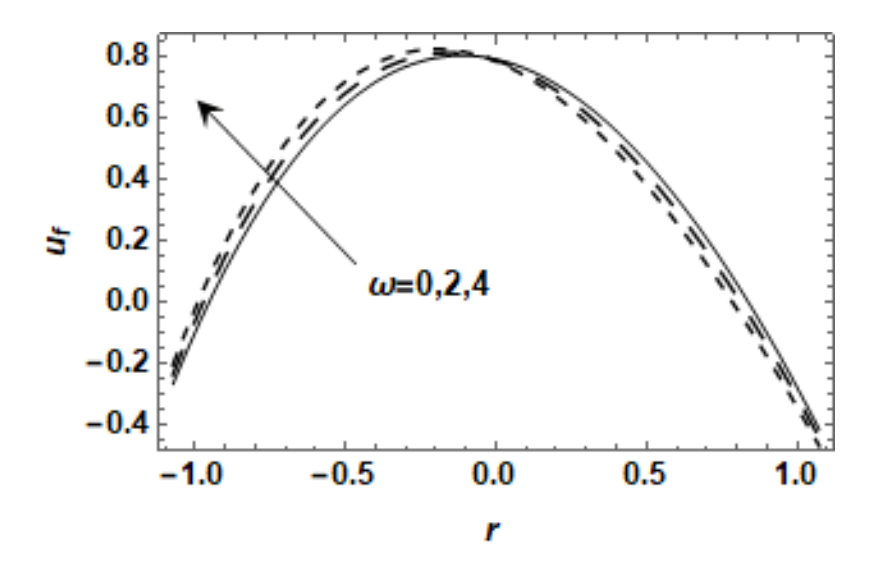


Fig 4.2: The fluid velocity profile with  $\beta = 0.3, M = 0, b = 0.8, a = 0.6, A = 0.5, \eta = 0.1,$   $Br = 0.5, Pr = 0.2, L = 5, \phi = \frac{\pi}{6}.$ 

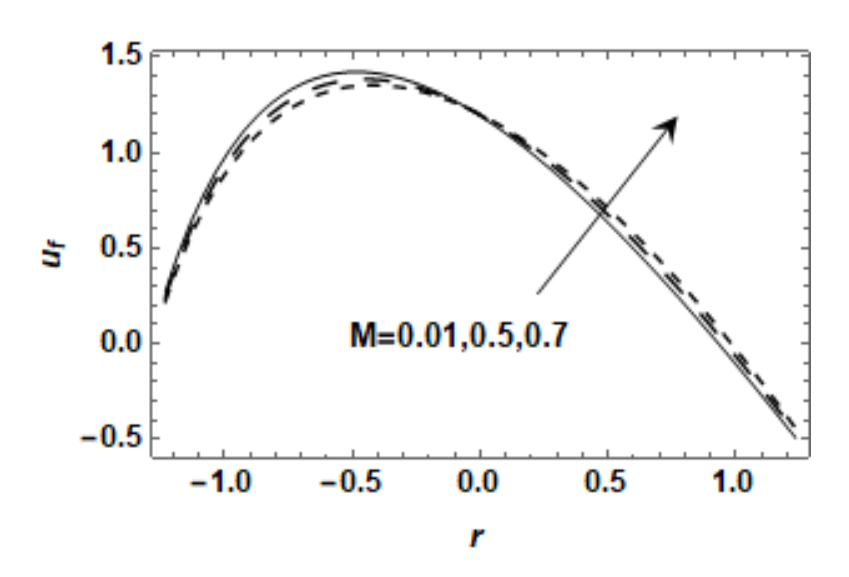


Fig 4.3: The fluid velocity profile with  $\beta = 0.3, b = 0.3, a = 0.3, A = 0.5, \eta = 0.2, Br = 0.3,$   $Pr = 0.2, L = 2, \omega = 3, \phi = \frac{\pi}{4}$ .

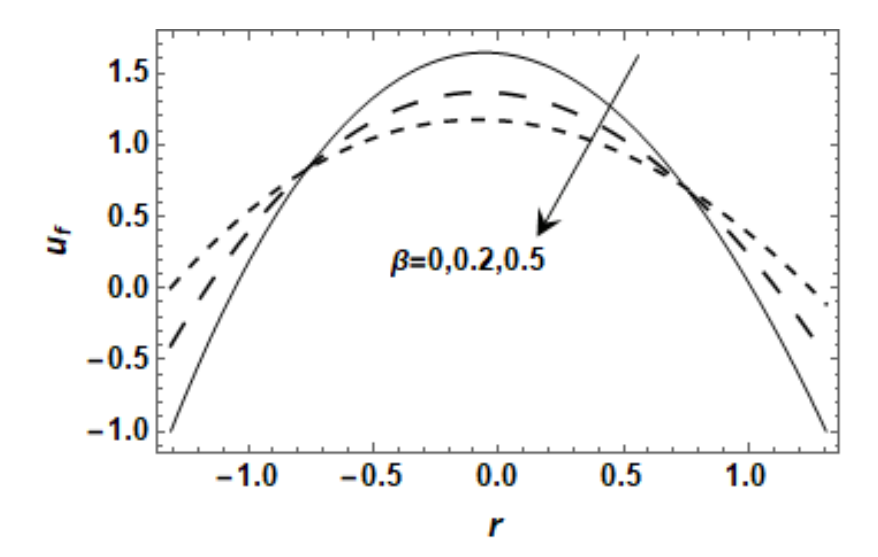


Fig 4.4: The fluid velocity profile with  $M=0.1, b=0.3, a=0.3, A=0.3, \eta=0.06, Br=0.1,$   $Pr=0.2, L=10.5, \omega=5, \phi=\frac{\pi}{3}.$ 

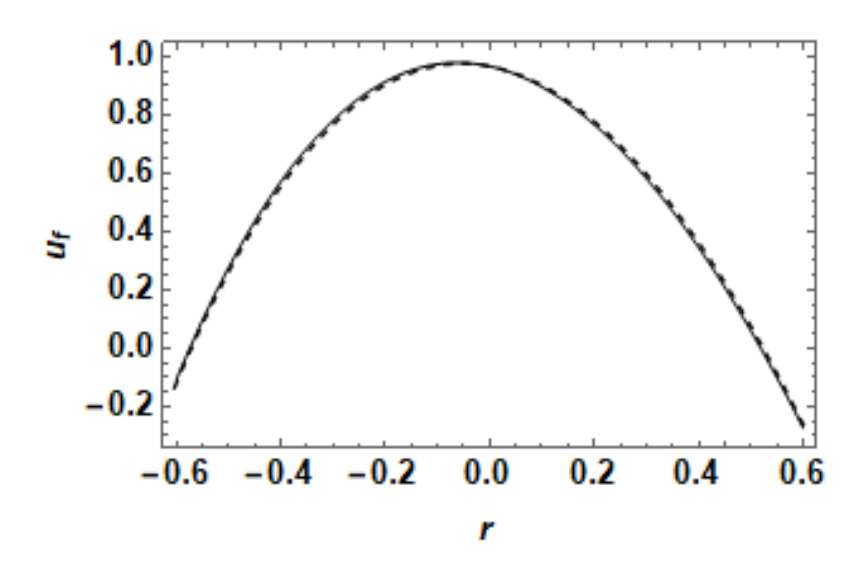


Fig 4.5: Comparison of HPM and NDSolver.

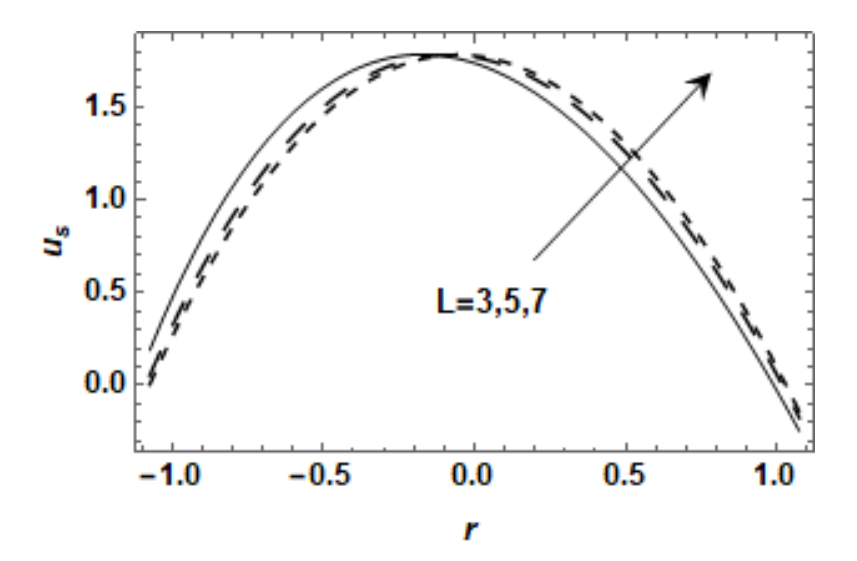


Fig 4.6: The particle velocity profile with  $\beta = 0.2$ , M = 0.1, b = 0.8, a = 0.6, A = 0.5  $\eta = 0.03$ , Br = 0.3, Pr = 0.02,  $\omega = 3$ ,  $\phi = \frac{\pi}{6}$ .

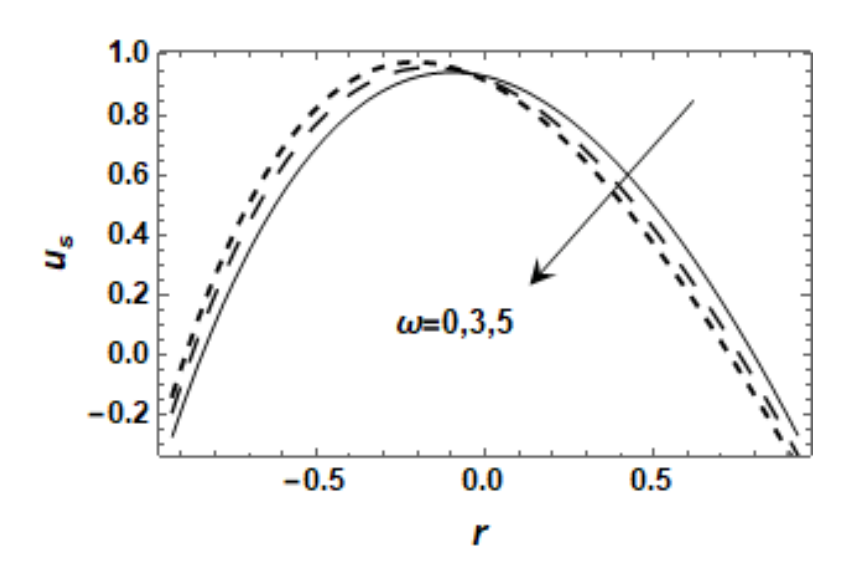


Fig 4.7: The particle velocity profile with  $\beta = 0.5$ , M = 0.1, b = 0.3, a = 0.8, A = 0.5,  $\eta = 0.03$ , Br = 0.1, Pr = 0.2, L = 3,  $\phi = \frac{\pi}{6}$ .

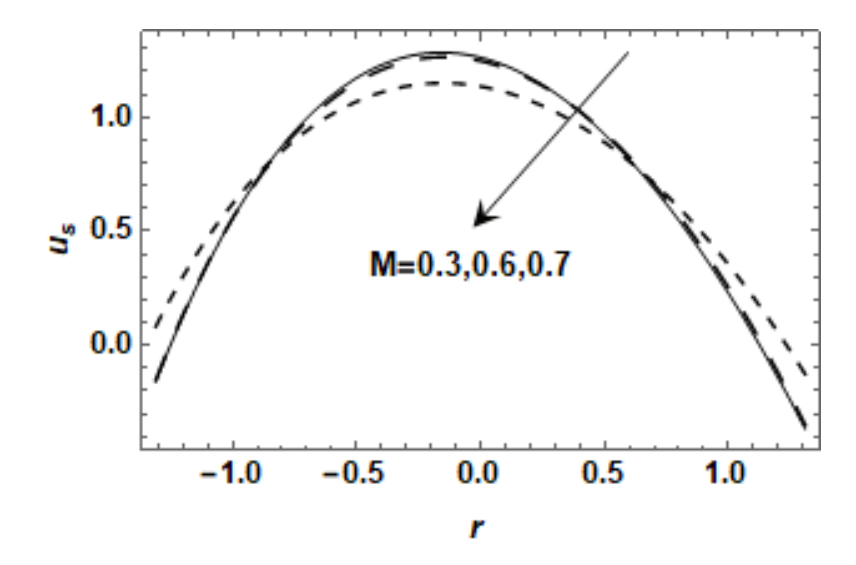


Fig 4.8: The particle velocity profile with  $\beta = 0.3$ , b = 0.6, a = 0.3, A = 0.3,  $\eta = 0.06$ , Br = 0.1, Pr = 0.2, L = 5,  $\omega = 5$ ,  $\phi = \frac{\pi}{3}$ .

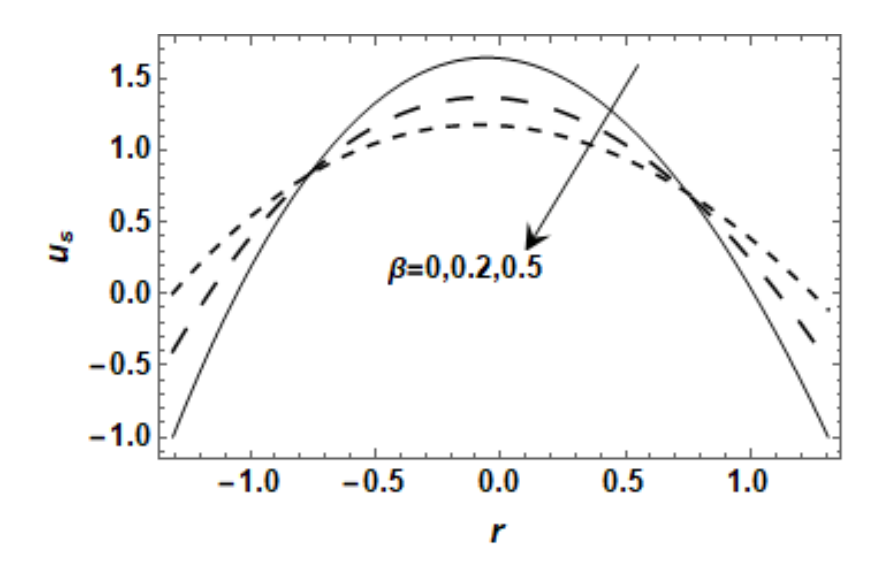


Fig 4.9: The particle velocity profile with M=0.1, b=0.3, a=0.3, A=0.3,  $\eta=0.06$ , Br=0.1, Pr=0.2, L=10.5,  $\omega=5$ ,  $\phi=\frac{\pi}{3}$ .

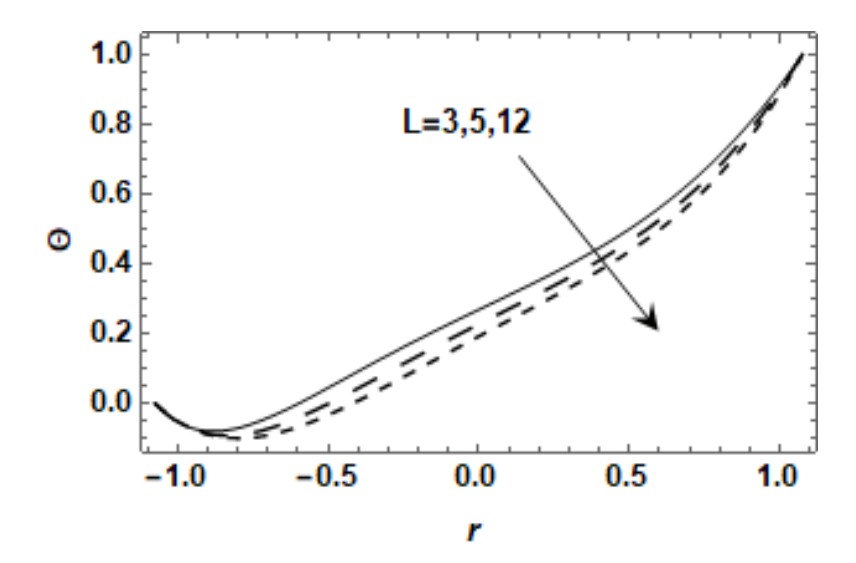


Fig 4.10: The fluid temperature profile with  $\beta = 0.2$ , M = 0.1, b = 0.8, a = 0.6, A = 0.5,  $\eta = 0.03$ , Br = 0.3, Pr = 0.02,  $\omega = 3$ ,  $\phi = \frac{\pi}{6}$ .

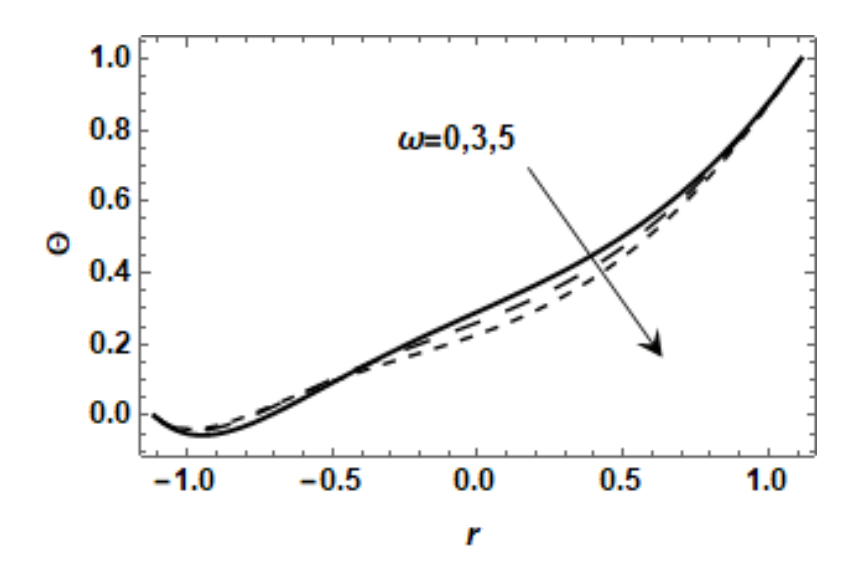


Fig 4.11: The fluid temperature profile with  $\beta = 0.5$ , M = 0.1, b = 0.3, a = 0.8, A = 0.5,  $\eta = 0.06$ , Br = 0.7, Pr = 0.6, L = 3.,  $\phi = 0.8$ .

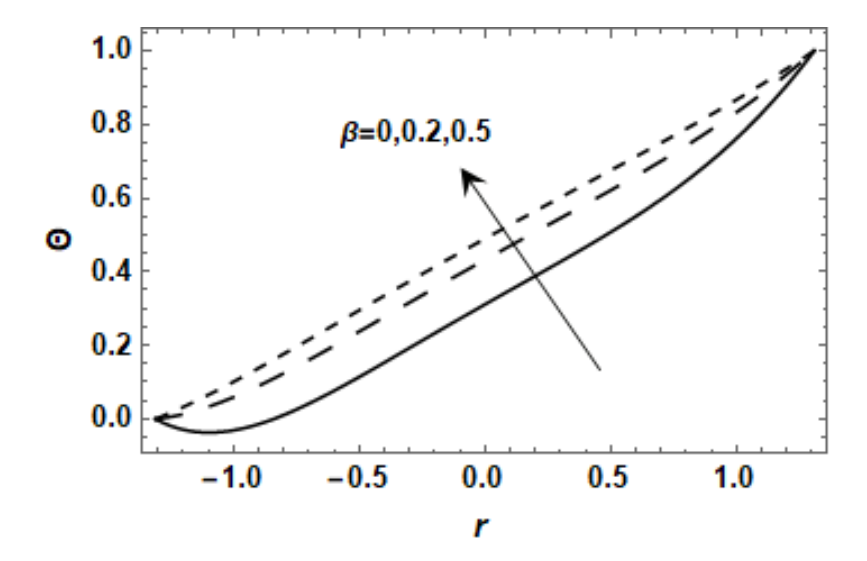


Fig 4.12: The fluid temperature profile with  $M=0.1, b=0.3, a=0.3, A=0.3, \eta=0.06,$   $Br=0.1, Pr=0.2, L=10.5, \omega=5, \phi=\frac{\pi}{3}.$ 

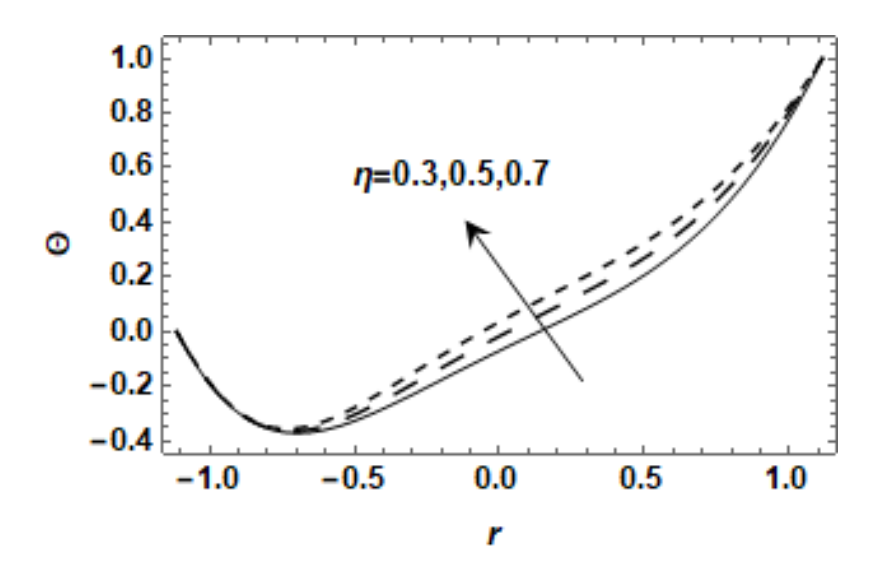


Fig 4.13: The fluid temperature profile with  $\beta = 0.2$ , M = 0.1, b = 0.3, a = 0.8, A = 0.5, Br = 0.6, Pr = 0.4, L = 10,  $\omega = 3$ ,  $\phi = 0.8$ .

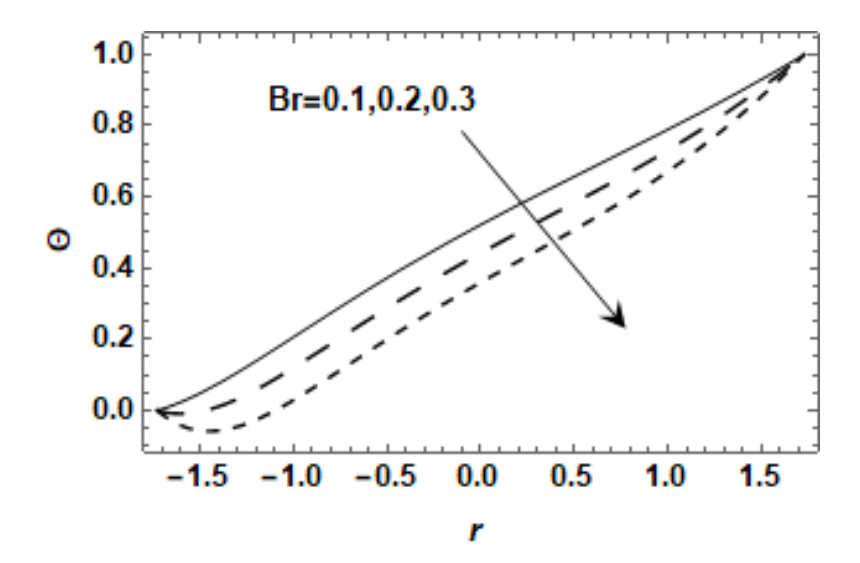


Fig 4.14: The fluid temperature profile with M = 0.1, b = 0.3, a = 0.8, A = 0.5,  $\eta = 0.6$ , Br = 0.1, Pr = 0.4, L = 10,  $\omega = 3$ ,  $\phi = 0.8$ .

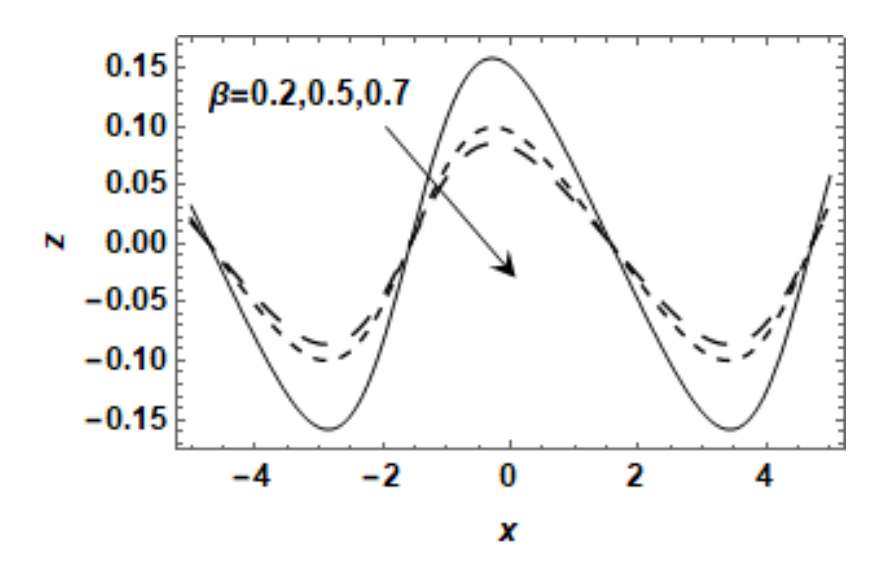


Fig 4.15: Heat transfer coefficient for slip parameter with M=0.1, b=0.3, a=0.8, A=0.5,  $\eta=0.6, Br=0.4, Pr=0.1, L=2, \omega=3, \phi=0.2, Q=2, Q_s=2.5, d=0.3.$ 

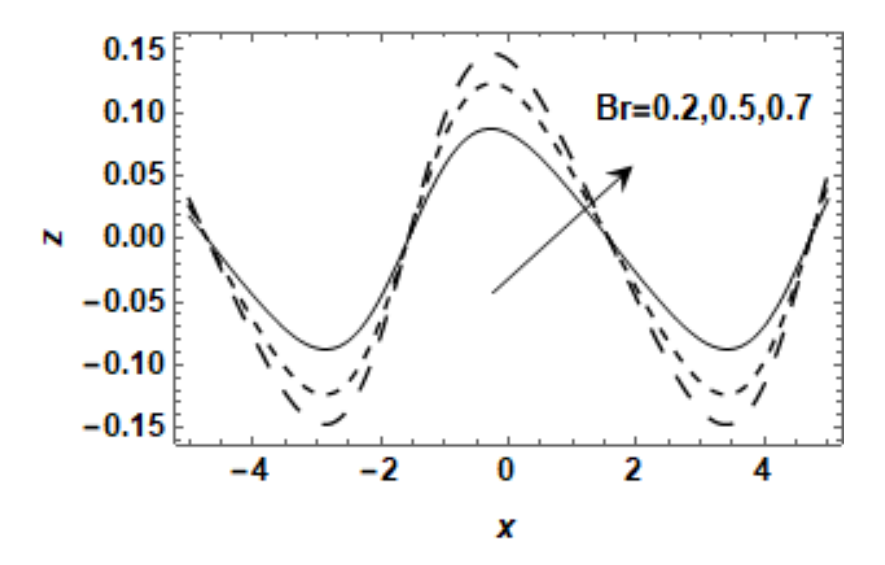


Fig 4.16: Heat transfer coefficient for thermal conductivity with M = 0.1, b = 0.3, a = 0.8, A = 0.5,  $\eta = 0.6$ ,  $\beta = 0.4$ , Pr = 0.1, L = 2,  $\omega = 3$ ,  $\phi = 0.2$ , Q = 2,  $Q_s = 2.5$ , d = 0.3, q = 1.

# **4.4 Conclusion**

The recent work focuses on the effects of MHD and non-uniform dispersion of solid particles on fluid and particle velocities and fluid temperature distribution. The geometry of the walls is curved and exhibiting peristaltic motion. Temperature profile is also analyzed under variable thermal conductivity. Important points of the study are:

- As density of particles increases the fluid and particle velocity exhibit same pattern of flow.
   i.e., fluid and particle velocities decrease in the vicinity of upper boundary and increase near lower boundary.
- The increase in particle density slows down heat transfer through the fluid.
- The presence of magnetic field reduces the fluid speed in lower region of the channel whereas opposite behavior in upper region of the channel.
- The particle velocity enhances near the walls due to magnetic field.

- By increasing curvature, both fluid and particle velocities decline near upper wall and enhance near lower wall. Increase in fluid temperature is also observed.
- Slip parameter slows down the fluid and particle velocities but temperature rises.
- High Brinkman number reduces temperature of fluid but increase in thermal conductivity results fast heat conduction.

# **Chapter 5**

# **Entropy Generation Analysis of Dusty Fluid with Peristalsis in Asymmetric Channel with Slip**

# **Effects**

Peristaltic dusty fluid flow with uniformly distributed dust particles is considered in this chapter. The passage of flow is asymmetric. Slip conditions have been incorporated in both momentum and thermal profiles. The mathematical model is constructed using laws of momentum and energy conservation. The resulting coupled equations are solved using small wave number approximation. Impacts of important quantities on temperature and velocity profiles of fluid along with solid particles have been debated through graphs. Entropy generation analysis has been carried out for influential parameters.

## **5.1 Problem Formulation**

The two-dimensional fluid flow is considered in asymmetric channel of width  $d_1 + d_2$ . Dust particles are distributed uniformly. Sinusoidal wave propagation is considered along the boundary walls. The geometry of the walls due to sinusoidal waves is expressed by the Eqns. (2.1a) and (2.1b).

The ruling equations describing fluid flow are

$$\frac{\partial U}{\partial X} + \frac{\partial V}{\partial Y} = 0, (5.1)$$

$$\rho \left[ \frac{\partial U}{\partial t} + U \frac{\partial U}{\partial x} + V \frac{\partial U}{\partial y} \right] = -\frac{\partial P}{\partial x} + \mu \nabla^2 U + k N (U_s - U), \tag{5.2}$$

$$\rho \left[ \frac{\partial V}{\partial t} + U \frac{\partial V}{\partial X} + V \frac{\partial V}{\partial Y} \right] = -\frac{\partial P}{\partial Y} + \mu \nabla^2 V + k N (V_s - V), \tag{5.3}$$

$$\rho C_p \left[ \frac{\partial T}{\partial t} + U \frac{\partial T}{\partial X} + V \frac{\partial T}{\partial Y} \right] = k^* [\nabla^2 T] + \frac{N C_p}{\tau_T} (T_s - T) + \frac{N}{\tau_V} (U_s - U)^2 + \Phi, \tag{5.4}$$

where viscous dissipation is

$$\Phi = \mu \left[ 2 \left\{ \left( \frac{\partial U}{\partial X} \right)^2 + \left( \frac{\partial V}{\partial Y} \right)^2 \right\} + \left( \frac{\partial U}{\partial Y} + \frac{\partial V}{\partial X} \right)^2 \right], \tag{5.5}$$

The ruling equations for dust particles are

$$\frac{\partial U_s}{\partial X} + \frac{\partial V_s}{\partial Y} = 0, \tag{5.6}$$

$$\frac{\partial U_s}{\partial t} + U_s \frac{\partial U_s}{\partial x} + V_s \frac{\partial U_s}{\partial y} = \frac{k}{m} (U - U_s), \tag{5.7}$$

$$\frac{\partial V_s}{\partial t} + U_s \frac{\partial V_s}{\partial X} + V_s \frac{\partial V_s}{\partial Y} = \frac{k}{m} (V - V_s), \tag{5.8}$$

$$\frac{\partial T_s}{\partial t} + U_s \frac{\partial T_s}{\partial X} + V_s \frac{\partial T_s}{\partial Y} = -\frac{c_p}{c_m} (T_s - T). \tag{5.9}$$

The coordinates (X, Y) in fixed frame of reference are transformed to the coordinates  $(\bar{x}, \bar{y})$  in wave frame of reference by the relation

$$\bar{y} = Y, \ \bar{x} = X - ct, \ \bar{v} = V, \ \bar{u} = U - c, \ \bar{u}_s = U_s - c, \ \bar{v}_s = V_s, \ \bar{T}(\bar{x}, \bar{y}) = T(X, Y, t),$$

$$\bar{T}_s(\bar{x}, \bar{y}) = T_s(X, Y, t), \ \bar{p}(\bar{x}, \bar{y}) = P(X, Y, t). \tag{5.10}$$

Using transformation (5.10), Eqns. (5.1) - (5.9) become

For fluid flow

$$\frac{\partial \bar{u}}{\partial \bar{x}} + \frac{\partial \bar{v}}{\partial \bar{y}} = 0, \tag{5.11}$$

$$\rho \left[ \bar{u} \frac{\partial \bar{u}}{\partial \bar{x}} + \bar{v} \frac{\partial \bar{u}}{\partial \bar{y}} \right] = -\frac{\partial P}{\partial \bar{x}} + N(\bar{u}_s - \bar{u})k + \mu \nabla^2 \bar{u}, \tag{5.12}$$

$$\rho \left[ \bar{u} \frac{\partial \bar{v}}{\partial \bar{x}} + \bar{v} \frac{\partial \bar{v}}{\partial \bar{y}} \right] = -\frac{\partial P}{\partial \bar{y}} + N(\bar{v}_s - \bar{v})k + \mu \nabla^2 \bar{v}, \tag{5.13}$$

$$\rho C_p \left[ \bar{u} \frac{\partial \bar{T}}{\partial \bar{x}} + \bar{v} \frac{\partial \bar{T}}{\partial \bar{y}} \right] = k^* \left[ \nabla^2 \bar{T} \right] + \frac{N C_p}{\tau_T} (\bar{T}_S - \bar{T}) + \frac{N}{\tau_V} (\bar{u}_S - \bar{u})^2 + \Phi, \tag{5.14}$$

Viscous dissipation term

$$\Phi = \mu \left[ 2 \left\{ \left( \frac{\partial \overline{u}}{\partial \overline{x}} \right)^2 + \left( \frac{\partial \overline{v}}{\partial \overline{y}} \right)^2 \right\} + \left( \frac{\partial \overline{u}}{\partial \overline{y}} + \frac{\partial \overline{v}}{\partial \overline{x}} \right)^2 \right], \tag{5.15}$$

For solid particles

$$\frac{\partial \bar{u}_s}{\partial \bar{x}} + \frac{\partial \bar{v}_s}{\partial \bar{y}} = 0, \tag{5.16}$$

$$\bar{u}_s \frac{\partial U_s}{\partial \bar{x}} + \bar{v}_s \frac{\partial U_s}{\partial \bar{v}} = \frac{k}{m} (\bar{u} - \bar{u}_s), \tag{5.17}$$

$$\bar{u}_s \frac{\partial V_s}{\partial \bar{x}} + \bar{v}_s \frac{\partial V_s}{\partial \bar{y}} = \frac{k}{m} (\bar{v} - \bar{v}_s), \tag{5.18}$$

$$\bar{u}_{S} \frac{\partial \bar{T}_{S}}{\partial \bar{x}} + \bar{v}_{S} \frac{\partial \bar{T}_{S}}{\partial \bar{y}} = -\frac{c_{p}}{c_{m}} (\bar{T}_{S} - \bar{T}). \tag{5.19}$$

The expressions of stream functions and dimensionless quantities for fluid phase and particle phase are:

$$x = \frac{\bar{x}}{\lambda}, \ y = \frac{\bar{y}}{d_1}, \ u = \frac{\bar{u}}{c}, \ v = \frac{\bar{v}}{\delta c}, \ u_S = \frac{\bar{u}_S}{c}, \ v_S = \frac{\bar{v}_S}{\delta c}, \ p = \frac{\bar{p}d_1^2}{\mu\lambda c}, \ \delta = \frac{d_1}{\lambda}, \ a = \frac{a_1}{d_1}, \ b = \frac{a_2}{d_1},$$

$$d = \frac{d_2}{d_1}, \ Re = \frac{\rho c d_1}{\mu}, \ Ec = \frac{c^2}{c_p(T_1 - T_0)}, \ Pr = \frac{\mu c_p}{k^*}, \ \Theta = \frac{T - T_0}{T_1 - T_0}, \ \Phi' = \frac{d_1^2 \Phi}{c^2 \mu}, \psi' = \frac{\psi}{c d_1}, \ \varphi' = \frac{\varphi}{c d_1},$$

$$u = \frac{\partial \psi}{\partial y}, \ v = -\delta \frac{\partial \psi}{\partial x}, \ u_S = \frac{\partial \varphi}{\partial y}, v_S = -\delta \frac{\partial \varphi}{\partial x}, \ A = \frac{kNd_1^2}{\mu}, \ B = \frac{kd_1}{mc}, \ A_1 = \frac{Nd_1^2}{\mu\tau_T}, \ B_1 = \frac{Nd_1^2}{\mu\tau_V},$$

$$C = \frac{c_p d_1}{C \cdot c}.$$

$$(5.20)$$

Using the quantities in Eqn. (5.20), momentum and energy equations for fluid and solid particles presented in Eqns. (5.11) - (5.19) become as:

For fluid flow

$$Re \, \delta \left[ \frac{\partial \psi}{\partial y} \, \frac{\partial^2 \psi}{\partial x \partial y} - \frac{\partial \psi}{\partial x} \frac{\partial^2 \psi}{\partial y^2} \right] = -\frac{\partial p}{\partial x} + \delta^2 \frac{\partial^3 \psi}{\partial x^2 \partial y} + \frac{\partial^3 \psi}{\partial y^3} + A \left( \frac{\partial \varphi}{\partial y} - \frac{\partial \psi}{\partial y} \right), \tag{5.21}$$

$$Re \ \delta^{3} \left[ \frac{\partial \psi}{\partial x} \frac{\partial^{2} \psi}{\partial x \partial y} - \frac{\partial \psi}{\partial y} \frac{\partial^{2} \psi}{\partial x^{2}} \right] = -\frac{\partial p}{\partial y} - \delta^{4} \frac{\partial^{3} \psi}{\partial x^{3}} - \delta^{2} \frac{\partial^{3} \psi}{\partial y^{2} \partial x} - \delta^{2} A \left( \frac{\partial \varphi}{\partial x} - \frac{\partial \psi}{\partial x} \right), \tag{5.22}$$

$$Re \ \delta \left[ \frac{\partial \Theta}{\partial x} \frac{\partial \psi}{\partial y} - \frac{\partial \Theta}{\partial y} \frac{\partial \psi}{\partial x} \right] = \frac{1}{pr} \left[ \delta^2 \frac{\partial^2 \Theta}{\partial x^2} + \frac{\partial^2 \Theta}{\partial y^2} \right] + A_1(\Theta_s - \Theta) + B_1 E c \left( \frac{\partial \varphi}{\partial y} - \frac{\partial \psi}{\partial y} \right)^2 + E c \ \Phi, \tag{5.23}$$

Viscous dissipation term in terms of stream function is

$$\Phi = 4\delta^2 \left(\frac{\partial^2 \psi}{\partial x \partial y}\right)^2 + \left(\frac{\partial^2 \psi}{\partial y^2} - \delta^2 \frac{\partial^2 \psi}{\partial x^2}\right)^2. \tag{5.24}$$

For solid particles

$$\delta\left(\frac{\partial\varphi}{\partial y}\frac{\partial^2\varphi}{\partial x\partial y} - \frac{\partial\varphi}{\partial x}\frac{\partial^2\varphi}{\partial y^2}\right) = B\left(\frac{\partial\psi}{\partial y} - \frac{\partial\varphi}{\partial y}\right),\tag{5.25}$$

$$\delta\left(-\frac{\partial\varphi}{\partial y}\frac{\partial^2\varphi}{\partial x^2} + \frac{\partial\varphi}{\partial x}\frac{\partial^2\varphi}{\partial x\partial y}\right) = B\left(\frac{\partial\psi}{\partial x} - \frac{\partial\varphi}{\partial x}\right),\tag{5.26}$$

$$\delta\left(\frac{\partial\varphi}{\partial y}\frac{\partial\Theta_{S}}{\partial x} - \frac{\partial\varphi}{\partial x}\frac{\partial\Theta_{S}}{\partial y}\right) = -\mathcal{C}(\Theta_{S} - \Theta). \tag{5.27}$$

Compatibility equations for fluid and solid particles are

$$Re\delta\left[\left(\frac{\partial\psi}{\partial y}\frac{\partial^3\psi}{\partial y^2\partial x}-\frac{\partial\psi}{\partial x}\frac{\partial^3\psi}{\partial y^3}\right)+\delta^2\left(\frac{\partial\psi}{\partial y}\frac{\partial^3\psi}{\partial x^3}-\frac{\partial\psi}{\partial x}\frac{\partial^3\psi}{\partial x^2\partial y}\right)\right]=2\delta^2\frac{\partial^4\psi}{\partial x^2\partial y^2}+\frac{\partial^4\psi}{\partial y^4}+\delta^4\frac{\partial^4\psi}{\partial x^4}+A(\nabla_1^2\varphi-\nabla_1^2\varphi-\nabla_2^2\varphi$$

$$\nabla_1^2 \psi), \tag{5.28}$$

$$\delta \left[ \frac{\partial \varphi}{\partial y} \frac{\partial}{\partial x} \nabla_1^2 \varphi - \frac{\partial \varphi}{\partial x} \frac{\partial}{\partial y} \nabla_1^2 \varphi \right] = B[\nabla_1^2 \psi - \nabla_1^2 \varphi], \tag{5.29}$$

where

$$\nabla_1^2 = \delta^2 \frac{\partial^2}{\partial x^2} + \frac{\partial^2}{\partial y^2}.$$
 (5.30)

The dimensionless description of walls is expressed by the Eqns. (2.25a) and (2.25b).

Non-dimensionalized boundary conditions are

$$\psi = \frac{F}{2}, \frac{\partial \psi}{\partial y} + \beta \tau_{xy} = -1, \quad \varphi = \frac{E}{2} \quad \text{at } y = h_1(x), \tag{5.31a}$$

$$\psi = -\frac{F}{2}, \frac{\partial \psi}{\partial y} - \beta \tau_{xy} = -1, \quad \varphi = -\frac{E}{2} \quad \text{at } y = h_2(x), \tag{5.31b}$$

$$\Theta - \varepsilon \frac{\partial \Theta}{\partial y} = 0$$
 at  $y = h_1(x)$ ,  $\Theta + \varepsilon \frac{\partial \Theta}{\partial y} = 1$  at  $y = h_2(x)$ . (5.31c)

$$\Theta_s - \varepsilon \frac{\partial \Theta_s}{\partial y} = 0$$
 at  $y = h_1(x)$ ,  $\Theta_s + \varepsilon \frac{\partial \Theta_s}{\partial y} = 1$  at  $y = h_2(x)$ . (5.31d)

# **5.2 Method of Solution:**

The perturbation technique is applied to solve the nonlinear differential equations. We use  $\delta$  to express fluid stream function  $\psi$ , particle stream function  $\varphi$ , pressure p, fluid temperature  $\Theta$ , particle temperature  $\Theta_s$ , time flow rate of fluid F and time flow rate of dust particle E as

$$\psi = \psi_0 + \delta \psi_1 + O(\delta^2), \tag{5.32}$$

$$\varphi = \varphi_0 + \delta \,\varphi_1 + O(\delta^2),\tag{5.33}$$

$$\Theta = \Theta_0 + \delta\Theta_1 + O(\delta^2), \tag{5.34}$$

$$\Theta_s = \Theta_{0s} + \delta\Theta_{1s} + O(\delta^2), \tag{5.35}$$

$$F = F_0 + \delta F_1 + O(\delta^2), \tag{5.36}$$

$$E = E_0 + \delta E_1 + O(\delta^2). \tag{5.37}$$

#### **5.2.1 Zeroth Order System:**

$$\frac{\partial^4 \psi_0}{\partial y^4} + A \left( \frac{\partial^2 \varphi_0}{\partial y^2} - \frac{\partial^2 \psi_0}{\partial y^2} \right) = 0, \tag{5.38}$$

$$B\left(\frac{\partial^2 \psi_0}{\partial v^2} - \frac{\partial^2 \varphi_0}{\partial v^2}\right) = 0,\tag{5.39}$$

$$\frac{1}{pr}\frac{\partial^2\Theta_0}{\partial y^2} + B_1 E c \left(\frac{\partial\varphi_0}{\partial y} - \frac{\partial\psi_0}{\partial y}\right)^2 + E c \left(\frac{\partial^2\psi_0}{\partial y^2}\right)^2 + A_1(\Theta_{0s} - \Theta_0) = 0, \tag{5.40}$$

$$C(\Theta_{0s} - \Theta_0) = 0. \tag{5.41}$$

Boundary conditions are

$$\psi_0 = \frac{F_0}{2}, \ \frac{\partial \psi_0}{\partial y} + \beta \tau_{0xy} = -1, \ \varphi_0 = \frac{E_0}{2}$$
 at  $y = h_1(x)$ , (5.42a)

$$\psi_0 = -\frac{F_0}{2}, \ \frac{\partial \psi_0}{\partial y} - \beta \tau_{0xy} = -1, \ \varphi_0 = -\frac{E_0}{2}$$
 at  $y = h_2(x)$ , (5.42b)

$$\Theta_0 - \varepsilon \frac{\partial \Theta_0}{\partial y} = 0$$
 at  $y = h_1(x)$ ,  $\Theta_0 + \varepsilon \frac{\partial \Theta_0}{\partial y} = 1$  at  $y = h_2(x)$ . (5.42c)

$$\Theta_{0s} - \varepsilon \frac{\partial \Theta_{0s}}{\partial y} = 0$$
 at  $y = h_1(x)$ ,  $\Theta_{0s} + \varepsilon \frac{\partial \Theta_{0s}}{\partial y} = 1$  at  $y = h_2(x)$ . (5.42d)

Applying DSolver command in Mathematica, solution of zeroth order system is obtained as

$$\psi_0(y) = \frac{(h_2 + h_1 - 2y)\left(2(h_2 - h_1)(h_2 - y)(h_1 - y) + F_0\left(h_2^2 + h_1^2 + 2h_1y - 2y^2 + 2h_2(-2h_1 + y - 3\beta) + 6h_1\beta\right)\right)}{2(h_2 - h_1)^2(h_2 - h_1 - 6\beta)}, \quad (5.43)$$

$$\varphi_0(y) = \frac{(h_2 + h_1 - 2y)(2(F_0 - h_2 + h_1)(h_2 - y)(-h_1 + y) + E_0(h_2 - h_1)(h_2 - h_1 - 6\beta))}{2(h_2 - h_1)^2(h_2 - h_1 - 6\beta)},$$
(5.44)

$$\Theta_0(y) = \frac{1}{4(h_2 - h_1)^4 (-h_2 + h_1 + 6\beta)^2} Br\left(-3F_0^2 (h_2 + h_1 - 2y)^4 + 2(h_2 - h_1)^2 y^2 (-36h_2^2 - 4h_1 + 6\beta)^2 \right) dy + 2(h_2 - h_1)^4 y^2 (-36h_2^2 - 4h_1 + 6\beta)^2 dy + 2(h_2 - h_1)^4 y^2 (-36h_2^2 - 4h_1 + 6\beta)^2 dy + 2(h_2 - h_1)^4 y^2 (-36h_2^2 - 4h_1 + 6\beta)^2 dy + 2(h_2 - h_1)^4 y^2 (-36h_2^2 - 4h_1 + 6\beta)^2 dy + 2(h_2 - h_1)^4 y^2 (-36h_2^2 - 4h_1 + 6\beta)^2 dy + 2(h_2 - h_1)^4 y^2 (-36h_2^2 - 4h_1 + 6\beta)^2 dy + 2(h_2 - h_1)^4 y^2 (-36h_2^2 - 4h_1 + 6\beta)^2 dy + 2(h_2 - h_1)^4 y^2 (-36h_2^2 - 4h_1 + 6\beta)^2 dy + 2(h_2 - h_1)^4 y^2 (-36h_2^2 - 4h_1 + 6\beta)^2 dy + 2(h_2 - h_1)^4 y^2 (-36h_2^2 - 4h_1 + 6\beta)^2 dy + 2(h_2 - h_1)^2 y^2 (-36h_2^2 - 4h_1 + 6\beta)^2 dy + 2(h_2 - h_1)^2 dy + 2(h_2 - h_$$

$$24y^{2} - 12E_{0}(h_{2} - h_{1})^{2}B_{1}\beta + 36E_{0}(h_{2} - h_{1})B_{1}\beta^{2}) + 2F_{0}(h_{2} - h_{1})y^{2}(72h_{2}^{2} + 144h_{2}h_{1} + 72h_{1}^{2} - h_{2}^{4}B_{1} + 4h_{2}^{3}h_{1}B_{1} - 6h_{2}^{2}h_{1}^{2}B_{1} + 4h_{2}h_{1}^{3}B_{1} - h_{1}^{4}B_{1} - 96h_{2}y - 96h_{1}y + 48y^{2} + 12(h_{2} - h_{1})^{3}B_{1}\beta - 36(h_{2} - h_{1})^{2}B_{1}\beta^{2}) + C1 + yC2.$$

$$(5.45)$$

### 5.2.2 First Order System:

$$Re\left(\frac{\partial\psi_0}{\partial y}\frac{\partial^3\psi_0}{\partial x\partial y^2} - \frac{\partial\psi_0}{\partial x}\frac{\partial^3\psi_0}{\partial y^3}\right) = \frac{\partial^4\psi_1}{\partial y^4} + A\left(\frac{\partial^2\varphi_1}{\partial y^2} - \frac{\partial^2\psi_1}{\partial y^2}\right),\tag{5.46}$$

$$\frac{\partial \varphi_0}{\partial y} \frac{\partial^3 \varphi_0}{\partial x \partial y^2} - \frac{\partial \varphi_0}{\partial x} \frac{\partial^3 \varphi_0}{\partial y^3} = B \left( \frac{\partial^2 \psi_1}{\partial y^2} - \frac{\partial^2 \varphi_1}{\partial y^2} \right), \tag{5.47}$$

$$Re \, \delta \left[ \frac{\partial \Theta_0}{\partial x} \frac{\partial \psi_0}{\partial y} - \frac{\partial \Theta_0}{\partial y} \frac{\partial \psi_0}{\partial x} \right] = \frac{1}{pr} \frac{\partial^2 \Theta_1}{\partial y^2} + A_1 (\Theta_{1s} - \Theta_1) + 2B_1 \, Ec \left( \frac{\partial \varphi_0}{\partial y} - \frac{\partial \psi_0}{\partial y} \right) \left( \frac{\partial \varphi_1}{\partial y} - \frac{\partial \psi_1}{\partial y} \right) + 2Ec \frac{\partial^2 \psi_1}{\partial y^2} \frac{\partial^2 \psi_0}{\partial y^2}, \tag{5.48}$$

$$\frac{\partial \varphi_0}{\partial y} \frac{\partial \Theta_{0s}}{\partial x} - \frac{\partial \varphi_0}{\partial x} \frac{\partial \Theta_{0s}}{\partial y} = C(\Theta_1 - \Theta_{1s}). \tag{5.49}$$

Boundary conditions are

$$\psi_1 = \frac{F_1}{2}, \ \frac{\partial \psi_1}{\partial y} + \beta \tau_{1xy} = 0, \ \varphi_1 = \frac{E_1}{2}$$
 at  $y = h_1(x)$ , (5.50a)

$$\psi_1 = -\frac{F_1}{2}, \ \frac{\partial \psi_1}{\partial y} - \beta \tau_{1xy} = 0, \ \varphi_1 = -\frac{E_1}{2}$$
 at  $y = h_2(x),$  (5.50b)

$$\Theta_1 - \varepsilon \frac{\partial \Theta_1}{\partial y} = 0$$
 at  $y = h_1(x)$ ,  $\Theta_1 + \varepsilon \frac{\partial \Theta_1}{\partial y} = 0$  at  $y = h_2(x)$ , (5.50c)

$$\Theta_{1s} - \varepsilon \frac{\partial \Theta_{1s}}{\partial y} = 0$$
 at  $y = h_1(x)$ ,  $\Theta_{1s} + \varepsilon \frac{\partial \Theta_{1s}}{\partial y} = 0$  at  $y = h_2(x)$ . (5.50d)

Solution of above system of differential equations has been obtained by applying DSolver command in Mathematica.

# 5.3 Entropy:

The entropy generation is described by the equation

$$S_E = \frac{k^*}{{T_0}^2} \left(\frac{\partial \mathbf{T}}{\partial y}\right)^2 + \frac{\mu}{T_0} \left(\frac{\partial u}{\partial y}\right)^2,$$

with dimensionless form as

$$N_s = \left(\frac{\partial \Theta}{\partial y}\right)^2 + Br.\Delta T \left(\frac{\partial^2 \psi}{\partial y^2}\right)^2$$
,

here  $N_S = \frac{S_E d_1^2 T_0^2}{k^* (T_1 - T_0)^2}$ , Br = Pr. Ec and  $\Delta T = \frac{T_0}{T_1 - T_0}$  represent entropy generation, Brinkman number and non-dimensionalized temperature difference.

The ratio of heat transfer irreversibility and total entropy is represented by Bejan number and given as:

$$Be = \frac{\text{Heat Transfer Irreversibility}}{\text{Total Irreversibility}},$$

$$Be = \frac{\left(\frac{\partial\Theta}{\partial y}\right)^2}{\left(\frac{\partial\Theta}{\partial y}\right)^2 + Br.\Delta T \left(\frac{\partial^2\psi}{\partial y^2}\right)^2}.$$

# 5.4 Graphical Analysis:

This section is reserved for graphical discussion of entropy generation, velocity, and temperature distribution of fluid and particles for various parameters.

#### **5.4.1 Fluid Flow Analysis**

The fluid velocity profile for slip parameter  $\beta$ , wave number  $\delta$ , and Reynolds number Re is plotted in Figs. 5.1-5.3. In Fig. 5.1, fluid flow behavior is discussed for various values of slip parameter  $\beta$ . Decrease in velocity profile is observed as slip parameter  $\beta$  increases. Physically, high values of slip parameter increase resistance that reduces velocity of the fluid. Fig. 5.2 represents results for different values of wave number  $\delta$ . As wave number  $\delta$  increases fluid velocity decreases. The Reynolds number Re impact on velocity behavior is illustrated in Fig. 5.3. Higher values of Reynolds number Re enhance fluid velocity. This is the consequence of dominant inertial forces.

#### **5.4.2 Solid Particle Flow Analysis**

The particle flow behavior for slip parameter  $\beta$ , wave number  $\delta$ , and Reynolds number Re is shown in Figs. 5.4-5.6. In Fig. 5.4, plots are presented for different values of slip parameter  $\beta$ . The increase in slip parameter  $\beta$  causes decline in particle velocity field. The effect of wave number  $\delta$  is depicted in Fig. 5.5. Increase in particle velocity is observed when wave number  $\delta$  increases. Fig. 5.6 is the demonstration of Reynolds number Re effect on particle flow. As Reynolds number Re increases particle velocity is enhanced. Impact of wave number  $\delta$  on particle velocity is opposite to that of fluid velocity.

## **5.4.3 Temperature Distribution Analysis**

Graphs of fluid and particle temperature distribution for wave number  $\delta$ , and Brinkman number Br have been discussed in Figs. 5.7-5.9. In Fig. 5.7, results to demonstrate effect of Brinkman number Br are simulated. Rise in fluid temperature is noticed with the increase in Brinkman number Br. Higher values of Brinkman number imply significant viscous dissipation impact that leads rise in heat transfer. Fig. 5.8 demonstrates the effect of wave number  $\delta$  on fluid temperature

profile. Higher temperature is noticed with the increasing values of wave number  $\delta$ . Behavior of temperature profile for dust particles is depicted in Fig. 5.9 for various values of Brinkman number Br. Temperature of dust particles increases as Brinkman number Br increases. Thus, impact of Brinkman number Br on fluid and particles temperature profile is same.

#### **5.4.4 Entropy Generation**

Entropy generation graphs are plotted for Brinkman number Br, wave number  $\delta$ , and thermal slip parameter  $\varepsilon$  in Figs. 5.10-5.12. In Fig. 5.10, entropy generation is discussed for different values of Brinkman number Br. Increase in entropy generation is observed as Brinkman number Br increases. As entropy generation is directly related to temperature therefore entropy generation also increases due to viscous dissipation impact. Graphical illustration of entropy generation for numerous values of wave number  $\delta$  is presented in Fig. 5.11. As wave number increases, dual results are obtained for entropy generation function. Fig. 5.12 represents effect of thermal slip parameter  $\varepsilon$  on entropy generation. As thermal slip parameter  $\varepsilon$  increases, entropy generation increases.

## 5.4.5 Bejan Number

The plots of Bejan number Be for Brinkman number Br, wave number  $\delta$ , and thermal slip parameter  $\varepsilon$  are shown in Figs. 5.13-5.15. The influence of Brinkman number Br on Bejan number is shown in Fig. 5.13. It can be seen that Bejan number Be decreases as Brinkman number Br increases. The influence of wave number  $\delta$  on Bejan number Be is portrayed in Fig. 5.14. Bejan number declines with the rise in wave number  $\delta$ . Fig. 5.15 exhibits thermal slip parameter  $\varepsilon$  effect on Bejan number Be. Increasing behavior of Bejan number Be is observed for increasing values of thermal slip parameter  $\varepsilon$ .

## **5.4.6 Validation of Present Study**

Fig. 5.16 presents the comparison of recent work with the results obtained by Kothandapani and Srinivas [90]. It shows that graph of velocity profile of fluid obtained in recent chapter exactly matches with the graph obtained by Kothandapani and Srinivas [90].

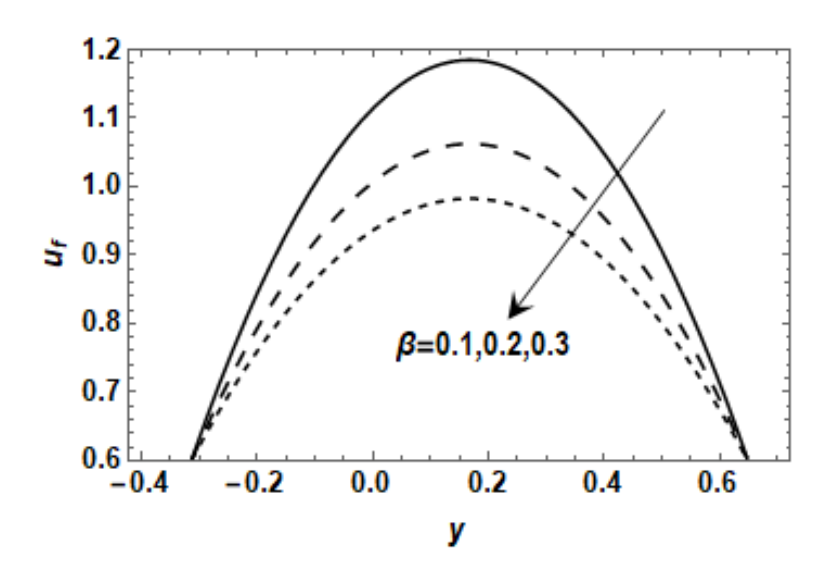
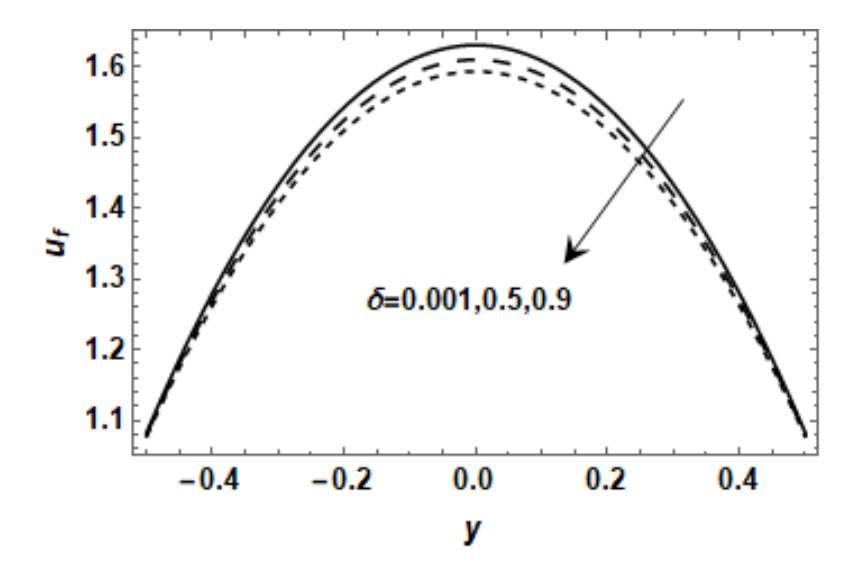
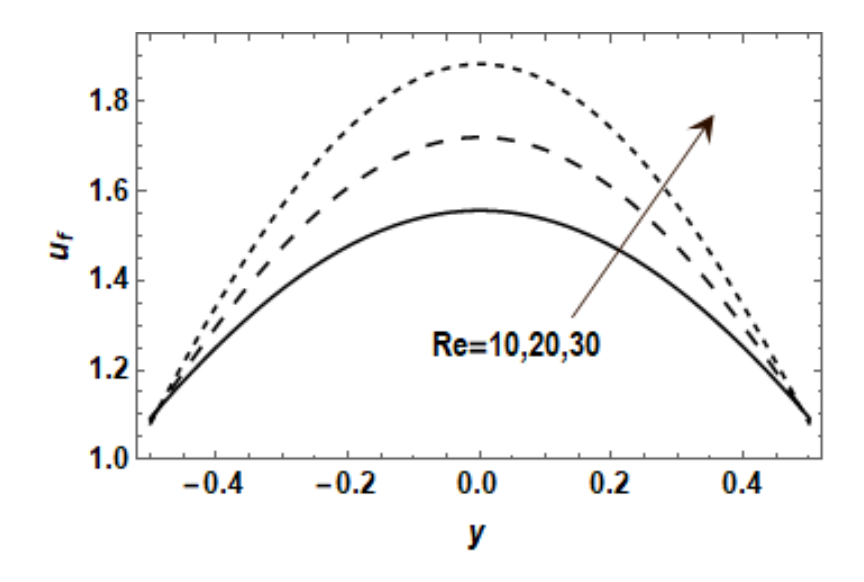


Fig 5.1: The fluid velocity with Re = 0.005, a = 0.3, b = 0.8, d = 0.1,  $\delta = 0.05$ ,  $\phi = \frac{\pi}{4}$ , A = 0.2, B = 0.3.



**Fig 5.2:** The fluid velocity with Re = 0.15, a = 0.2, b = 0.8, d = 0.6,  $\beta = 0.1$ ,  $\phi = \frac{\pi}{6}$ , A = 0.2, B = 0.3.



**Fig 5.3:** The fluid velocity with  $\beta = 0.5$ ,  $\alpha = 0.2$ , b = 0.8, d = 0.6,  $\phi = \frac{\pi}{6}$ , A = 0.2, B = 0.3,  $\delta = 0.2$ .

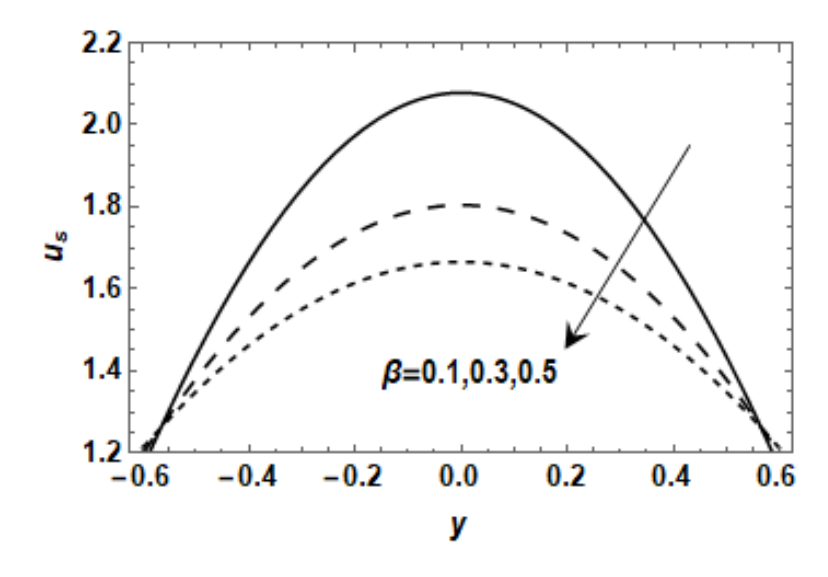


Fig 5.4: The particle velocity with Re = 0.15, a = 0.2, b = 0.8, d = 0.6,  $\phi = \frac{\pi}{6}$ , A = 0.2, B = 0.3,  $\delta = 0.01$ .

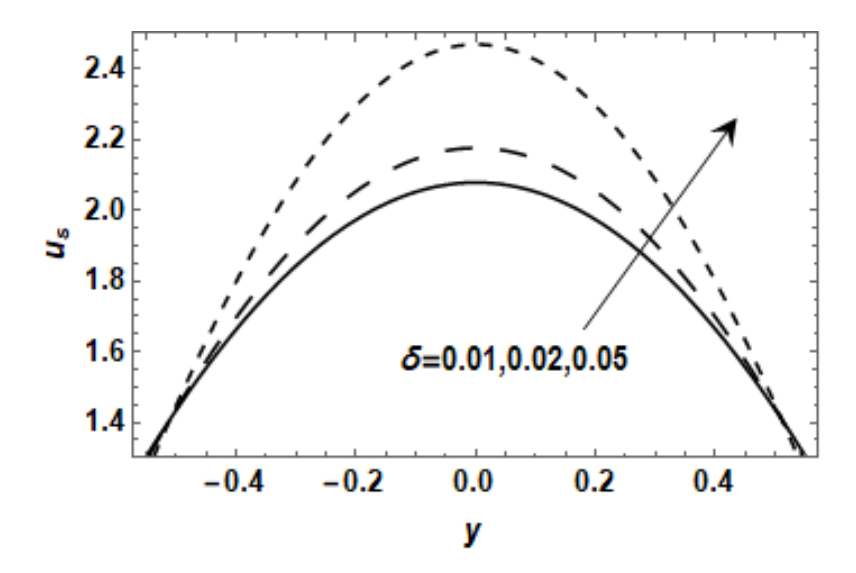


Fig 5.5: The particle velocity with  $\beta = 0.1$ , Re = 0.15, a = 0.2, b = 0.8, d = 0.6,  $\phi = \frac{\pi}{6}$ , A = 0.2, B = 0.3.

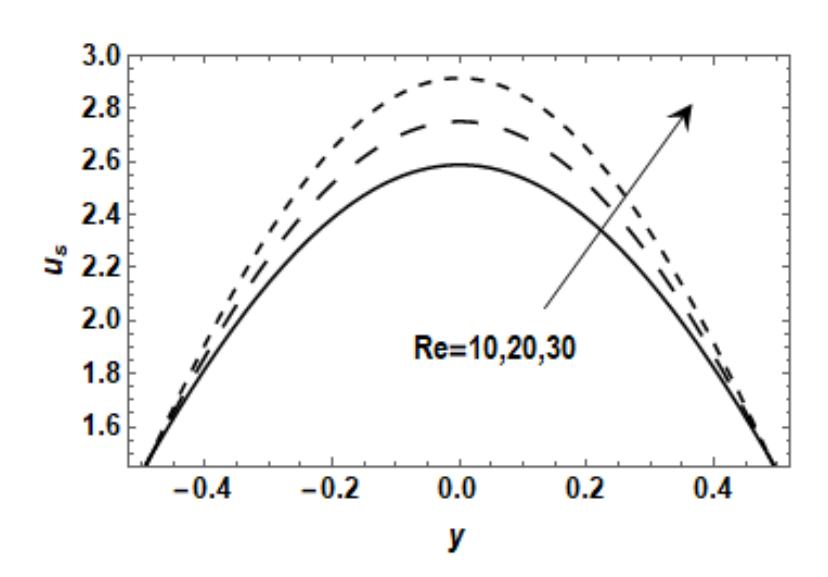
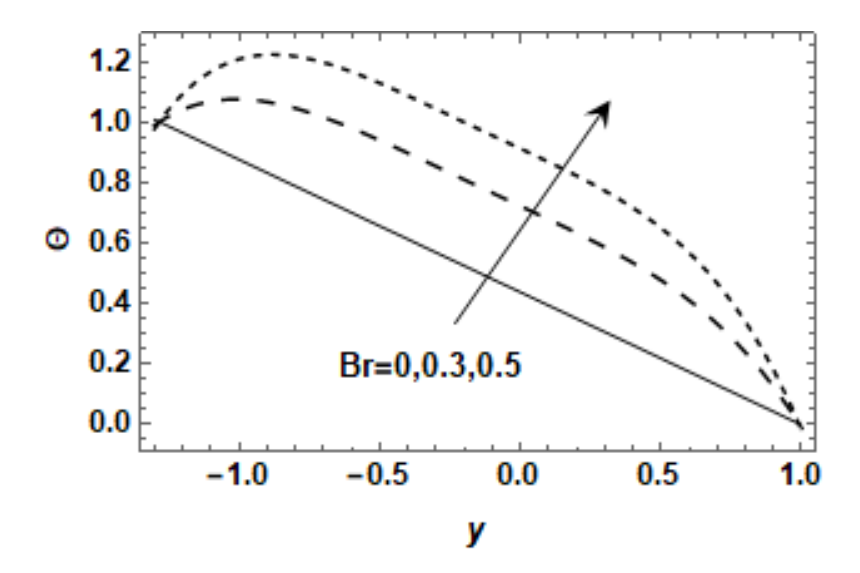
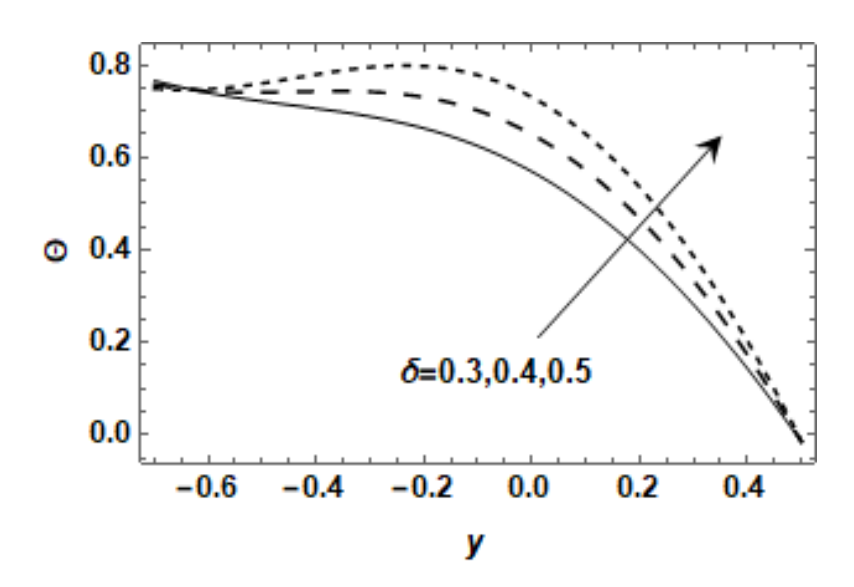


Fig 5.6: The particle velocity with  $\beta = 0.5$ , a = 0.2, b = 0.8, d = 0.6,  $\phi = \frac{\pi}{6}$ , A = 0.2, B = 0.3,  $\delta = 0.2$ .



**Fig 5.7:** Fluid temperature profile with  $Pr = 0.9, Re = 0.2, \beta = 0.2, a = 0.2, b = 0.8, d = 0.6,$   $\delta = 0.01, \varepsilon = 0.01, \phi = \frac{\pi}{3}, A = 0.2, B = 0.3, C = 1.5, B_1 = 0.3, A_1 = 0.5, L = 0.7.$ 



**Fig 5.8:** Fluid temperature profile with Pr = 0.7, Re = 10,  $\beta = 0.2$ , a = 0.2, b = 0.8, d = 0.6, Br = 0.2,  $\varepsilon = 0.4$ ,  $\phi = \frac{\pi}{3}$ , A = 0.2, B = 0.3, C = 0.5,  $B_1 = 0.1$ ,  $A_1 = 0.3$ , L = 0.7.

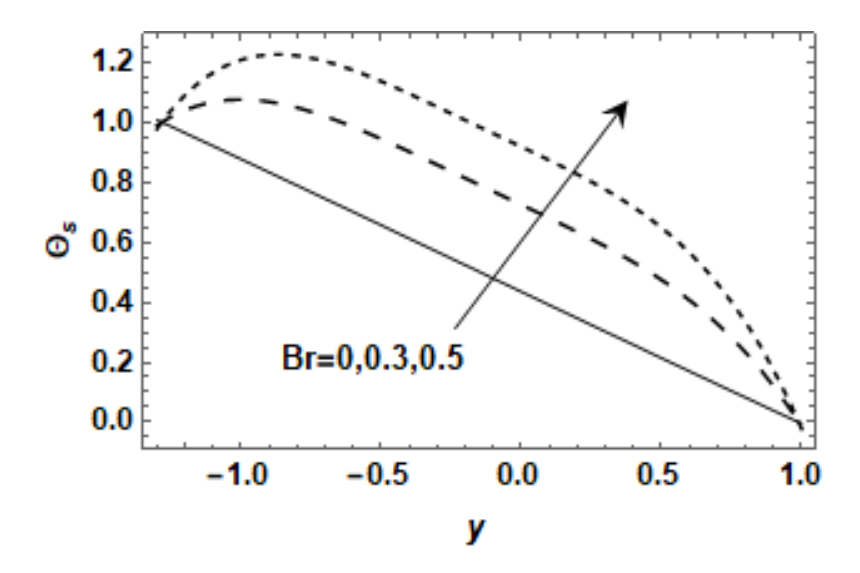
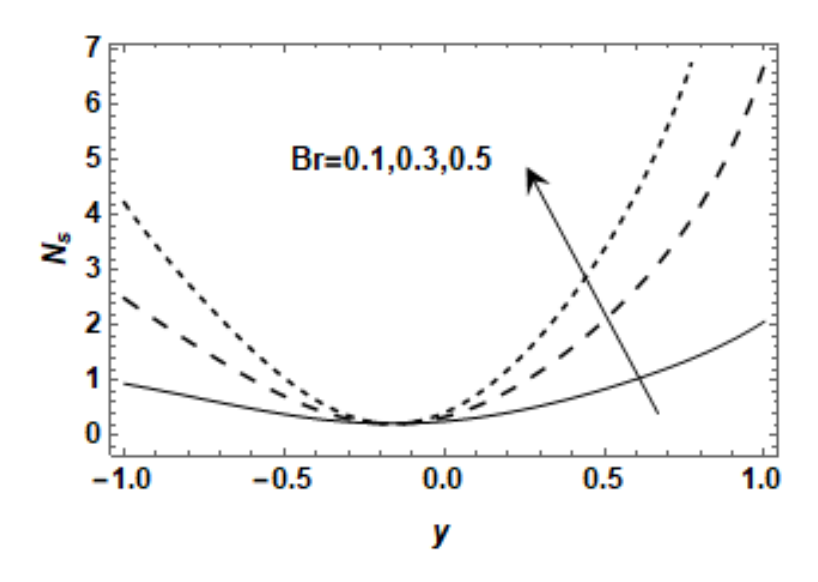
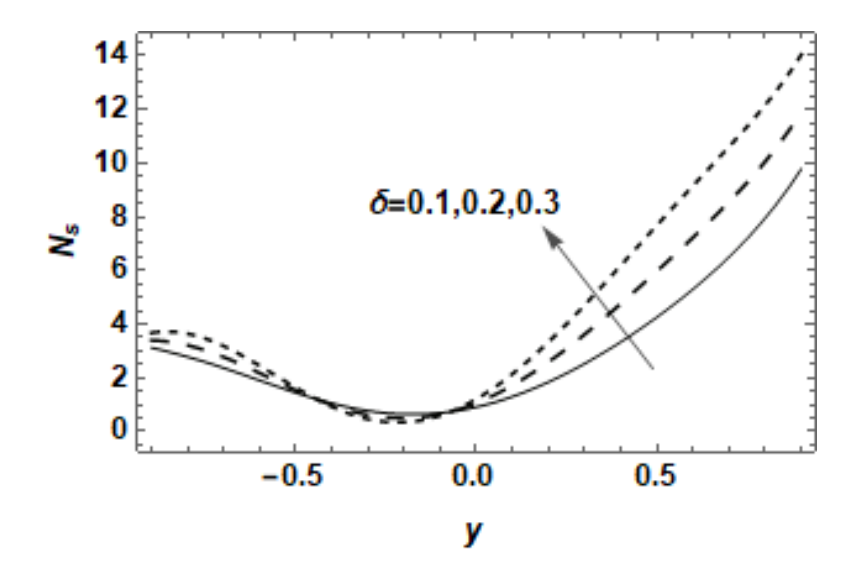


Fig 5.9: Particle temperature profile with  $Pr = 0.9, Re = 2, \beta = 0.2, a = 0.2, b = 0.8, d = 0.6,$   $\delta = 0.01, \varepsilon = 0.01, \phi = \frac{\pi}{3}, A = 0.2, B = 0.3, C = 1.5, B_1 = 0.3, A_1 = 0.5, L = 0.7.$ 



**Fig 5.10:** Entropy generation function with Pr=0.5, Re=0.5,  $\beta=0.2$ ,  $\alpha=0.2$ , b=0.8, d=0.6,  $\delta=0.2$ ,  $\varepsilon=0.1$ ,  $\phi=\frac{\pi}{3}$ , A=0.2, B=0.3, C=0.5,  $B_1=0.5$ ,  $A_1=0.3$ , L=0.7,  $\Delta T=0.9$ .



**Fig 5.11:** Entropy generation function with Pr=0.5, Re=5,  $\beta=0.2$ , a=0.2, b=0.8, d=0.6, Br=0.3,  $\varepsilon=0.5$ ,  $\phi=\frac{\pi}{4}$ , A=0.2, B=0.3, C=0.5,  $B_1=0.5$ ,  $A_1=0.3$ , L=0.7,  $\Delta T=0.9$ .

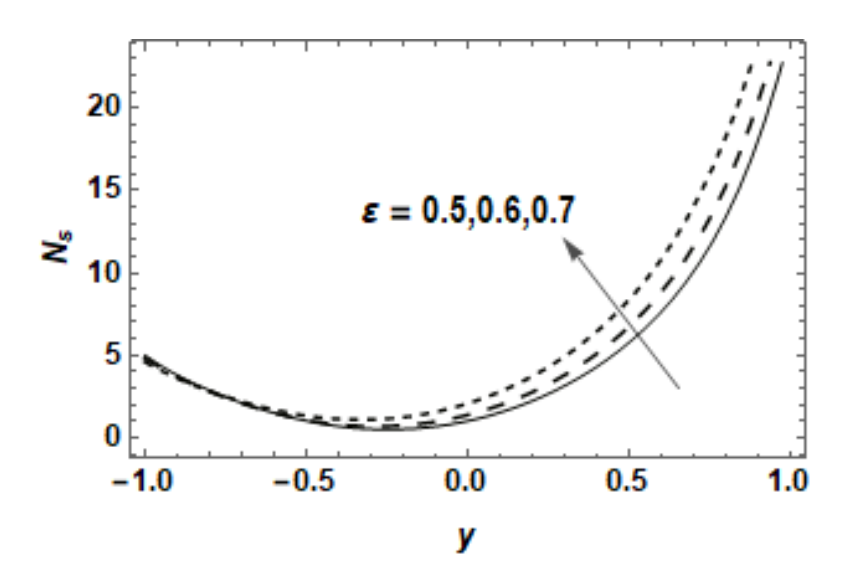


**Fig 5.12:** Entropy generation function with Pr = 0.5, Re = 0.5,  $\beta = 0.2$ ,  $\alpha = 0.2$ , b = 0.8, d = 0.6,  $\delta = 0.2$ , Br = 0.7,  $\phi = \frac{\pi}{3}$ , A = 0.2, B = 0.3, C = 0.5,  $B_1 = 0.5$ ,  $A_1 = 0.3$ , L = 0.7,  $\Delta T = 0.9$ .

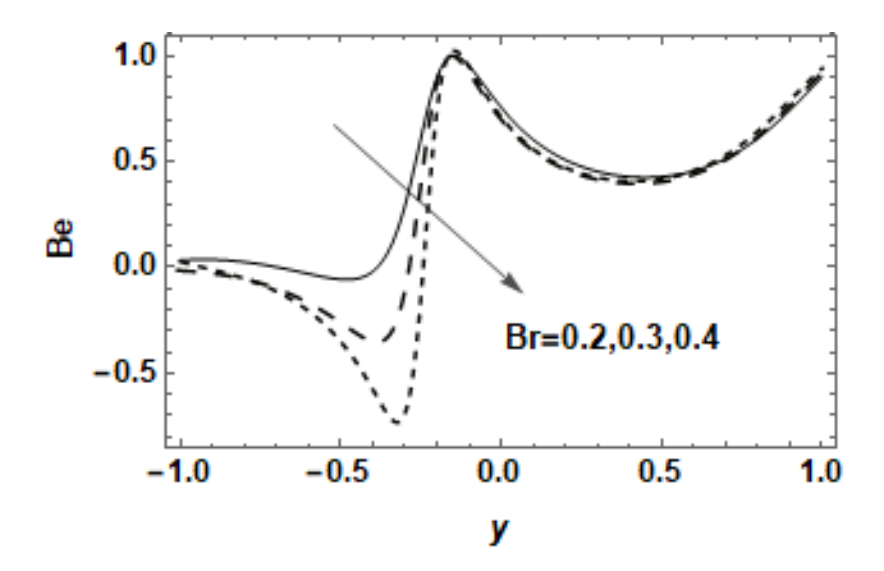


Fig 5.13: Bejan number with Re = 20,  $\beta = 0.2$ ,  $B_1 = 0.5$ ,  $A_1 = 0.3$ ,  $\varepsilon = 0.4$ ,  $\Delta T = 0.9$ , L = 0.7, a = 0.2, b = 0.8, d = 0.6,  $\phi = \frac{\pi}{3}$ , A = 0.2, B = 0.3, C = 0.5, Pr = 0.5,  $\delta = 0.07$ .

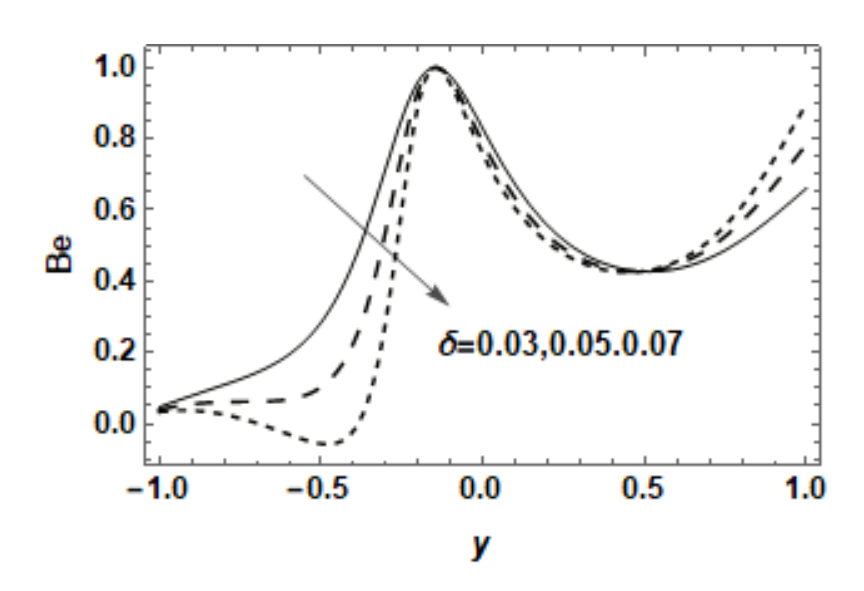


Fig 5.14: Bejan number with Re = 20,  $\beta = 0.2$ ,  $B_1 = 0.5$ ,  $A_1 = 0.3$ ,  $\varepsilon = 0.4$ ,  $\Delta T = 0.9$ , L = 0.7, a = 0.2, b = 0.8, d = 0.6,  $\phi = \frac{\pi}{3}$ , A = 0.2, B = 0.3, C = 0.5, Pr = 0.5, Br = 0.2.

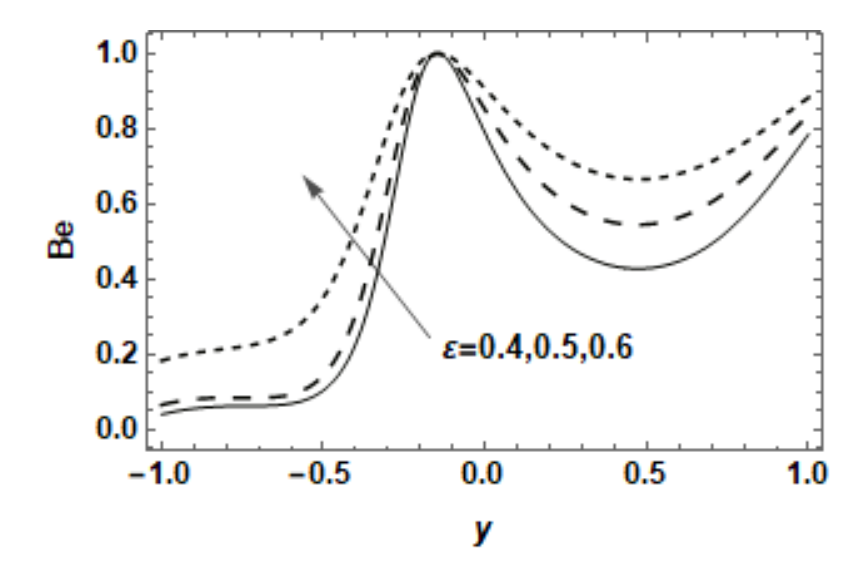
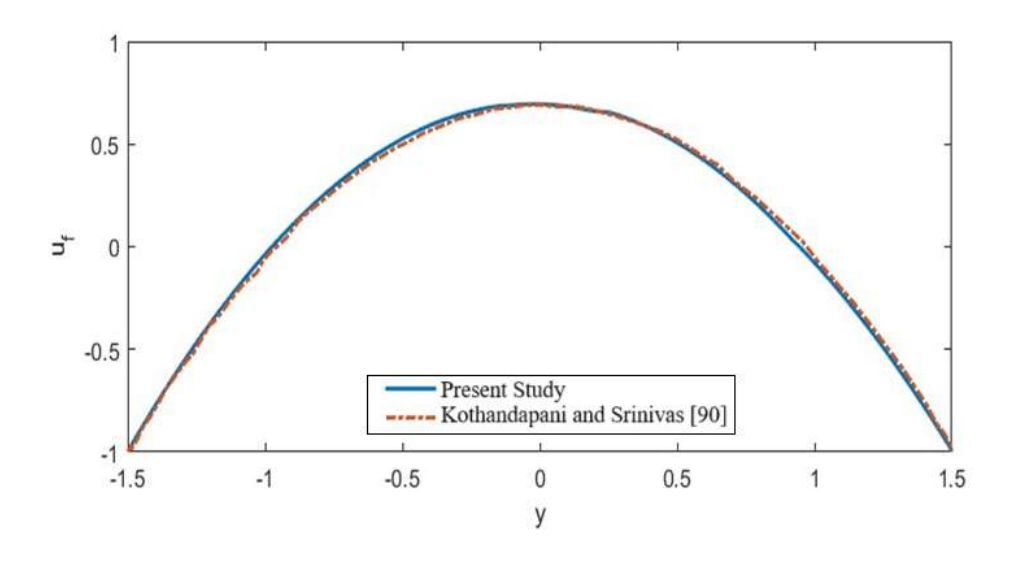


Fig 5.15: Bejan number with Re = 20,  $\beta = 0.2$ ,  $B_1 = 0.5$ ,  $A_1 = 0.3$ ,  $\delta = 0.05$ ,  $\Delta T = 0.9$ , L = 0.7, a = 0.2, b = 0.8, d = 0.6,  $\phi = \frac{\pi}{3}$ , A = 0.2, B = 0.3, C = 0.5, Pr = 0.5, Br = 0.2.



**Fig 5.16:** Comparison of velocity profile for Re = 0,  $\beta = 0$  with the results of Kothandapani and Srinivas [90].

## **5.5 Conclusion**

Effects of wall slip have been discussed for velocity profile of viscous fluid travelling through an asymmetric channel. Simulations to illustrate effects of thermal slip on temperature profile have been presented. Discussion on entropy generation is also included. Some significant results of recent study are listed as:

- Fluid velocity is enhanced by increasing Reynolds number while decreases by increasing slip parameter and wave number.
- Particle velocity increases with increase in Reynolds number and wave number while declines by increasing slip parameter.
- Fluid temperature rises by increasing wave number and Brinkman number. Also, solid particle temperature increases by increasing Brinkman number.
- Entropy generation rate increases by increasing Brinkman number and thermal slip.
- Bejan number decreases by growing Brinkman number and wave number and reducing thermal slip parameter.

# Chapter 6

# Thermal and Magnetic Effects on Second Grade

# **Dusty Liquid with Peristaltic Propagation in**

# **Porous Medium**

The chapter is dedicated for the discussion of heat transfer effects on MHD second grade dusty fluid propelling peristaltically. A porous medium carries the fluid in an asymmetric channel. Stream functions have been introduced to simplify governing equations. Analytic solution of coupled equations has been obtained using perturbation method under small wave number approximation. The results of fluid and dust particle profiles have been debated graphically. Graphs have been employed to carry out comparisons of influential parameters for fluid and solid particle velocity. Furthermore, temperature distribution analysis has been performed for significant quantities. Pressure distribution graphs have also been studied.

## **6.1 Problem Formulation**

A two-dimensional second grade peristaltic fluid with dust particles suspended in it is flowing through a porous medium. The channel is asymmetric of width  $d_1 + d_2$ . An applied magnetic field  $B_0$  is incorporated along y-direction. Sinusoidal wave propagation is deliberated along the boundary walls. The geometry of walls due to sinusoidal waves is expressed by Eqns. (2.1a) and (2.1b).

The Stress tensor  $\tau$  for second grade fluid is

$$\tau = \mu A_1 + \alpha_1 A_2 + \alpha_2 A_1^2, \tag{6.1}$$

where

$$\boldsymbol{A}_{1} = (\nabla \cdot \boldsymbol{V}) + (\nabla \cdot \boldsymbol{V})^{T}, \ \boldsymbol{A}_{2} = \frac{d\boldsymbol{A}_{1}}{dt} + \boldsymbol{A}_{1}(\nabla \cdot \boldsymbol{V}) + (\nabla \cdot \boldsymbol{V})^{T}\boldsymbol{A}_{1}. \tag{6.2}$$

The momentum and energy equations describing fluid flow are

$$\frac{\partial U}{\partial x} + \frac{\partial V}{\partial y} = 0, ag{6.3}$$

$$\rho \left[ \frac{\partial U}{\partial t} + U \frac{\partial U}{\partial X} + V \frac{\partial U}{\partial Y} \right] = -\frac{\partial P}{\partial X} + \frac{\partial \tau_{XX}}{\partial X} + \frac{\partial \tau_{XY}}{\partial Y} + kN(U_s - U) - \frac{\mu}{k_1}U - \sigma B_o^2 U, \tag{6.4}$$

$$\rho \left[ \frac{\partial V}{\partial t} + U \frac{\partial V}{\partial X} + V \frac{\partial V}{\partial Y} \right] = -\frac{\partial P}{\partial Y} + \frac{\partial \tau_{XY}}{\partial X} + \frac{\partial \tau_{YY}}{\partial Y} + kN(V_S - V) - \frac{\mu}{k_1} V, \tag{6.5}$$

$$\rho C_p \left[ \frac{\partial T}{\partial t} + U \frac{\partial T}{\partial x} + V \frac{\partial T}{\partial y} \right] = k^* \left[ \frac{\partial^2 T}{\partial x^2} + \frac{\partial^2 T}{\partial y^2} \right] + \frac{NC_p}{\tau_T} (T_S - T) + \frac{N}{\tau_U} (U_S - U)^2 + \Phi, \tag{6.6}$$

where viscous dissipation is

$$\Phi = \tau_{XX} \frac{\partial U}{\partial X} + \tau_{XY} \frac{\partial U}{\partial Y} + \tau_{YX} \frac{\partial V}{\partial Y} + \tau_{YY} \frac{\partial V}{\partial Y}, \tag{6.7}$$

The momentum and energy equations for dust particles are

$$\frac{\partial U_S}{\partial X} + \frac{\partial V_S}{\partial Y} = 0,\tag{6.8}$$

$$\frac{\partial U_S}{\partial t} + U_S \frac{\partial U_S}{\partial X} + V_S \frac{\partial U_S}{\partial Y} = \frac{k}{m} (U - U_S), \tag{6.9}$$

$$\frac{\partial V_S}{\partial t} + U_S \frac{\partial V_S}{\partial X} + V_S \frac{\partial V_S}{\partial Y} = \frac{k}{m} (V - V_S), \tag{6.10}$$

$$\frac{\partial T_S}{\partial t} + U_S \frac{\partial T_S}{\partial X} + V_S \frac{\partial T_S}{\partial Y} = -\frac{C_p}{C_m} (T_S - T). \tag{6.11}$$

The coordinates (X, Y) in fixed frame of reference are transformed to the coordinates  $(\bar{x}, \bar{y})$  in wave frame of reference by the relation

$$\bar{y} = Y, \bar{x} = X - ct, \bar{v} = V, \bar{u} = U - c, \bar{u}_s = U_s - c, \bar{v}_s = V_s, \bar{p}(x) = P(X, t).$$
 (6.12)

The expressions of stream functions and dimensionless quantities for fluid and solid particles are

$$x = \frac{\bar{x}}{\lambda}, y = \frac{\bar{y}}{d_{1}}, p = \frac{\bar{p}d_{1}^{2}}{\mu\lambda c}, \delta = \frac{d_{1}}{\lambda}, a = \frac{a_{1}}{d_{1}}, b = \frac{a_{2}}{d_{1}}, d = \frac{d_{2}}{d_{1}}, Re = \frac{\rho c d_{1}}{\mu}, \alpha'_{1} = \frac{\alpha_{1} c}{\mu d_{1}}, \alpha'_{2} = \frac{\alpha_{2} c}{\mu d_{1}},$$

$$\tau' = \frac{\tau d_{1}}{\mu c}, Ec = \frac{c^{2}}{C_{p}(T_{1} - T_{0})}, Pr = \frac{\mu C_{p}}{k^{*}}, \Theta = \frac{T - T_{0}}{T_{1} - T_{0}}, \Phi = \frac{d_{1}^{2} \Phi}{c^{2} \mu}, \psi' = \frac{\psi}{c d_{1}}, \varphi' = \frac{\varphi}{c d_{1}}, u = \frac{\partial \psi}{\partial y},$$

$$v = -\delta \frac{\partial \psi}{\partial x}, u_{S} = \frac{\partial \varphi}{\partial y}, v_{S} = -\delta \frac{\partial \varphi}{\partial x}, A = \frac{kNd_{1}^{2}}{\mu}, B = \frac{kd_{1}}{mc}, A_{1} = \frac{Nd_{1}^{2}}{\tau_{T}\mu}, B_{1} = \frac{Nd_{1}^{2}}{\mu\tau_{u}}, M^{2} = \frac{\sigma B_{0}^{2} d_{1}^{2}}{\mu},$$

$$m_{0} = \frac{d_{1}^{2}}{k_{1}}, C = \frac{C_{p}d_{1}}{C_{m}c}, K = m + M^{2},$$

$$(6.13)$$

where a, b, d are non-dimensional lengths describing the channel and  $A, B, C, A_1$ , and  $B_1$  are dimensionless quantities.

Using above quantities, momentum and energy equations become as:

For fluid flow

$$Re \ \delta \left[ \frac{\partial \psi}{\partial y} \frac{\partial^2 \psi}{\partial x \partial y} - \frac{\partial \psi}{\partial x} \frac{\partial^2 \psi}{\partial y^2} \right] = -\frac{\partial p}{\partial x} + \delta \left[ \frac{\partial \tau_{xx}}{\partial x} + \frac{\partial \tau_{xy}}{\partial y} + A \left( \frac{\partial \varphi}{\partial y} - \frac{\partial \psi}{\partial y} \right) - K \left( \frac{\partial \psi}{\partial y} + 1 \right), \tag{6.14}$$

$$Re \,\delta^{3} \left[ \frac{\partial \psi}{\partial x} \, \frac{\partial^{2} \psi}{\partial x \partial y} - \frac{\partial \psi}{\partial y} \frac{\partial^{2} \psi}{\partial x^{2}} \right] = -\frac{\partial p}{\partial x} + \delta^{3} \frac{\partial \tau_{xy}}{\partial x} + \delta^{3} \frac{\partial \tau_{yy}}{\partial y} + \delta^{2} A \left( \frac{\partial \psi}{\partial x} - \frac{\partial \varphi}{\partial x} \right), \tag{6.15}$$

$$Re \, \delta \left[ \frac{\partial \Theta}{\partial x} \frac{\partial \psi}{\partial y} - \frac{\partial \Theta}{\partial y} \frac{\partial \psi}{\partial x} \right] = \frac{1}{pr} \left[ \delta^2 \frac{\partial^2 \Theta}{\partial x^2} + \frac{\partial^2 \Theta}{\partial y^2} \right] + A_1(\Theta_s - \Theta) + B_1 \, Ec \left( \frac{\partial \varphi}{\partial y} - \frac{\partial \psi}{\partial y} \right)^2 + Ec \, \Phi. \tag{6.16}$$

Stresses in terms of stream functions are

$$\tau_{xx} = 2\delta \frac{\partial^2 \psi}{\partial x \partial y} + \alpha_1 \left[ 2\delta^2 \frac{\partial \psi}{\partial y} \frac{\partial^3 \psi}{\partial x^2 \partial y} - 2\delta^2 \frac{\partial \psi}{\partial x} \frac{\partial^3 \psi}{\partial x \partial y^2} + \delta^4 \left( \frac{\partial^2 \psi}{\partial x^2} \right)^2 - \left( \frac{\partial^2 \psi}{\partial y^2} \right)^2 \right], \tag{6.17}$$

$$\tau_{xy} = \left(\frac{\partial^2 \psi}{\partial y^2} - \delta^2 \frac{\partial^2 \psi}{\partial x^2}\right) + \alpha_1 \left[ -\delta^3 \frac{\partial \psi}{\partial y} \frac{\partial^3 \psi}{\partial x^3} + \delta \frac{\partial \psi}{\partial y} \frac{\partial^3 \psi}{\partial x \partial y^2} + \delta^3 \frac{\partial \psi}{\partial x} \frac{\partial^3 \psi}{\partial x^2 \partial y} - \delta \frac{\partial \psi}{\partial x} \frac{\partial^3 \psi}{\partial y^3} + 2\delta \frac{\partial^2 \psi}{\partial y^2} \frac{\partial^2 \psi}{\partial x \partial y} + 2\delta \frac{\partial^2 \psi}{\partial y^2} \frac{\partial^2 \psi}{\partial x \partial y} \right],$$
(6.18)

$$\tau_{yy} = -2\delta \frac{\partial^2 \psi}{\partial x \partial y} + \alpha_1 \left[ -2\delta^2 \frac{\partial \psi}{\partial y} \frac{\partial^3 \psi}{\partial x^2 \partial y} + 2\delta^2 \frac{\partial \psi}{\partial x} \frac{\partial^3 \psi}{\partial x \partial y^2} - \delta^4 \left( \frac{\partial^2 \psi}{\partial x^2} \right)^2 + \left( \frac{\partial^2 \psi}{\partial y^2} \right)^2 \right]. \tag{6.19}$$

Viscous dissipation term in terms of stream function is

$$\Phi = 2\delta^{2} \left(\frac{\partial^{2}\psi}{\partial x\partial y}\right)^{2} + 2\delta^{3} \left(\frac{\partial^{2}\psi}{\partial x\partial y}\right)^{2} + \left(\frac{\partial^{2}\psi}{\partial y^{2}}\right)^{2} - \delta^{2} \frac{\partial^{2}\psi}{\partial x^{2}} \frac{\partial^{2}\psi}{\partial y^{2}} - \delta^{2} \frac{\partial^{2}\psi}{\partial x\partial y} \frac{\partial^{2}\psi}{\partial y^{2}} + \delta^{4} \frac{\partial^{2}\psi}{\partial x^{2}} \frac{\partial^{2}\psi}{\partial x\partial y} + \delta^{4} \frac{\partial^{2}\psi}{\partial x^{2}} \frac{\partial^{2}\psi}{\partial x^{2}} + \delta^{4} \frac{\partial^{2}\psi}{\partial x\partial y} + \delta^{4} \frac{\partial^{2}\psi}{\partial x^{2}} \frac{\partial^{2}\psi}{\partial x^{2}} + \delta^{4} \frac{\partial^{2}\psi}{\partial x\partial y} + \delta^{4} \frac{\partial^{2}\psi}{\partial x^{2}} \frac{\partial^{2}\psi}{\partial x^{2}} + \delta^{4} \frac{\partial^{2}\psi}{\partial x\partial y} + \delta^{4} \frac{\partial^{2}\psi}{\partial x^{2}} \frac{\partial^{2}\psi}{\partial x^{2}} + \delta^{4} \frac{\partial^{2}\psi}{\partial x\partial y} + \delta^{4} \frac{\partial^{2}\psi}{\partial x^{2}} \frac{\partial^{2}\psi}{\partial x^{2}} + \delta^{4} \frac{\partial^{2}\psi}{\partial x\partial y} + \delta^{4} \frac{\partial^{2}\psi}{\partial x^{2}} \frac{\partial^{2}\psi}{\partial x^{2}} + \delta^{4} \frac{\partial^{2}\psi}{\partial x\partial y} + \delta^{4} \frac{\partial^{2}\psi}{\partial x^{2}} \frac{\partial^{2}\psi}{\partial x^{2}} \frac{\partial^{2}\psi}{\partial x^{2}} + \delta^{4} \frac{\partial^{2}\psi}{\partial x^{2}} \frac{\partial^{2}\psi}{\partial x^{$$

For solid particles

$$\frac{\partial \varphi}{\partial y} \frac{\partial^2 \varphi}{\partial x \partial y} - \delta \frac{\partial \varphi}{\partial x} \frac{\partial^2 \varphi}{\partial y^2} = \frac{k}{m} \left( \frac{\partial \psi}{\partial y} - \frac{\partial \varphi}{\partial y} \right), \tag{6.21}$$

$$-\frac{\partial \varphi}{\partial y}\frac{\partial^2 \varphi}{\partial x^2} + \delta \frac{\partial \varphi}{\partial x}\frac{\partial^2 \varphi}{\partial x \partial y} = \frac{k}{m} \left( \frac{\partial \varphi}{\partial x} - \frac{\partial \psi}{\partial x} \right),\tag{6.22}$$

$$\delta\left(\frac{\partial\varphi}{\partial y}\frac{\partial\Theta_S}{\partial x} - \frac{\partial\varphi}{\partial x}\frac{\partial\Theta_S}{\partial y}\right) = -C(\Theta_S - \Theta). \tag{6.23}$$

Compatibility equations are:

For fluid flow

$$Re\left[\delta\left(\frac{\partial\psi}{\partial y}\frac{\partial^3\psi}{\partial y\partial x\partial y}-\frac{\partial\psi}{\partial x}\frac{\partial^3\psi}{\partial y^3}\right)-\delta^3\left(\frac{\partial\psi}{\partial x}\frac{\partial^3\psi}{\partial x\partial y\partial x}-\frac{\partial\psi}{\partial y}\frac{\partial^3\psi}{\partial x^3}\right)\right]=\delta\frac{\partial^2}{\partial x\partial y}\left(\tau_{xx}-\tau_{yy}\right)+\left(\frac{\partial^2}{\partial y^2}-\frac{\partial^2\psi}{\partial y^3}\right)$$

$$\delta^2 \frac{\partial^2}{\partial x^2} \tau_{xy} + A(\nabla_1^2 \varphi - \nabla_1^2 \psi) - K \nabla_1^2 \psi. \tag{6.24}$$

For dust particles

$$\delta \left[ \frac{\partial \varphi}{\partial y} \frac{\partial}{\partial x} \nabla_1^2 \varphi - \frac{\partial \varphi}{\partial x} \frac{\partial}{\partial y} \nabla_1^2 \varphi \right] = B[\nabla_1^2 \psi - \nabla_1^2 \varphi], \tag{6.25}$$

where

$$\nabla_1^2 = \delta^2 \frac{\partial^2}{\partial x^2} + \frac{\partial^2}{\partial y^2}.$$
 (6.26)

The dimensionless description of walls is given by Eqns. (2.25a) and (2.25b).

Boundary conditions in dimensionless form are

$$\psi = \frac{F}{2}, \frac{\partial \psi}{\partial y} + \beta \tau_{xy} = -1, \quad \varphi = \frac{E}{2} \quad \text{at } y = h_1(x), \tag{6.27a}$$

$$\psi = -\frac{F}{2}, \frac{\partial \psi}{\partial y} - \beta \tau_{xy} = -1, \quad \varphi = -\frac{E}{2} \quad \text{at } y = h_2(x), \tag{6.27b}$$

$$\Theta - \varepsilon \frac{\partial \Theta}{\partial y} = 0$$
 at  $y = h_1(x)$ , (6.28a)

$$\Theta + \varepsilon \frac{\partial \Theta}{\partial y} = 1$$
 at  $y = h_2(x)$ . (6.28b)

$$\Theta_s - \varepsilon \frac{\partial \Theta_s}{\partial y} = 0$$
 at  $y = h_1(x)$ , (6.29a)

$$\Theta_s + \varepsilon \frac{\partial \Theta_s}{\partial y} = 1$$
 at  $y = h_2(x)$ . (6.29b)

### **6.2 Method of Solution**

The modeled nonlinear differential equations are evaluated by perturbation method. We use  $\delta$  to express fluid stream function  $\psi$ , particle stream function  $\varphi$ , pressure p, fluid temperature  $\Theta$ , particle temperature  $\Theta_p$ , time flow rate of fluid F, and time flow rate of dust particles E as

$$\psi = \psi_0 + \delta \psi_1 + O(\delta^2), \tag{6.30}$$

$$\varphi = \varphi_0 + \delta \varphi_1 + O(\delta^2), \tag{6.31}$$

$$p = p_0 + \delta p_1 + O(\delta^2), \tag{6.32}$$

$$\Theta = \Theta_0 + \delta\Theta_1 + O(\delta^2), \tag{6.33}$$

$$\Theta_{\rm S} = \Theta_{\rm 0S} + \delta\Theta_{\rm 1S} + O(\delta^2),\tag{6.34}$$

$$F = F_0 + \delta F_1 + O(\delta^2), \tag{6.35}$$

$$E = E_0 + \delta E_1 + O(\delta^2). \tag{6.36}$$

#### 6.2.1 Zeroth Order System

$$\frac{\partial^2 S_{0xy}}{\partial y^2} + A \left( \frac{\partial^2 \varphi_0}{\partial y^2} - \frac{\partial^2 \psi_0}{\partial y^2} \right) - K \frac{\partial^2 \psi_0}{\partial y^2} = 0, \tag{6.37}$$

$$B\left(\frac{\partial^2 \psi_0}{\partial y^2} - \frac{\partial^2 \varphi_0}{\partial y^2}\right) = 0,\tag{6.38}$$

$$\frac{1}{Pr}\frac{\partial^2\Theta_0}{\partial y^2} + B_1 E c \left(\frac{\partial \varphi_0}{\partial y} - \frac{\partial \psi_0}{\partial y}\right)^2 + E c \Phi_0 + A_1(\Theta_{0s} - \Theta_0) = 0, \tag{6.39}$$

$$C(\Theta_{0s} - \Theta_0) = 0, (6.40)$$

where

$$\tau_{0xy} = \frac{\partial^2 \psi_0}{\partial y^2},\tag{6.41}$$

$$\Phi_0 = \left(\frac{\partial^2 \psi_0}{\partial y^2}\right)^2,\tag{6.42}$$

$$\frac{dp_0}{dx} = \frac{\partial \tau_{0xy}}{\partial y} + A \left( \frac{\partial \varphi_0}{\partial y} - \frac{\partial \psi_0}{\partial y} \right) - K \left( \frac{\partial \psi_0}{\partial y} + 1 \right). \tag{6.43}$$

Boundary conditions are

$$\psi_0 = \frac{F_0}{2}, \frac{\partial \psi_0}{\partial y} + \beta \tau_{0xy} = -1, \ \varphi_0 = \frac{E_0}{2}$$
 at  $y = h_1(x)$ , (6.44a)

$$\psi_0 = -\frac{F_0}{2}, \frac{\partial \psi_0}{\partial y} - \beta \tau_{0xy} = -1, \ \varphi_0 = -\frac{E_0}{2}$$
 at  $y = h_2(x)$ , (6.44b)

$$\Theta_0 - \varepsilon \frac{\partial \Theta_0}{\partial y} = 0$$
 at  $y = h_1(x)$ , (6.45a)

$$\Theta_0 + \varepsilon \frac{\partial \Theta_0}{\partial y} = 1$$
 at  $y = h_2(x)$ . (6.45b)

$$\Theta_{0s} - \varepsilon \frac{\partial \Theta_{0s}}{\partial y} = 0$$
 at  $y = h_1(x)$ , (6.46a)

$$\Theta_{0s} + \varepsilon \frac{\partial \Theta_{0s}}{\partial y} = 1$$
 at  $y = h_2(x)$ . (6.46b)

#### 6.2.2 First Order System

$$Re\left(\frac{\partial\psi_0}{\partial y}\frac{\partial^3\psi_0}{\partial x\partial y^2} - \frac{\partial\psi_0}{\partial x}\frac{\partial^3\psi_0}{\partial y^3}\right) = \frac{\partial^2}{\partial x\partial y}\left(\tau_{0xx} - \tau_{0yy}\right) - \frac{\partial^2\tau_{1xy}}{\partial y^2} + A\left(\frac{\partial^2\varphi_1}{\partial y^2} - \frac{\partial^2\psi_1}{\partial y^2}\right) - K\frac{\partial^2\psi_1}{\partial y^2}, \quad (6.47)$$

$$\frac{\partial \varphi_0}{\partial y} \frac{\partial^3 \varphi_0}{\partial x \partial y^2} - \frac{\partial \varphi_0}{\partial x} \frac{\partial^3 \varphi_0}{\partial y^3} = B \left( \frac{\partial^2 \psi_1}{\partial y^2} - \frac{\partial^2 \varphi_1}{\partial y^2} \right), \tag{6.48}$$

$$Re \, \delta \left[ \frac{\partial \Theta_0}{\partial x} \frac{\partial \psi_0}{\partial y} - \frac{\partial \Theta_0}{\partial y} \frac{\partial \psi_0}{\partial x} \right] = \frac{1}{Pr} \frac{\partial^2 \Theta_1}{\partial y^2} + A_1 (\Theta_{1s} - \Theta_1) + 2B_1 \, Ec \left( \frac{\partial \varphi_0}{\partial y} - \frac{\partial \psi_0}{\partial y} \right) \left( \frac{\partial \varphi_1}{\partial y} - \frac{\partial \psi_1}{\partial y} \right) + Ec \, \Phi_1, \tag{6.49}$$

$$\frac{\partial \varphi_0}{\partial y} \frac{\partial \Theta_{0s}}{\partial x} - \frac{\partial \varphi_0}{\partial x} \frac{\partial \Theta_{0s}}{\partial y} = -C(\Theta_{1s} - \Theta_1), \tag{6.50}$$

$$\frac{dp_1}{dx} = -Re\left(\frac{\partial\psi_0}{\partial y}\frac{\partial^2\psi_0}{\partial x\partial y} - \frac{\partial\psi_0}{\partial x}\frac{\partial^2\psi_0}{\partial y^2}\right) + \frac{\partial\tau_{0xx}}{\partial x} + \frac{\partial\tau_{1xy}}{\partial y} + A\left(\frac{\partial\varphi_1}{\partial y} - \frac{\partial\psi_1}{\partial y}\right) - K\left(\frac{\partial\psi_1}{\partial y}\right),\tag{6.51}$$

where

$$\tau_{0yy} = \tau_{0xx} = -\alpha_1 \left(\frac{\partial^2 \psi_0}{\partial y^2}\right)^2,\tag{6.52}$$

$$\tau_{1xy} = \frac{\partial^2 \psi_1}{\partial y^2} + \alpha_1 \left( \frac{\partial \psi_0}{\partial y} \frac{\partial^3 \psi_0}{\partial x \partial y^2} - \frac{\partial \psi_0}{\partial x} \frac{\partial^3 \psi_0}{\partial y^3} + 2 \frac{\partial^2 \psi_0}{\partial y^2} \frac{\partial^2 \psi_0}{\partial x \partial y} \right), \tag{6.53}$$

$$\Phi_{1} = \left(\frac{\partial^{2}\psi_{1}}{\partial y^{2}}\right)^{2} + \alpha_{1} \left(\frac{\partial^{2}\psi_{0}}{\partial x \partial y} \left(\frac{\partial^{2}\psi_{0}}{\partial y^{2}}\right)^{2} + \frac{\partial\psi_{0}}{\partial y} \frac{\partial^{2}\psi_{0}}{\partial y^{2}} \frac{\partial^{3}\psi_{0}}{\partial x \partial y^{2}} - \frac{\partial\psi_{0}}{\partial x} \frac{\partial^{2}\psi_{0}}{\partial y^{2}} \frac{\partial^{3}\psi_{0}}{\partial y^{3}}\right), \tag{6.54}$$

with boundary conditions

$$\psi_1 = \frac{F_1}{2}, \frac{\partial \psi_1}{\partial y} + \beta \tau_{1xy} = 0, \ \varphi_1 = \frac{E_1}{2}$$
 at  $y = h_1(x)$ , (6.55a)

$$\psi_1 = -\frac{F_1}{2}, \frac{\partial \psi_1}{\partial y} - \beta \tau_{1xy} = 0, \ \varphi_1 = -\frac{E_1}{2}$$
 at  $y = h_2(x)$ , (6.55b)

$$\Theta_1 - \varepsilon \frac{\partial \Theta_1}{\partial y} = 0$$
 at  $y = h_1(x)$ , (6.56a)

$$\Theta_1 + \varepsilon \frac{\partial \Theta_1}{\partial y} = 0$$
 at  $y = h_2(x)$ . (6.56b)

$$\Theta_{1s} - \varepsilon \frac{\partial \Theta_{1s}}{\partial y} = 0$$
 at  $y = h_1(x)$ , (6.57a)

$$\Theta_{1s} + \varepsilon \frac{\partial \Theta_{1s}}{\partial y} = 0$$
 at  $y = h_2(x)$ . (6.57b)

Above system of differential equations has been solved by applying DSolver command in Mathematica.

### 6.3 Graphical Analysis

For better illustration of flow behavior, results for fluid velocity, particle velocity, pressure gradient, and temperature distribution have been demonstrated graphically for various parameters in this section.

#### **6.3.1 Fluid Flow Analysis**

Figs. 6.1-6.5 show behavior of fluid velocity for second grade parameter  $\alpha_1$ , slip parameter  $\beta$ , wave number  $\delta$ , porosity parameter  $m_0$ , and Hartman number M. Results for fluid velocity for different values of  $\alpha_1$  are shown in Fig. 6.1. It is noticed that by increasing second grade parameter  $\alpha_1$ , velocity of the fluid increases. Increase in second grade parameter  $\alpha_1$  results in low fluid viscosity therefore fluid flows swiftly. In Fig. 6.2, fluid velocity graphs are drawn to discuss impact of slip parameter  $\beta$ . It portrays that fluid velocity declines by raising  $\beta$ . Thus, slip parameter  $\beta$  and second grade parameter  $\alpha_1$  have opposite impact on velocity of the fluid. Fig. 6.3, depicts variation of velocity profile when wave number  $\delta$  varies. It depicts that increase in wave number  $\delta$  enhances velocity profile significantly. High wave number implies small wavelength. Therefore, frequency of waves along channel walls increases. Physically fluid is squeezed frequently that accelerates the fluid flow. When medium is porous it hinders the velocity of the fluid therefore velocity declines with the rise of porosity parameter  $m_0$  and it is deliberated in Fig. 6.4. Fig. 6.5 is illustration of velocity field under the impact of MHD. Decline in velocity is noticed by growing Hartmann number M. The decreasing behavior of velocity is due to the friction that is incorporated by increasing electromagnetic forces.

#### **6.3.2 Solid Particle Flow Analysis**

Figs. 6.6 and 6.7 demonstrates analysis of particle velocity for second grade parameter  $\alpha_1$  and porosity parameter  $m_0$ . In Fig. 6.6, graphs are plotted for different values of second grade parameter  $\alpha_1$ . It expresses increasing trend of velocity profile with enhancement of  $\alpha_1$ . Fig. 6.7 represents particle velocity trend under the effect of porous parameter  $m_0$ . Increasing behavior of particle velocity is observed when porosity increases. In contrast to velocity profile, porosity  $m_0$  and second grade parameter  $\alpha_1$  have minimal effects on solid particle velocity.

#### **6.3.3 Pressure Gradient Graphs**

Pressure gradient graphs versus x are plotted in Figs. 6.8-6.10 for several values of second grade parameter  $\alpha_1$ , slip parameter  $\beta$ , and wave number  $\delta$ . In Fig. 6.8, plots are drawn for various values of  $\alpha_1$ . With an increase in  $\alpha_1$ , the pressure gradient decreases. Fig. 6.9 provides a graphic representation of how slip parameter affects pressure gradient. Pressure gradient decreases as  $\beta$  grows. The influence of wave number  $\delta$  on pressure gradient is discussed in Fig. 6.10 by drawing graphs for different values of  $\delta$ . Pressure gradient declines as  $\delta$  increases.

### **6.3.4** Temperature Distribution Analysis

For fluid, temperature distribution graphs for wave number  $\delta$ , Eckert number Ec, and Reynolds number Re have been discussed in Figs. 6.11-6.13. Parabolic behavior is observed in presence of slip. In Fig. 6.11, graphs are presented for different values of Eckert number Ec. It is noticed that fluid temperature rises when Eckert number Ec increases. Eckert number Ec is the ratio of fluid kinetic energy to enthalpy driving force. The increasing trend of Eckert number Ec implies higher kinetic energy due to higher fluid velocity relative to temperature difference at the walls. The presence of viscous dissipation converts this kinetic energy into heat that results increase in fluid

temperature. In Fig. 6.12, graphs are plotted for several values of wave number  $\delta$ . Increase in temperature is observed when wave number increases. It is noticed that effect of wave number  $\delta$  on temperature distribution is same as on velocity distribution. Fig. 6.13 is graphical representation of temperature distribution for Reynolds number Re. It illustrates that temperature decreases as Reynolds number Re increases. This is consequence of low viscosity.

Graphs of temperature distribution for solid particle for wave number  $\delta$  and Eckert number Ec have been drawn in Figures 6.14 and 6.15. Fig. 6.14 demonstrates effect of wavenumber on temperature of solid particles. As wavenumber increases, temperature also increases. In Fig. 6.15, effect of Eckert number Ec on particle temperature profile has been shown. Higher temperature is observed for higher values of Ec. The impact of wave number  $\delta$  and Eckert number Ec on particle temperature is same as on fluid temperature.

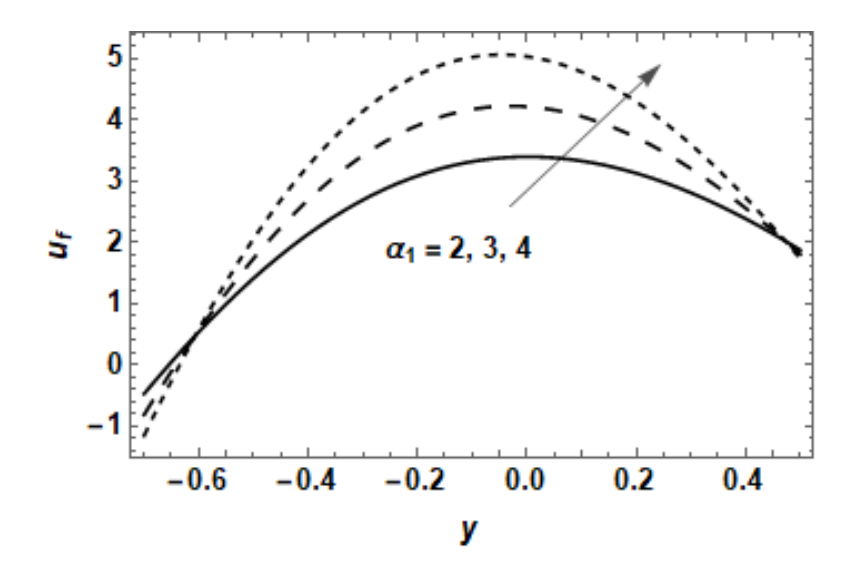
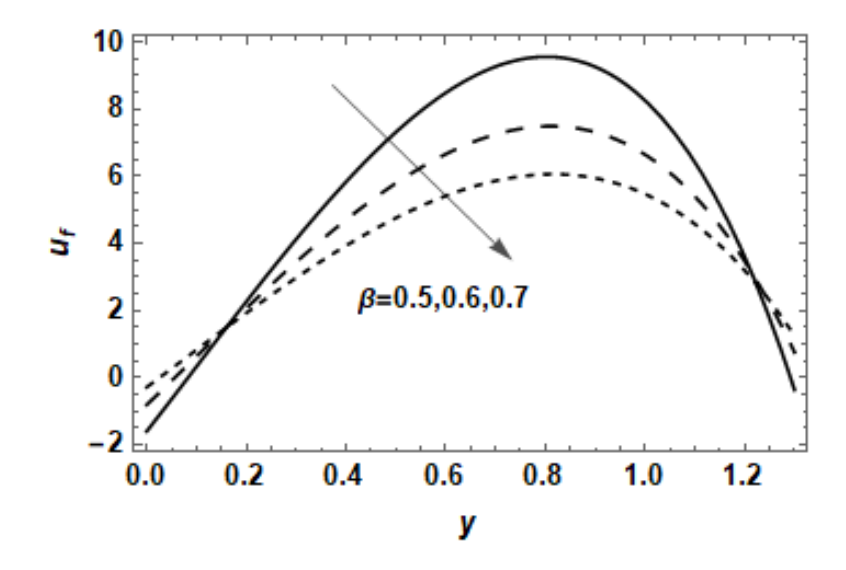


Fig 6.1: The fluid velocity with  $\beta=0.2$ , Re=0.15,  $m_0=0.1$ , M=0.5,  $\alpha=0.2$ , b=0.8, d=0.3,  $\delta=0.01$ ,  $\phi=\frac{\pi}{3}$ , A=0.2, B=0.1.



**Fig 6.2:** The fluid velocity with Re = 0.3,  $m_0 = 0.01$ , M = 0.4, a = 0.2, b = 0.6, d = 0.3,  $\delta = 0.01$ ,  $\phi = \frac{\pi}{6}$ , A = 0.1, B = 0.1,  $\alpha_1 = 0.2$ .

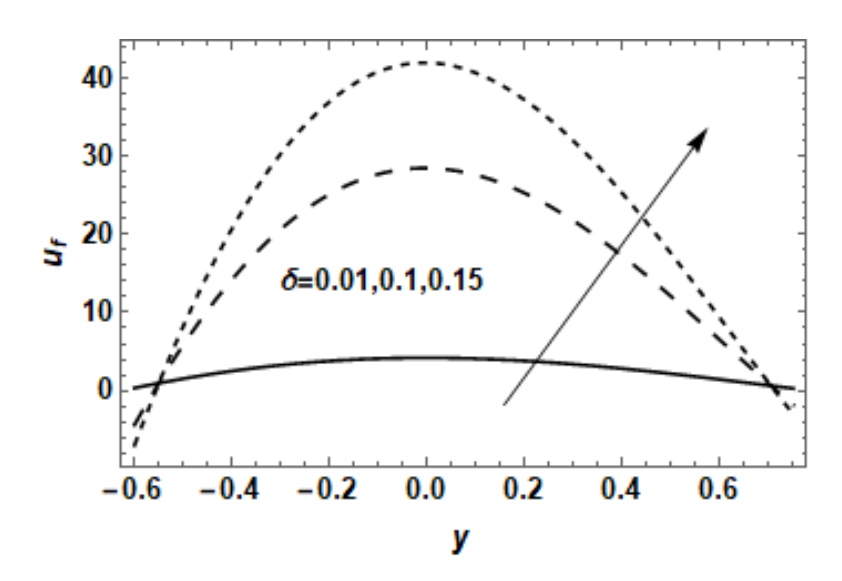


Fig 6.3: The fluid velocity with  $\beta = 0.2$ , Re = 0.15, K = 0.3, a = 0.2, b = 0.8, d = 0.3,  $\phi = \frac{\pi}{3}$ , A = 0.2, B = 0.1,  $\alpha_1 = 2$ .

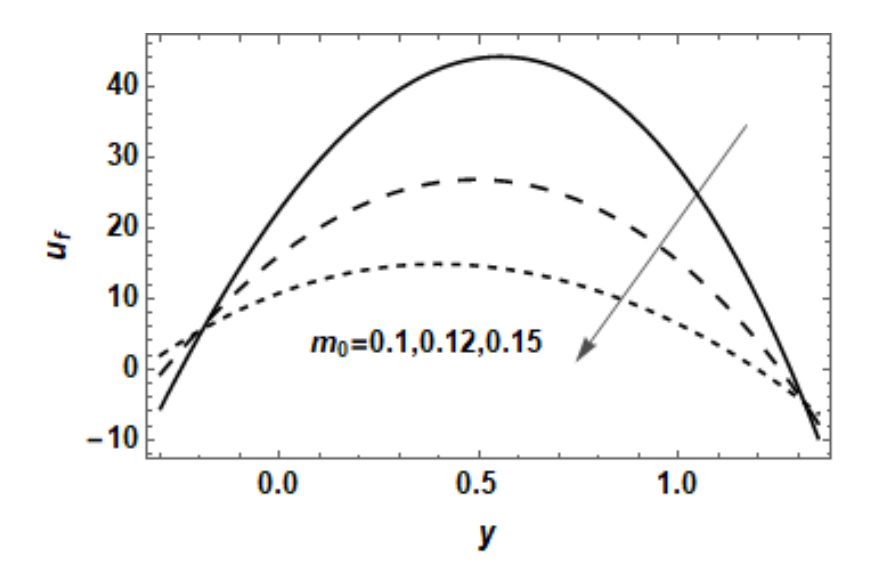


Fig 6.4: The fluid velocity with  $\beta = 0.2$ , Re = 0.15,  $m_0 = 0.1$ , a = 0.3, b = 0.8, d = 0.3,  $\phi = \frac{\pi}{3}$ , A = 0.2, B = 0.1,  $\alpha_1 = 2$ ,  $\delta = 0.01$ .

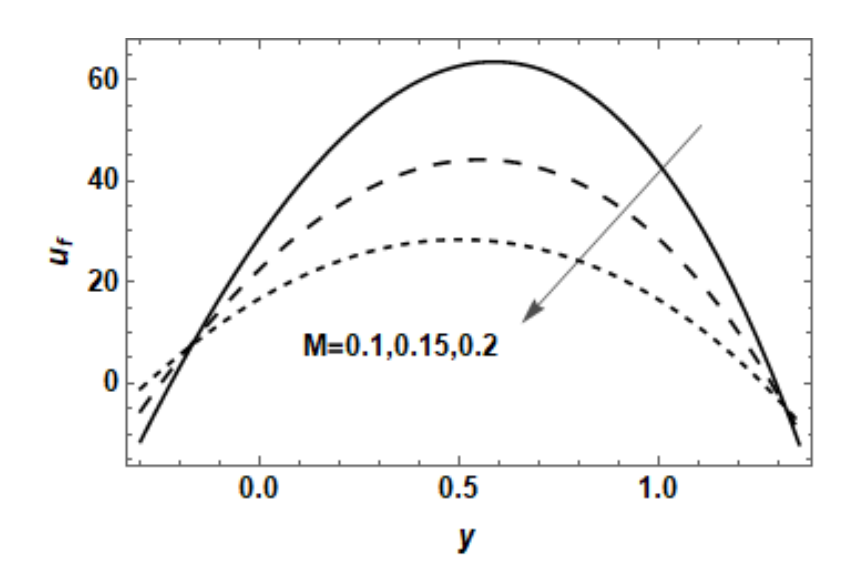


Fig 6.5: The fluid velocity with  $\beta = 0.2$ , Re = 0.15, M = 0.15,  $\alpha = 0.3$ , b = 0.8, d = 0.3,  $\phi = \frac{\pi}{3}$ , A = 0.2, B = 0.1,  $\alpha_1 = 2$ ,  $\delta = 0.01$ .

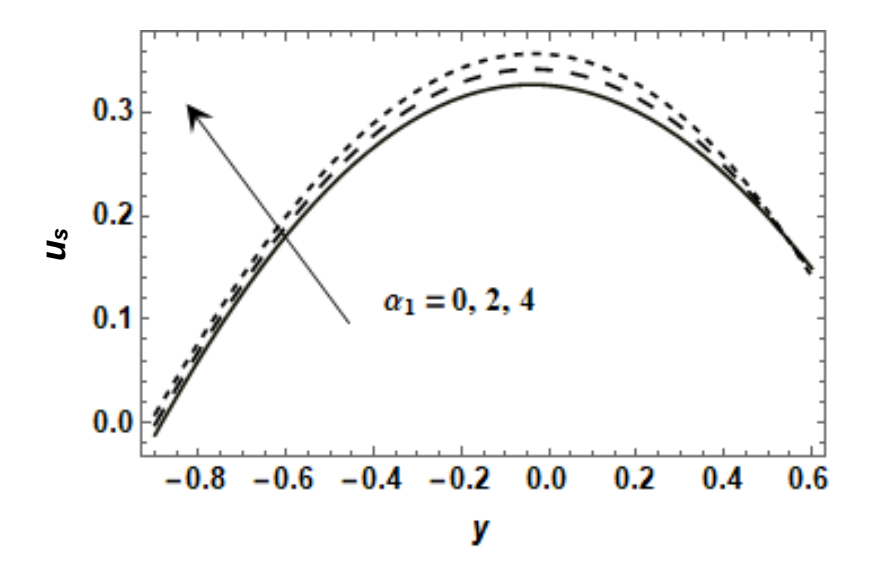


Fig 6.6: The particle velocity with  $\beta=0.6$ , Re=0.15, a=0.2, b=0.5, d=0.9,  $\phi=\frac{\pi}{6}$ , A=0.6, B=0.8,  $\delta=0.01$ ,  $m_0=0.3$ , M=0.5.

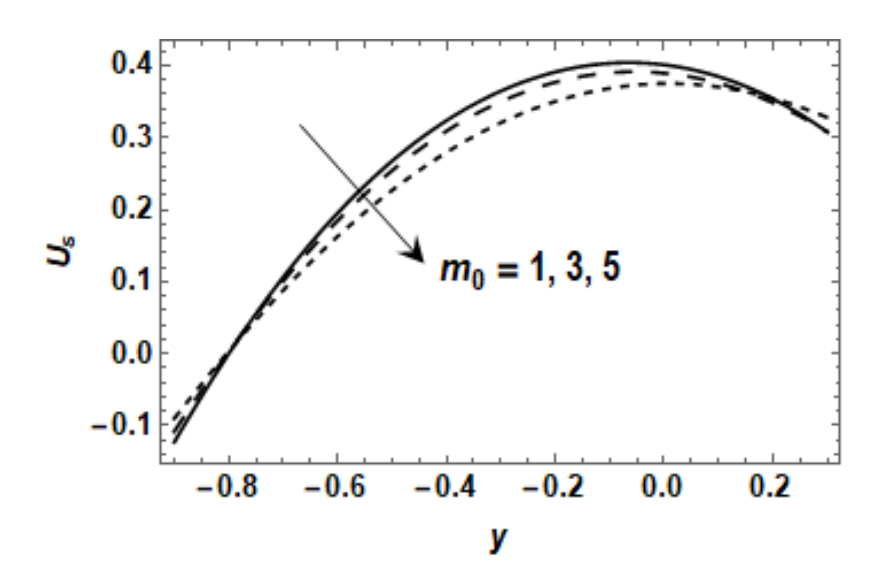


Fig 6.7: The particle velocity with  $\beta = 0.4$ , Re = 0.15, M = 0.1, a = 0.3, b = 0.5, d = 0.9,  $\phi = \frac{\pi}{6}$ , A = 0.6, B = 0.8,  $\alpha_1 = 2$ ,  $\delta = 0.01$ .

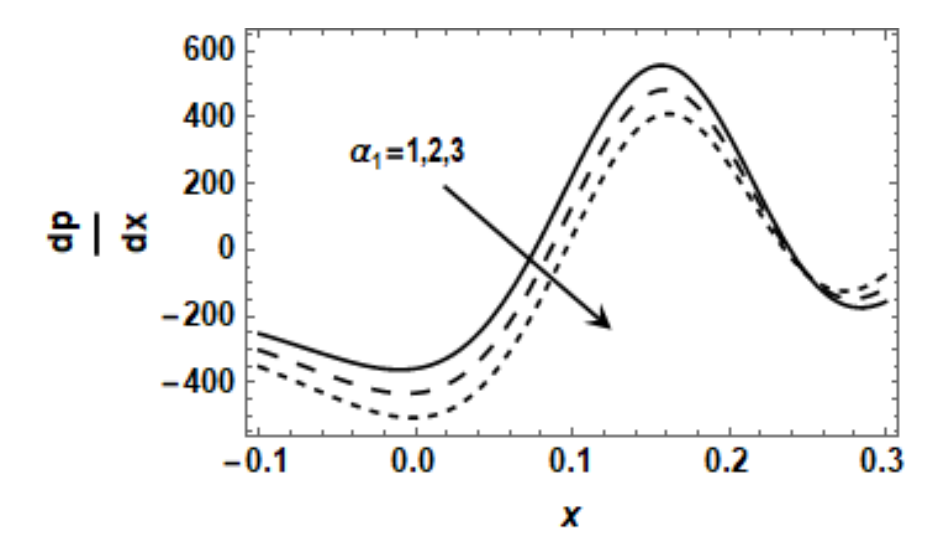


Fig 6.8: The pressure gradient with  $\beta = 0.1$ , Re = 0.1, a = 0.2, b = 0.4, d = 0.6,  $\phi = \frac{\pi}{6}$ , A = 0.9, B = 1.5,  $\delta = 0.01$ , K = 40.

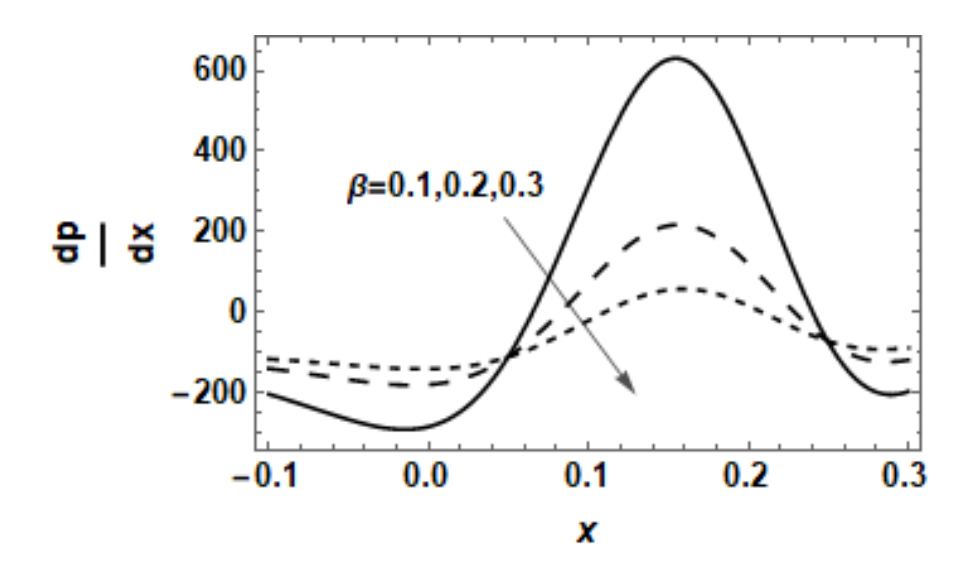


Fig 6.9: The pressure gradient with  $\delta = 0.01, Re = 0.1, a = 0.2, b = 0.4, d = 0.6, \phi = \frac{\pi}{6},$   $A = 0.9, B = 1.5, \alpha_1 = 0.01, K = 40.$ 

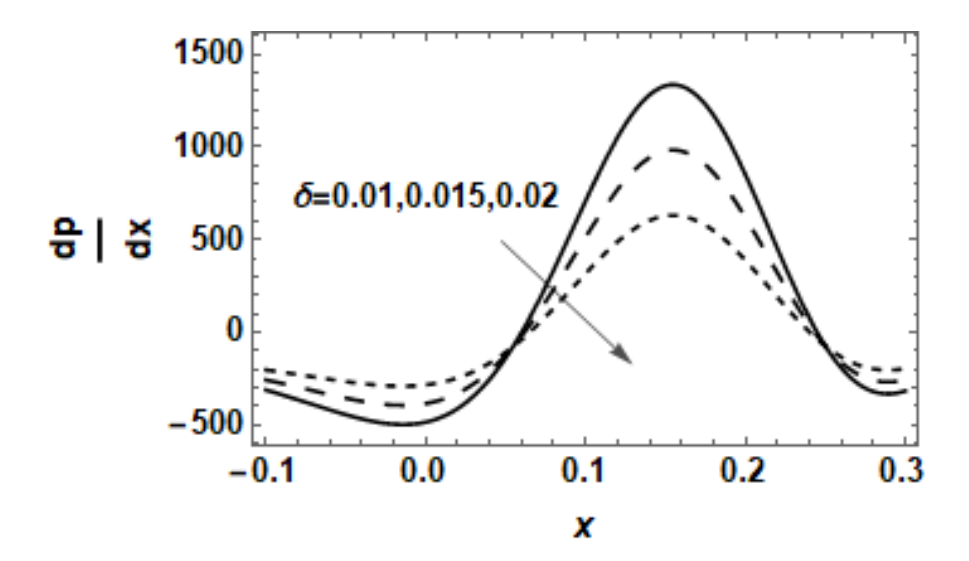
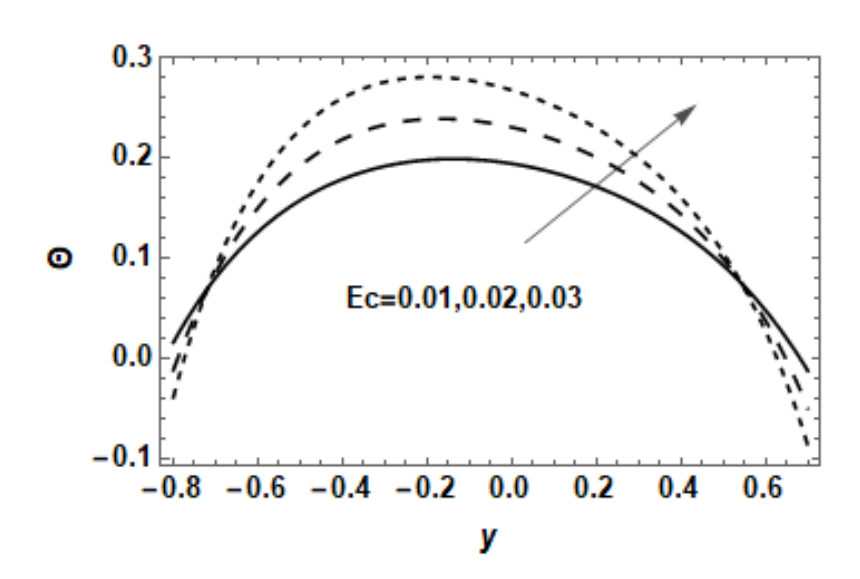
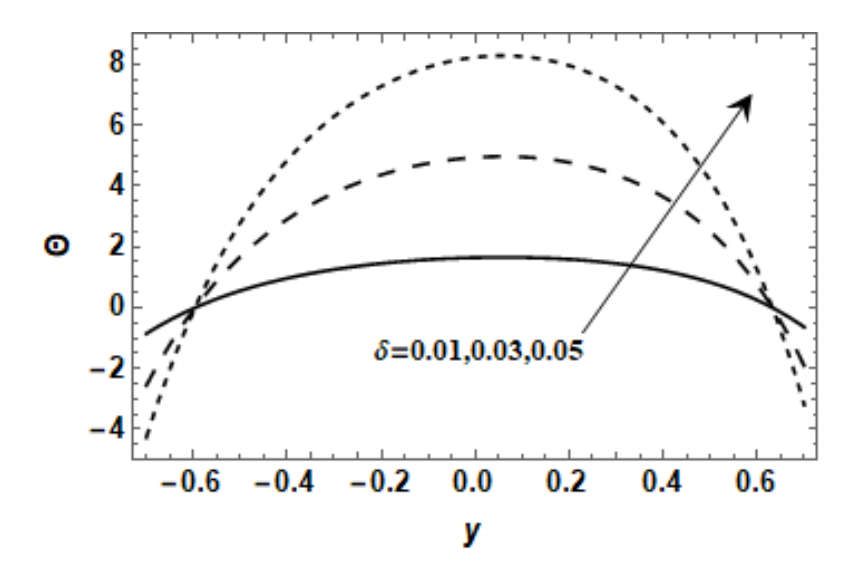


Fig 6.10: The pressure gradient with  $\beta = 0.1$ , Re = 0.1, a = 0.2, b = 0.4, d = 0.6,  $\phi = \frac{\pi}{6}$ , A = 0.9, B = 1.5,  $\alpha_1 = 0.01$ , K = 40.



**Fig 6.11:** Temperature distribution with Pr=0.03, Re=0.2,  $B_1=0.5$ ,  $\beta=0.2$ , K=0.5,  $\alpha=0.3$ , b=0.5, d=0.9,  $\delta=0.01$ ,  $\varepsilon=0.2$ ,  $\phi=\frac{\pi}{6}$ , A=0.6, B=0.8,  $\alpha_1=2$ .



**Fig 6.12:** Temperature distribution with Pr = 0.1, Re = 0.2, Ec = 0.02,  $B_1 = 0.5$ ,  $\beta = 0.2$ ,  $\varepsilon = 0.2$ , K = 0.5,  $\alpha = 0.3$ , b = 0.4, d = 0.6,  $\phi = \frac{\pi}{3}$ , A = 0.5, B = 0.8,  $\alpha_1 = 2$ .

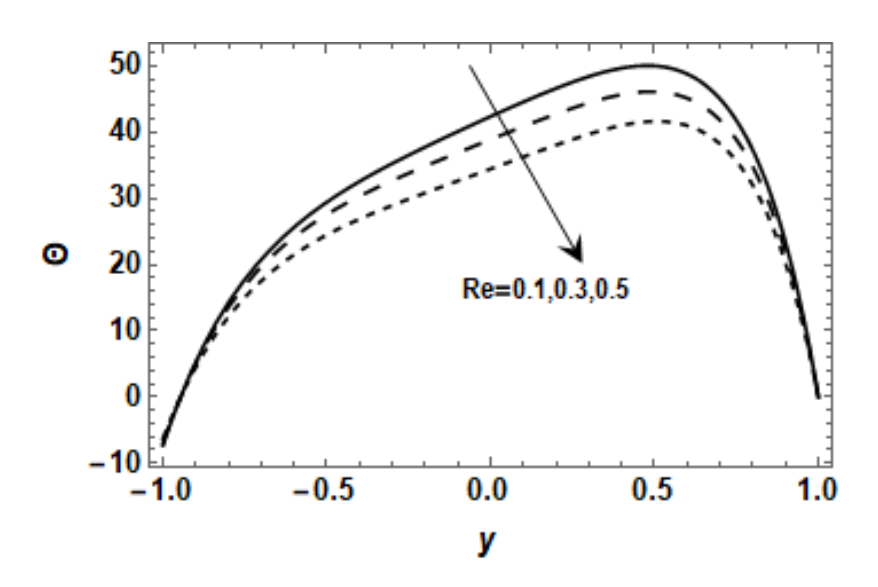


**Fig 6.13:** Temperature distribution with Pr = 0.07, Ec = 0.02,  $B_1 = 0.5$ ,  $\beta = 0$ , K = 0.5,  $\alpha = 0.3$ , b = 0.4, d = 0.6,  $\delta = 0.01$ ,  $\phi = \frac{\pi}{3}$ , A = 0.5, B = 0.8,  $\alpha_1 = 2$ ,  $\varepsilon = 0$ .

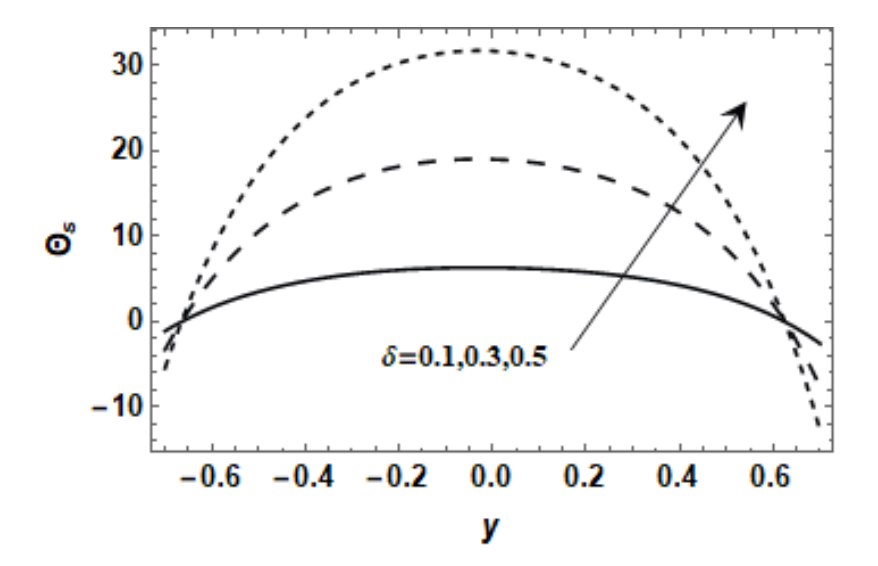


Fig 6.14: Particle temperature distribution with Re = 0.2, Ec = 0.02,  $B_1 = 0.5$ ,  $\beta = 0.2$ , K = 0.5,  $\alpha = 0.3$ , b = 0.5, d = 0.6,  $\phi = \frac{\pi}{3}$ , A = 0.5, B = 0.8,  $\alpha_1 = 2$ ,  $\varepsilon = 0.2$ , C = 5, Pr = 0.03.

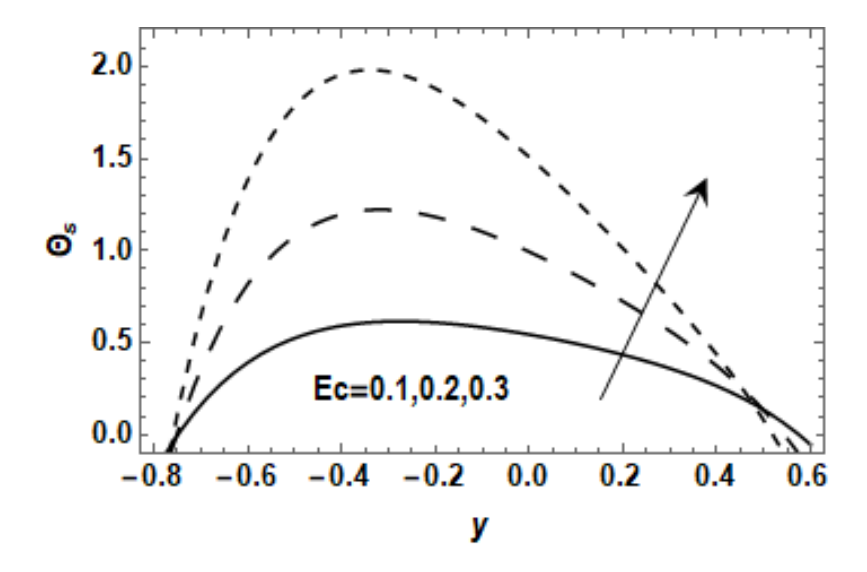


Fig 6.15: Re = 0.2, Pr = 0.03,  $B_1 = 0.5$ ,  $\beta = 0.2$ , K = 0.5, a = 0.3, b = 0.5, d = 0.9,  $\delta = 0.01$ ,  $\phi = \frac{\pi}{6}$ , A = 0.6, B = 0.8,  $\alpha_1 = 2$ ,  $\varepsilon = 0.2$ , C = 5.

## **6.4 Conclusion**

The current investigation highlights the impacts of heat transfer on the flow of second-grade dusty fluid with peristalsis. In an asymmetric channel, fluid is considered to propagate through a porous media. Some important findings of the study are listed as follows:

- Fluid is accelerated by increasing second grade parameter and wave number while decreases by increasing slip parameter and porosity.
- Particle velocity increases by increasing second grade parameter and porosity.
- Pressure gradient decreases by increasing wave number, slip parameter and second grade parameter.
- Fluid temperature rises by increasing Eckert number and wave number. Temperature declines by increasing Reynolds number.
- Particle temperature rises by increasing Eckert number and wave number.

# Chapter 7

# Theoretical Analysis of Peristaltic Dusty Fluid

# under Temperature Varying Thermal

# **Conductivity and Viscosity Passing Through**

# **Curved Geometry**

This chapter presents an analysis of a Newtonian fluid with viscosity dependent upon temperature. The fluid is assumed to pass through a peristaltic curved channel. Moreover, thermal conductivity also varies with temperature. Boundary conditions considered are convective. The ruling equations under prescribed assumptions are nonlinear and therefore solved numerically using Mathematica. The simulations for velocity and temperature of fluid and particles are discussed under the effect of various physical properties.

### 7.1 Problem Formulation

We consider Newtonian fluid flow with solid spherical particles dispersed in the fluid. Channel has curved walls propagating peristaltically. Viscosity and thermal conductivity depend upon temperature. Convective boundary conditions are considered at the walls of the curved channel. Peristaltic wave along the walls is travelling with speed c, wave length  $\lambda$  and amplitude b. Under above assumption, mathematical expression of the walls is given by Eqns. (3.1) and (3.2).

The equations for the fluid flow and heat transfer are:

$$R^* \frac{\partial \bar{U}}{\partial \bar{X}} + \frac{\bar{V}}{(\bar{R} + R^*)} + (\bar{R} + R^*) \frac{\partial \bar{V}}{\partial \bar{R}} = 0, \tag{7.1}$$

$$\rho\left(\frac{\partial \overline{V}}{\partial t} + \overline{V}\frac{\partial \overline{V}}{\partial \overline{R}} + \frac{R^*}{\overline{R} + R^*}\overline{U}\frac{\partial \overline{V}}{\partial \overline{X}} - \frac{\overline{U}^2}{\overline{R} + R^*}\right) = \frac{1}{\overline{R} + R^*}\frac{\partial}{\partial \overline{R}}\left(2(\overline{R} + R^*)\mu(\overline{T})\frac{\partial \overline{V}}{\partial \overline{R}}\right) + \frac{R^*}{\overline{R} + R^*}\frac{\partial}{\partial \overline{X}}\left(\mu(\overline{T})\left(\frac{R^*}{\overline{R} + R^*}\frac{\partial \overline{V}}{\partial \overline{X}} + \frac{R^*}{\overline{R} + R^*}\frac{\partial}{\partial \overline{X}}\right)\right)$$

$$\frac{\partial \bar{U}}{\partial \bar{R}} - \frac{\bar{U}}{\bar{R} + R^*} \bigg) - \frac{2\mu(\bar{T})}{\bar{R} + R^*} \bigg( \frac{R^*}{\bar{R} + R^*} \frac{\partial \bar{U}}{\partial \bar{X}} + \frac{\bar{V}}{\bar{R} + R^*} \bigg) - \frac{\partial \bar{P}}{\partial \bar{R}} + kN(\bar{V}_S - \bar{V}), \tag{7.2}$$

$$\rho\left(\frac{\partial \overline{U}}{\partial t} + \overline{V}\frac{\partial \overline{U}}{\partial \overline{R}} + \frac{R^*}{\overline{R} + R^*}\overline{U}\frac{\partial \overline{U}}{\partial \overline{X}} + \frac{\overline{U}\overline{V}}{\overline{R} + R^*}\right) = \frac{1}{(\overline{R} + R^*)^2}\frac{\partial}{\partial \overline{R}}\left((\overline{R} + R^*)^2\mu(\overline{T})\left(\frac{R^*}{\overline{R} + R^*}\frac{\partial \overline{V}}{\partial \overline{X}} - \frac{\overline{U}}{\overline{R} + R^*} + \frac{\partial \overline{U}}{\partial \overline{R}}\right)\right) + \frac{1}{(\overline{R} + R^*)^2}\frac{\partial}{\partial \overline{R}}\left((\overline{R} + R^*)^2\mu(\overline{T})\left(\frac{R^*}{\overline{R} + R^*}\frac{\partial \overline{V}}{\partial \overline{X}} - \frac{\overline{U}}{\overline{R} + R^*} + \frac{\partial \overline{U}}{\partial \overline{R}}\right)\right) + \frac{1}{(\overline{R} + R^*)^2}\frac{\partial}{\partial \overline{R}}\left((\overline{R} + R^*)^2\mu(\overline{T})\left(\frac{R^*}{\overline{R} + R^*}\frac{\partial \overline{V}}{\partial \overline{X}} - \frac{\overline{U}}{\overline{R} + R^*}\right)\right)$$

$$\frac{R^*}{\bar{R}+R^*} \frac{\partial}{\partial \bar{X}} \left( 2\mu(\bar{T}) \left( \frac{R^*}{\bar{R}+R^*} \frac{\partial \bar{U}}{\partial \bar{X}} + \frac{\bar{V}}{\bar{R}+R^*} \right) \right) - \frac{R^*}{\bar{R}+R^*} \frac{\partial \bar{P}}{\partial \bar{X}} + kN(\bar{U}_S - \bar{U}), \tag{7.3}$$

$$\rho C_P \left( \frac{\partial \bar{T}}{\partial t} + \bar{V} \frac{\partial \bar{T}}{\partial \bar{R}} + \frac{R^*}{\bar{R} + R^*} \bar{U} \frac{\partial \bar{T}}{\partial \bar{X}} \right) = \mu(\bar{T}) \left[ 2 \left( \frac{\partial \bar{V}}{\partial \bar{R}} \right)^2 + \left( \frac{R^*}{\bar{R} + R^*} \frac{\partial \bar{V}}{\partial \bar{X}} - \frac{\bar{U}}{\bar{R} + R^*} \right) \left( \frac{\partial \bar{U}}{\partial \bar{R}} - \frac{\bar{U}}{\bar{R} + R^*} + \frac{R^*}{\bar{R} + R^*} \frac{\partial \bar{V}}{\partial \bar{X}} \right) + \frac{1}{\bar{R} + R^*} \frac{\partial \bar{V}}{\partial \bar{X}} \right) \right]$$

$$\frac{\partial \overline{U}}{\partial \overline{R}} \left( \frac{\partial \overline{U}}{\partial \overline{R}} - \frac{\overline{U}}{\overline{R} + R^*} + \frac{R^*}{\overline{R} + R^*} \frac{\partial \overline{V}}{\partial \overline{X}} \right) + 2 \left( \frac{R^*}{\overline{R} + R^*} \frac{\partial \overline{U}}{\partial \overline{X}} + \frac{\overline{V}}{\overline{R} + R^*} \right)^2 - \nabla \left( -K(\overline{T}) \nabla \overline{T} \right) + \frac{NC_P}{\tau_T} (\overline{T}_S - \overline{T}) + \frac{N}{\tau_U} (\overline{U}_S - \overline{T}) + \frac{NC_P}{\tau_T} (\overline{T}_S - \overline{T}) + \frac{NC_P}{\tau_T} (\overline{$$

$$\overline{U}$$
)<sup>2</sup>, (7.4)

where thermal conductivity  $K(\bar{T})$  and viscosity  $\mu(\bar{T})$  depend on temperature and described as

$$K(\bar{T}) = K_0 (1 + \eta(\bar{T} - T_0)),$$
 (7.5)

$$\mu(\bar{T}) = \mu_0 e^{-\zeta(\bar{T} - T_0)} \cong \mu_0 (1 - \zeta(\bar{T} - T_0)),\tag{7.6}$$

where  $K_0$ ,  $\mu_0$  denote constant thermal conductivity.

The flow and heat transfer equations for solid particles are

$$R^* \frac{\partial \bar{U}_S}{\partial \bar{X}} + \frac{\bar{V}_S}{(\bar{R} + R^*)} + (\bar{R} + R^*) \frac{\partial \bar{V}_S}{\partial \bar{R}} = 0, \tag{7.7}$$

$$\left(\frac{\partial \bar{V}_S}{\partial t} + \bar{V}_S \frac{\partial \bar{V}_S}{\partial \bar{R}} + \frac{R^*}{\bar{R} + R^*} \bar{U}_S \frac{\partial \bar{V}_S}{\partial \bar{X}} - \frac{\bar{U}_S^2}{\bar{R} + R^*}\right) = \frac{k}{m} (\bar{V} - \bar{V}_S), \tag{7.8}$$

$$\left(\frac{\partial \overline{U}_S}{\partial t} + \overline{V}_S \frac{\partial \overline{U}_S}{\partial \overline{R}} + \frac{R^*}{\overline{R} + R^*} \overline{U}_S \frac{\partial \overline{U}_S}{\partial \overline{X}} + \frac{\overline{U}_S \overline{V}_S}{\overline{R} + R^*}\right) = \frac{k}{m} (\overline{U} - \overline{U}_S).$$
(7.9)

$$\left(\frac{\partial \bar{T}_S}{\partial t} + \bar{V}_S \frac{\partial \bar{T}_S}{\partial \bar{R}} + \frac{R^*}{\bar{R} + R^*} \bar{U}_S \frac{\partial \bar{T}_S}{\partial \bar{X}}\right) = -\frac{C_P}{C_m} (\bar{T} - \bar{T}_S), \tag{7.10}$$

Problem is transformed from fixed frame with coordinates  $(\bar{R}, \bar{X})$  to the coordinates (r, x) in moving frame using the relation

$$\bar{R} = r, \bar{X} = x + ct, \bar{U} = u + c, \bar{U}_S = u_S + c, \bar{V} = v, \bar{V}_S = v_S, \bar{T} = T, \bar{T}_S = T_S, \bar{P} = P. \tag{7.11}$$

Problem is further simplified by introducing the dimensionless quantities and stream functions described as:

$$u' = \frac{u}{c}, v' = \frac{v}{\delta c}, u'_{S} = \frac{u_{S}}{c}, v'_{S} = \frac{v_{S}}{\delta c}, x' = \frac{x}{\lambda}, \quad L = \frac{\hat{R}}{a}, r' = \frac{r}{a}, \quad P = \frac{p\lambda\mu_{0}c}{a^{2}}, \quad \Theta = \frac{T-T_{0}}{T_{1}-T_{0}}, \Theta_{S} = \frac{T_{S}-T_{0}}{T_{1}-T_{0}}, \Omega_{S} = \frac{T_{S}$$

where  $A, B, A_1, B_1$  and C are dimensionless quantities.

Using Eqns. (7.11) and (7.12) in Eqns. (7.1) -(7.10), compatibility equations for fluid and particles are obtained as

$$\begin{split} Re\delta\left(\frac{1}{L}\frac{\partial^2\psi}{\partial r\partial x} + \frac{(r+L)}{L}\frac{\partial^3\psi}{\partial r^2\partial x} - \frac{\partial^2\psi}{\partial x^2}\frac{\partial^2\psi}{\partial r^2} - \frac{\partial\psi}{\partial x}\frac{\partial^3\psi}{\partial r^3} - \frac{\partial^2\psi}{\partial r^2}\frac{\partial^2\psi}{\partial r\partial x} - \frac{\partial^3\psi}{\partial r^2\partial x}\left(1 - \frac{\partial\psi}{\partial r}\right) - \frac{1}{r+L}\frac{\partial\psi}{\partial x}\frac{\partial^2\psi}{\partial r^2} + \\ \frac{1}{r+L}\frac{\partial^2\psi}{\partial x^2}\left(1 - \frac{\partial\psi}{\partial r}\right) - \frac{1}{(r+L)^2}\frac{\partial\psi}{\partial x}\left(1 - \frac{\partial\psi}{\partial r}\right) - \frac{L}{r+L}\frac{\partial^3\psi}{\partial x^3} + \frac{L}{(r+L)^2}\left(\frac{\partial^2\psi}{\partial x^2}\right)^2 - \delta^2\left(-2\frac{L^2}{(r+L)^3}\frac{\partial\psi}{\partial x}\frac{\partial^2\psi}{\partial x^2} + \frac{L^2}{(r+L)^2}\frac{\partial\psi}{\partial x}\frac{\partial^2\psi}{\partial x^2} + \frac{L^2}{(r+L)^2}\frac{\partial^3\psi}{\partial x^3}\left(1 - \frac{\partial\psi}{\partial r}\right) + \frac{2}{r+L}\left(1 - \frac{\partial\psi}{\partial r}\right)\frac{\partial^2\psi}{\partial r\partial x}\right) = \frac{2\delta^2}{r+L}\frac{\partial^2}{\partial r\partial x}\left(r + \frac{\partial\psi}{\partial r}\right) + \frac{L\delta^2}{r+L}\frac{\partial^2\psi}{\partial x^2}\left(1 - \omega_0\Theta\right)\left(\delta^2\left(\frac{L}{r+L}\right)^2\frac{\partial^2\psi}{\partial x^2} - \frac{\partial^2\psi}{\partial r^2} - \frac{1}{r+L}\left(1 - \frac{\partial\psi}{\partial r}\right)\right)\right) - \\ L)(1 - \omega_0\Theta)\frac{\partial}{\partial r}\left(\frac{L}{r+L}\frac{\partial\psi}{\partial x}\right) + \frac{L\delta^2}{r+L}\frac{\partial^2}{\partial x^2}\left(1 - \omega_0\Theta\right)\left(\delta^2\left(\frac{L}{r+L}\right)^2\frac{\partial^2\psi}{\partial x^2} - \frac{\partial^2\psi}{\partial r^2} - \frac{1}{r+L}\left(1 - \frac{\partial\psi}{\partial r}\right)\right)\right) - \\ \frac{\partial\psi}{\partial r}\left(\frac{L}{r+L}\frac{\partial\psi}{\partial x}\right) + \frac{L\delta^2}{r+L}\frac{\partial^2\psi}{\partial x^2}\left(1 - \omega_0\Theta\right)\left(\delta^2\left(\frac{L}{r+L}\right)^2\frac{\partial^2\psi}{\partial x^2} - \frac{\partial^2\psi}{\partial r^2} - \frac{1}{r+L}\left(1 - \frac{\partial\psi}{\partial r}\right)\right)\right) - \\ \frac{\partial\psi}{\partial r}\left(\frac{L}{r+L}\frac{\partial\psi}{\partial x}\right) + \frac{L\delta^2}{r+L}\frac{\partial^2\psi}{\partial x^2}\left(1 - \omega_0\Theta\right)\left(\delta^2\left(\frac{L}{r+L}\right)^2\frac{\partial^2\psi}{\partial x^2} - \frac{\partial^2\psi}{\partial r^2} - \frac{1}{r+L}\left(1 - \frac{\partial\psi}{\partial r}\right)\right)\right) - \\ \frac{\partial\psi}{\partial r}\left(\frac{L}{r+L}\frac{\partial\psi}{\partial x}\right) + \frac{L\delta^2}{r+L}\frac{\partial^2\psi}{\partial x^2}\left(1 - \omega_0\Theta\right)\left(\delta^2\left(\frac{L}{r+L}\right)^2\frac{\partial^2\psi}{\partial x^2} - \frac{\partial^2\psi}{\partial r^2} - \frac{1}{r+L}\left(1 - \frac{\partial\psi}{\partial r}\right)\right)\right) - \\ \frac{\partial\psi}{\partial r}\left(\frac{L}{r+L}\frac{\partial\psi}{\partial x}\right) + \frac{L\delta^2}{r+L}\frac{\partial^2\psi}{\partial x^2}\left(1 - \omega_0\Theta\right)\left(\delta^2\left(\frac{L}{r+L}\right)^2\frac{\partial^2\psi}{\partial x^2} - \frac{\partial^2\psi}{\partial r^2} - \frac{1}{r+L}\left(1 - \frac{\partial\psi}{\partial r}\right)\right)\right) - \\ \frac{\partial\psi}{\partial r}\left(\frac{L}{r+L}\frac{\partial\psi}{\partial x}\right) + \frac{L\delta^2}{r+L}\frac{\partial^2\psi}{\partial x^2}\left(1 - \omega_0\Theta\right)\left(\delta^2\left(\frac{L}{r+L}\right)^2\frac{\partial^2\psi}{\partial x^2} - \frac{\partial^2\psi}{\partial r^2} - \frac{1}{r+L}\left(1 - \frac{\partial\psi}{\partial r}\right)\right)\right) - \\ \frac{\partial\psi}{\partial r}\left(\frac{L}{r+L}\frac{\partial\psi}{\partial x}\right) + \frac{L\delta^2}{r+L}\frac{\partial^2\psi}{\partial x^2}\left(1 - \omega_0\Theta\right)\left(\delta^2\left(\frac{L}{r+L}\right)^2\frac{\partial^2\psi}{\partial x^2} - \frac{1}{r+L}\left(1 - \frac{\partial\psi}{\partial r}\right)\right) + \frac{L\delta^2}{r+L}\frac{\partial\psi}{\partial x}\left(1 - \frac{\partial\psi}{\partial r}\right)\right) + \frac{L\delta^2}{r+L}\frac{\partial\psi}{\partial x}\left(1 - \frac{\partial\psi}{\partial r}\right) + \frac{L\delta^2}{r+L}\frac{\partial\psi}{\partial r}\right)$$

$$\frac{2\delta^{2}}{r+L}\frac{\partial}{\partial x}\left((1-\omega_{0}\Theta)\left(-\frac{L}{r+L}\frac{\partial^{2}\psi}{\partial r\partial x} + \frac{L}{(r+L)^{2}}\frac{\partial\psi}{\partial x}\right)\right) - \frac{\partial}{\partial r}\left[\frac{1}{L(r+L)}\frac{\partial}{\partial r}\left((r+L)^{2}(1-\omega_{0}\Theta)\left(\delta^{2}\left(\frac{L}{r+L}\right)^{2}\frac{\partial^{2}\psi}{\partial x^{2}} - \frac{\partial^{2}\psi}{\partial r^{2}} - \frac{1}{r+L}\left(1-\frac{\partial\psi}{\partial r}\right)\right)\right]\right] - \delta^{2}\frac{\partial^{2}}{\partial r\partial x}\left(2(1-\omega_{0}\Theta)\left(-\frac{L}{r+L}\frac{\partial^{2}\psi}{\partial r\partial x} + \frac{\partial^{2}\psi}{\partial r\partial x} + \frac{L}{(r+L)^{2}}\frac{\partial\psi}{\partial x}\right)\right) + A\left(\delta^{2}\frac{L}{r+L}\frac{\partial^{2}}{\partial x^{2}} + \frac{\partial^{2}}{\partial r^{2}}\right)(\varphi-\psi), \tag{7.13}$$

$$\delta\left(\frac{1}{L}\frac{\partial^{2}\varphi}{\partial r\partial x} + \frac{(r+L)}{L}\frac{\partial^{3}\varphi}{\partial r^{2}\partial x} - \frac{1}{r+L}\frac{\partial\varphi}{\partial x}\frac{\partial^{2}\varphi}{\partial r^{2}} - \frac{\partial^{2}\varphi}{\partial x^{2}}\frac{\partial^{2}\varphi}{\partial r^{2}} - \frac{\partial\varphi}{\partial x}\frac{\partial^{3}\varphi}{\partial r^{3}} + \frac{\partial^{2}\varphi}{\partial r^{2}}\frac{\partial^{2}\varphi}{\partial r\partial x} - \frac{\partial^{3}\varphi}{\partial r^{2}\partial x}\left(1-\frac{\partial\varphi}{\partial r}\right) + \frac{1}{r+L}\frac{\partial^{2}\varphi}{\partial r\partial x}\left(1-\frac{\partial\varphi}{\partial r}\right) - \frac{1}{(r+L)^{2}}\left(1-\frac{\partial\varphi}{\partial r}\right)\frac{\partial\varphi}{\partial x} - \frac{L}{r+L}\frac{\partial^{3}\varphi}{\partial x^{3}} + \frac{L^{2}}{(r+L)^{2}}\left(\frac{\partial^{2}\varphi}{\partial r^{2}}\right)^{2} - \delta^{2}\left(-\frac{L}{r+L}\frac{\partial^{3}\varphi}{\partial x^{3}} + \frac{L^{2}}{(r+L)^{2}}\frac{\partial^{2}\varphi}{\partial r\partial x}\right) - \frac{L}{r+L}\frac{\partial^{3}\varphi}{\partial x^{3}}\left(1-\frac{\partial\varphi}{\partial r}\right) + \frac{L^{2}}{(r+L)^{2}}\frac{\partial^{2}\varphi}{\partial x^{2}}\left(1-\frac{\partial\varphi}{\partial r}\right)\right) - B\left(\frac{(r+L)}{L}\left(\frac{\partial^{2}\varphi}{\partial r^{2}} - \frac{\partial^{2}\psi}{\partial r^{2}}\right) + \frac{L}{L}\left(\frac{\partial\varphi}{\partial r} - \frac{\partial\psi}{\partial r}\right) - \frac{L}{r+L}\delta^{2}\frac{\partial^{2}\varphi}{\partial x^{2}}\left(\psi-\varphi\right)\right). \tag{7.14}$$

For fluid and dust fragments, the energy equations are nondimensionalized as:

$$Re\delta\left[-\frac{\partial\Theta}{\partial x} + \frac{L}{r+L}\frac{\partial\psi}{\partial x}\frac{\partial\Theta}{\partial r} + \frac{L}{r+L}\left(1 - \frac{\partial\psi}{\partial r}\right)\frac{\partial\Theta}{\partial x}\right] = (1 + \eta\Theta)\left\{\frac{\partial^{2}\Theta}{\partial r^{2}} + \frac{1}{r+L}\frac{\partial\Theta}{\partial r}\right\} + \varepsilon\left(\frac{\partial\Theta}{\partial r}\right)^{2} + \delta^{2}\left(\frac{L}{r+L}\right)^{2}\left\{(1 + \eta\Theta)\frac{\partial^{2}\Theta}{\partial x^{2}} + \eta\left(\frac{\partial\Theta}{\partial x}\right)^{2}\right\} + Br(1 - \omega_{0}\Theta)\left(2\delta^{2}\left(\frac{\partial}{\partial r}\left(\frac{1}{r+L}\frac{\partial\psi}{\partial x}\right)\right)^{2} + 2\delta^{2}\left(-\frac{L}{r+L}\frac{\partial^{2}\psi}{\partial r\partial x} + \frac{1}{r+L}\frac{\partial\Theta}{\partial x}\right)^{2}\right\} + \left(\delta^{2}\left(\frac{L}{r+L}\right)^{2}\frac{\partial^{2}\psi}{\partial x^{2}} - \frac{1}{r+L}\left(1 - \frac{\partial\psi}{\partial r}\right) - \frac{\partial^{2}\psi}{\partial r^{2}}\right)^{2}\right) + A_{1}\Pr(\Theta_{S} - \Theta) + B_{1}Br\left(\frac{\partial\varphi}{\partial r} - \frac{\partial\psi}{\partial r}\right)^{2},$$

$$(7.15)$$

$$\delta\left[-\frac{\partial\Theta_{S}}{\partial x} + \frac{L}{r+L}\frac{\partial\varphi}{\partial x}\frac{\partial\Theta_{S}}{\partial r} + \frac{L}{r+L}\left(1 - \frac{\partial\varphi}{\partial r}\right)\frac{\partial\Theta_{S}}{\partial x}\right] = -C(\Theta_{S} - \Theta). \tag{7.16}$$

### 7.2 Method of Solution

Assuming wavelength large and low Reynolds number small, Eqns. (7.13) -(7.16) take the form

$$\frac{\partial}{\partial r} \left[ \frac{1}{L(r+L)} \frac{\partial}{\partial r} \left( (r+L)^2 (1 - \omega_0 \Theta) \left( -\frac{\partial^2 \psi}{\partial r^2} - \frac{1}{r+L} \left( 1 - \frac{\partial \psi}{\partial r} \right) \right) \right) \right] - A \frac{\partial^2}{\partial r^2} (\varphi - \psi) = 0, \tag{7.17}$$

$$B\left(\frac{(r+L)}{L}\left(\frac{\partial^2 \varphi}{\partial r^2} - \frac{\partial^2 \psi}{\partial r^2}\right) + \frac{1}{L}\left(\frac{\partial \varphi}{\partial r} - \frac{\partial \psi}{\partial r}\right)\right) = 0,\tag{7.18}$$

$$(1+\eta\Theta)\left\{\frac{\partial^2\Theta}{\partial r^2} + \frac{1}{r+L}\frac{\partial\Theta}{\partial r}\right\} + \eta\left(\frac{\partial\Theta}{\partial r}\right)^2 + Br(1-\omega_0\Theta)\left(\frac{1}{r+L}\left(1-\frac{\partial\psi}{\partial r}\right) + \frac{\partial^2\psi}{\partial r^2}\right)^2 + A_1\Pr(\Theta_s-\Theta) + \frac{\partial^2\Psi}{\partial r^2}\left(\frac{\partial\Psi}{\partial r}\right)^2 + A_1\Pr(\Theta_s-\Theta) + \frac{\partial\Psi}{\partial r}\left(\frac{\partial\Psi}{\partial r}\right)^2 + \frac{\partial\Psi}{\partial r}\left(\frac{\partial\Psi}{\partial r}\right)^2$$

$$B_1 Br \left(\frac{\partial \varphi}{\partial r} - \frac{\partial \psi}{\partial r}\right)^2 = 0, \tag{7.19}$$

$$\Theta_s - \Theta = 0. ag{7.20}$$

The non-dimensional form of the configuration are given by Eqn. (3.22).

Boundary conditions in dimensionless form are

$$\psi = -\frac{E}{2}$$
,  $\phi = -\frac{F}{2}$ ,  $\frac{\partial \psi}{\partial r} = -1$ , at  $r = -h$ , (7.21)

$$\psi = \frac{E}{2}$$
,  $\phi = \frac{F}{2}$ ,  $\frac{\partial \psi}{\partial r} = -1$ , at  $r = h$ , (7.22)

$$\frac{\partial \Theta}{\partial r} + \beta_1 (1 - \Theta) = 0$$
 at  $r = -h$ , (7.23)

$$\frac{\partial \Theta}{\partial r} + \beta_2 \Theta = 0$$
 at  $r = h$ , (7.24)

$$\frac{\partial \Theta_s}{\partial r} + \beta_1 (1 - \Theta_s) = 0 \quad \text{at } r = h, \tag{7.25}$$

$$\frac{\partial \Theta_s}{\partial r} + \beta_2 \Theta_s = 0$$
 at  $r = -h$ , (7.26)

where  $\beta_1$  and  $\beta_2$  are Biot numbers at lower and upper wall of the channel.

## 7.3 Graphical Analysis

A comprehensive analysis of the problem has been performed by plotting graphs of velocity and temperature profiles by varying curvature parameter L, viscosity parameter  $\omega_0$ , thermal conductivity parameter  $\eta$ , biot numbers  $\beta_1$ , and  $\beta_2$ .

#### 7.3.1 Fluid Flow Analysis

Figs. 7.1 and 7.2 show graphical results for velocity of fluid propagation. The flow behavior of fluid is parabolic. Fig. 7.1 is graphical view of fluid velocity for various values of curvature parameter L. As curvature parameter increases velocity of fluid decrease below central line and increase above central line. This is due to the fact that near the upper boundary path is straighter than lower boundary and fluid flow becomes smooth and fast. The fluid velocity profile for varying viscosity parameter  $\omega_0$  has been portrayed in Fig. 7.2. Flow is accelerated near center and deaccelerated near upper boundary of the passage as  $\omega_0$  grows. Viscosity effects the fluid near the walls more considerably therefore increase in viscosity reduces the speed of the fluid close to the walls and it has less effect in the center therefore fluid moves freely in the central part of the passage.

#### 7.3.2 Solid Particle Flow

Figs. 7.3 and 7.4 depict locomotion of dust particles under the impact of curvature parameter and viscosity parameter. In Fig. 7.3, particle velocity trends are shown as curvature parameter L varies. As curvature parameter L increases, velocity of particles decreases below center and increases above central line of the channel. Fig. 7.4 illustrates the impact of variable viscosity parameter  $\omega_0$  on particle flow. In the vicinity of center, particles speed increases whereas in the neighborhood

of upper wall speed of the particles declines. The effects of curvature and viscosity parameter are same on fluid velocity and particle velocity.

#### 7.3.3 Temperature Distribution Analysis

Temperature profile plots are shown in Figs. 7.5-7.9 portraying the effect of curvature parameter L, viscosity parameter  $\omega_0$ , thermal conductivity parameter  $\eta$ , Biot numbers  $\beta_1$ ,  $\beta_2$ , and Brinkman number Br. Fig. 7.5 represents variation in temperature with the varying values of viscosity parameter  $\omega_0$ . As viscosity parameter grows temperature transference becomes slow. The behavior of temperature profile under the impact of thermal conductivity parameter  $\eta$  is depicted in Fig. 7.6. The enhancement of thermal conductivity parameter  $\eta$  implies slow heat transfer through the fluid. Plot in Fig. 7.7 shows the effect of Brinkman number Br on temperature distribution. The large values of Brinkman number Br gives rise to temperature profile of fluid.  $\beta_1$  is Biot number at the lower wall. Significant decline in temperature profile is observed by increasing values of  $\beta_1$  as shown in Fig. 7.8.  $\beta_2$  is Biot number at the upper wall of the channel. Slow heat transfer is noticed with the rise in  $\beta_2$ . The effect is prominent near upper wall as revealed in Fig. 7.9. The Biot number is ratio of resistance for conduction of the solid boundary to the resistance for convection at the surface of the boundary. As Biot number becomes high, the conduction inside the boundary becomes slow as compared to convection inside the fluid. Therefore, heat travels from the fluid to the boundary that results in fall of temperature of the fluid.

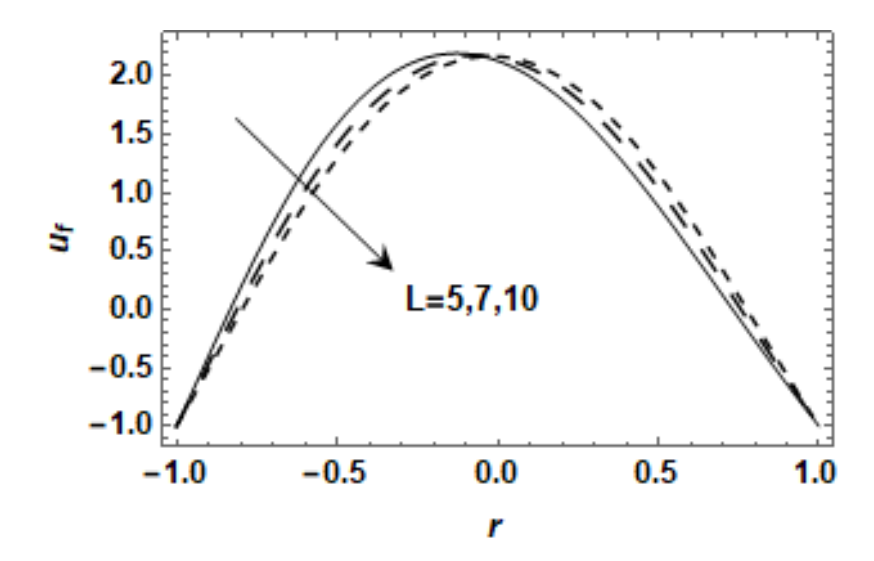


Fig 7.1: Flow behavior of fluid for curvature with  $\eta = 0.1$ , Br = 0.3,  $\omega_0 = 0.6$ , d = 0.2, b = 0.8, A = 0.5,  $\beta_1 = 2.5$ ,  $\beta_2 = 0.3$ .

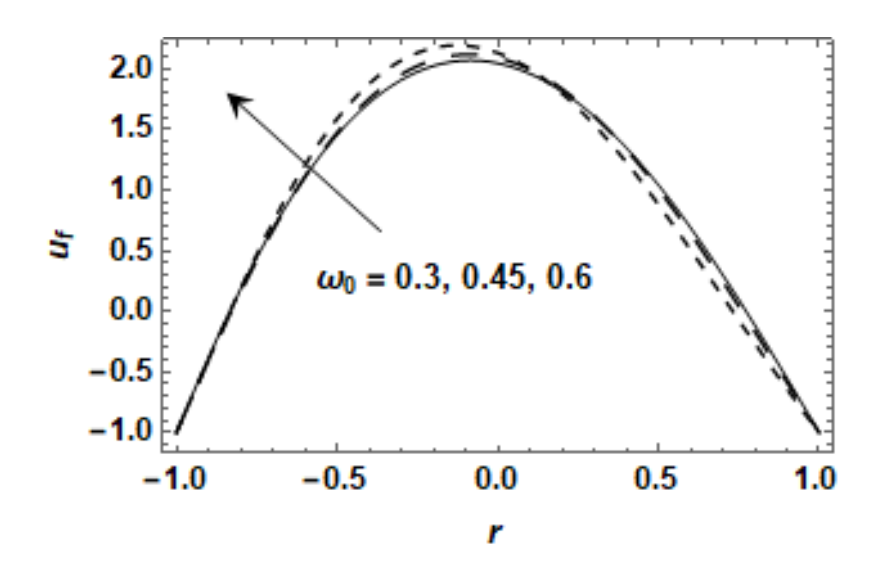


Fig 7.2: Flow behavior of fluid for viscosity parameter with  $\eta=0.1, Br=0.3, L=5, d=0.2,$   $b=0.8, A=0.5, \beta_1=2.5, \beta_2=0.3.$ 

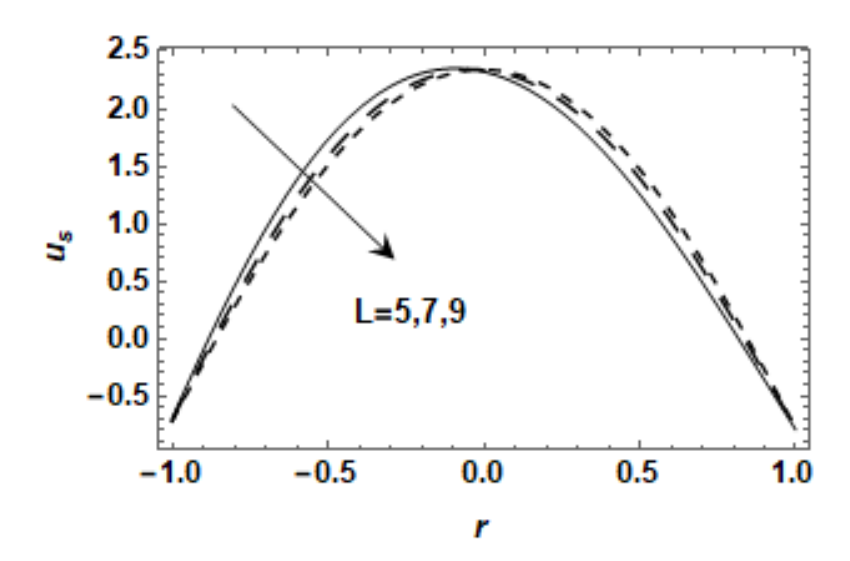


Fig 7.3: Dust particles flow behavior for curvature with  $\eta = 0.1, Br = 0.3, \omega_0 = 0.4, d = 0.2,$   $b = 0.8, A = 0.5, \beta_1 = 2.5, \beta_2 = 0.3.$ 

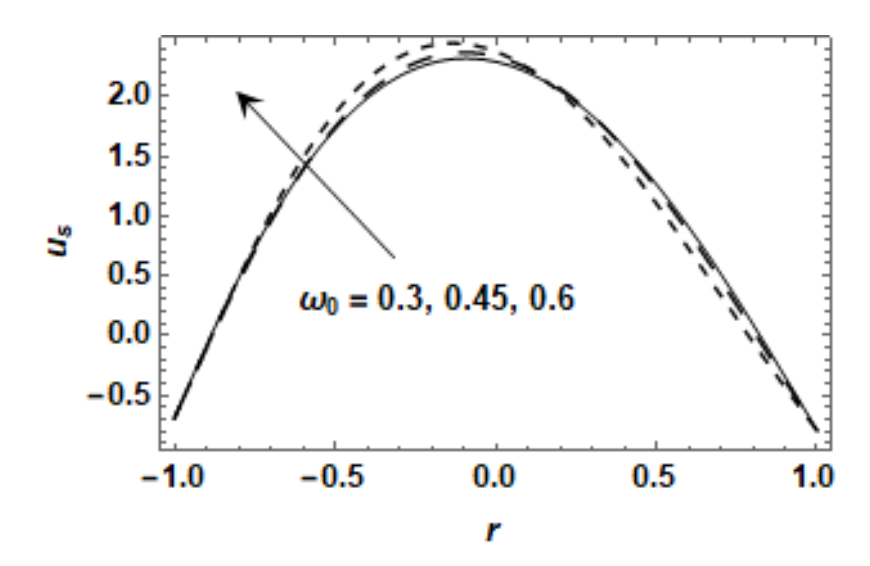


Fig 7.4: Dust particles flow behavior for viscosity parameter with  $\eta=0.1$ , Br=0.3, L=5, d=0.2, b=0.8, A=0.5,  $\beta_1=2.5$ ,  $\beta_2=0.3$ .

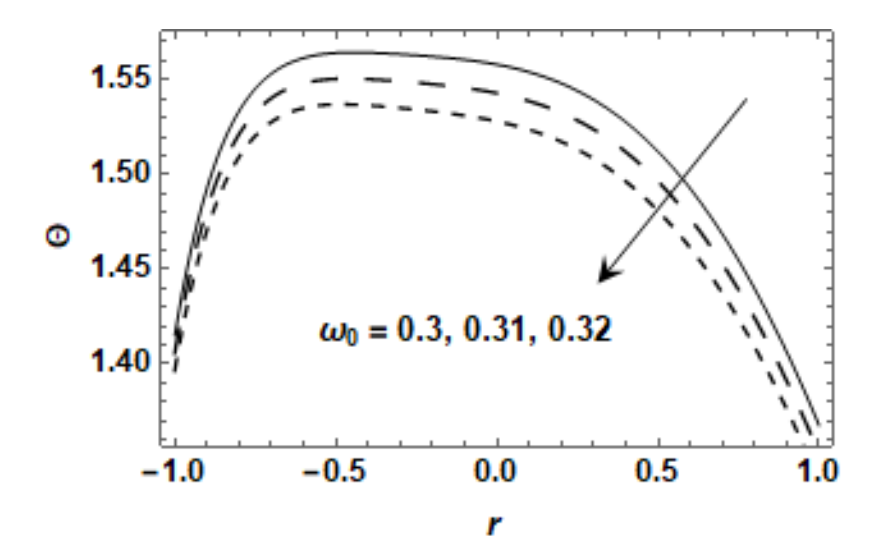


Fig 7.5: Fluid temperature distribution for viscosity parameter with  $\eta=0.1, Br=0.1, L=3, d=0.8, b=0.7, A=0.8, \beta_1=2.5, \beta_2=0.3.$ 

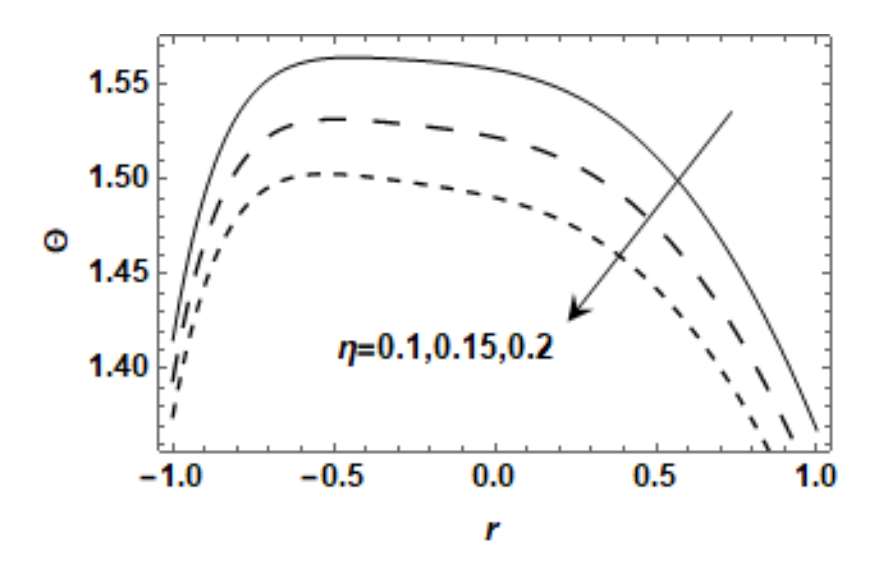


Fig 7.6: Fluid temperature distribution for thermal conductivity with  $\omega_0=0.3$ , Br=0.1, L=3, d=0.7, b=0.7, A=0.8,  $\beta_1=2.5$ ,  $\beta_2=0.3$ .

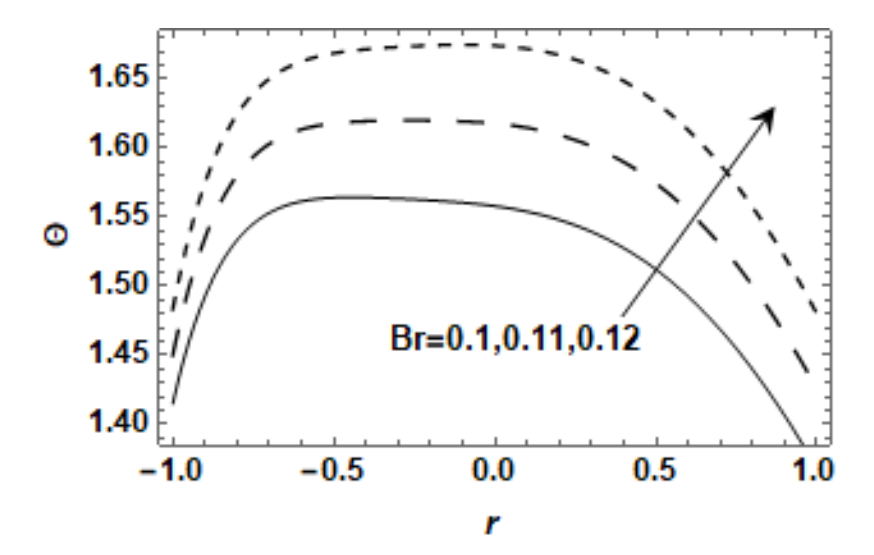


Fig 7.7: Fluid temperature distribution for thermal conductivity with  $\omega_0 = 0.3$ ,  $\eta = 0.1$ , L = 3, d = 0.8, b = 0.7, A = 0.8,  $\beta_1 = 2.5$ ,  $\beta_2 = 0.3$ .

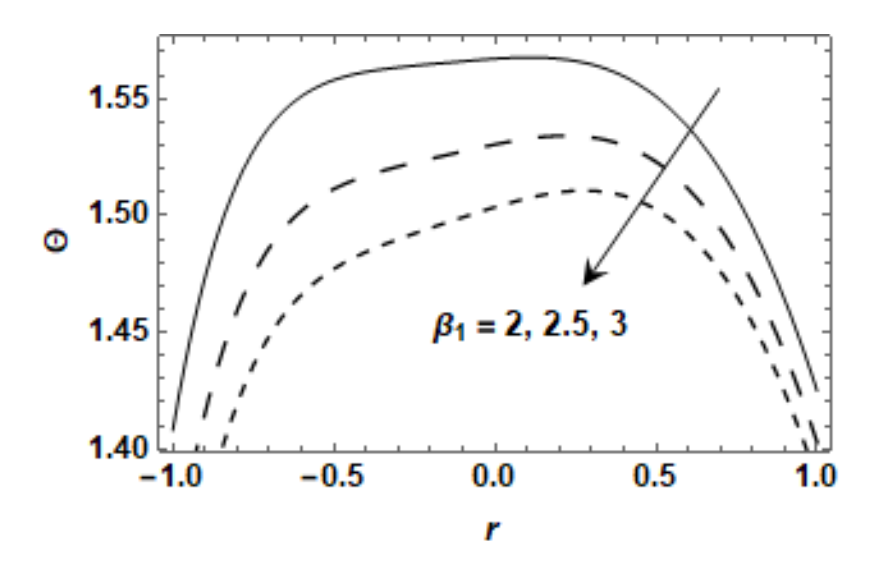


Fig 7.8: Fluid temperature distribution for Biot number  $\beta_1$  with  $\omega_0 = 0.3$ , Br = 0.1,  $\eta = 0.1$ , L = 5, d = 0.8, b = 0.7, A = 0.8,  $\beta_2 = 0.3$ .

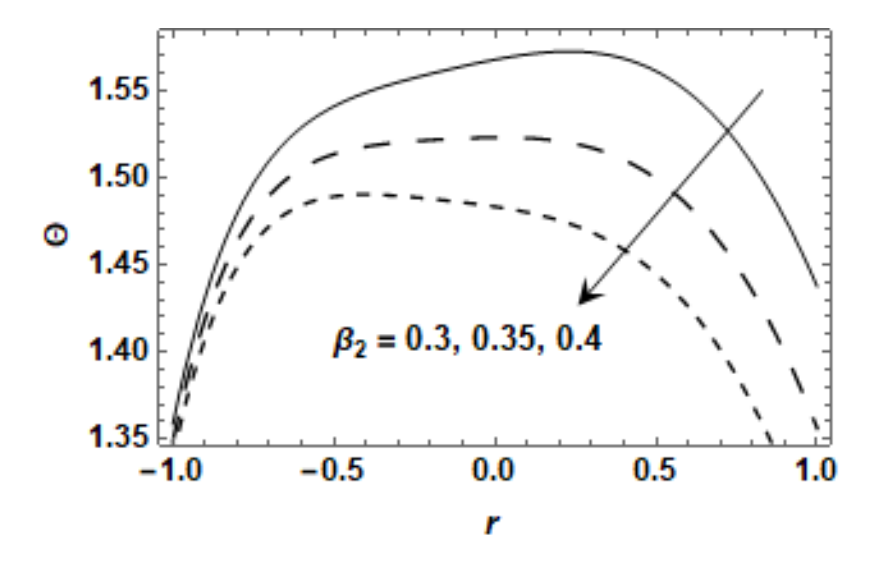


Fig 7.9: Fluid temperature distribution for Biot number  $\beta_2$  with  $\omega_0=0.3, Br=0.1, \eta=0.1,$   $L=5,\ d=0.8,\ b=0.7, A=0.8, \beta_1=2.5.$ 

## 7.4 Conclusion

In the current study Newtonian fluid with uniform distribution is investigated. The peristaltic progression of fluid is considered through symmetric channel with curved walls. Velocities of both fluid phase and particle phase are examined for variable viscosity and curvature parameter. Heat transfer analysis is carried out and effects of variable viscosity and thermal conductivity along with Biot numbers are discussed. The key findings of the study are listed as:

- Velocity profiles of fluid and dust particles are parabolic in shape.
- In both cases increase in curvature decreases velocity close to the lower wall and increases in the vicinity of upper wall.
- Due to increase in viscosity parameter, velocities of both fluid and particles increase near center of flow and reduce in the locality of upper boundary.

- Variable viscosity and thermal conductivity both are responsible to slow down the heat transfer through the fluid. Temperature profile declines due to increase in the values of Biot numbers.
- By increasing Brinkman number, temperature of the fluid rises.

# **Chapter 8**

## **Conclusions**

This dissertation aimed to conduct thermal analysis of peristaltic dusty fluids theoretically. The presence of particles in many biological and industrial fluids affects thermal conductivity of the fluids. Therefore, heat transfer analysis of particulate fluids is an influential factor in designing devices with optimum performance.

In chapter 1, basic definitions, fundamental mathematical equations, non-dimensional parameters, and their significance and comprehensive discussion on literature history are presented.

In chapter 2, Walter's B dusty fluid with radiation and MHD effects has been considered. Study shows that high values of Reynolds number result in fast movement of blood through vessels. Consequently, nutrients are delivered to tissues and organs efficiently. It has been noticed that when the radiation parameter is increased, heat transfer becomes faster within the fluid. In industry, engineers select the design and material of furnaces and boilers to get the optimum results of radiation to obtain the desired temperature of the fluid inside boilers and furnaces. The fluid in joints has characteristics of Walter's B fluid, so this study is helpful in assessing the joints health. In chapter 3, the movement of visco-elastic fluid following Jeffrey fluid model with the distribution of dust particles has been examined. The passage of flow is curved. Effects of relaxation and retardation time on bolus movement and velocity profiles of fluid and particles are key findings of the study. It has been observed that fluid takes more time to return to equilibrium. As retardation time increases, fluid response to applied stresses is delayed, and therefore bolus movement towards

left (backward) is observed. The analysis of bolus movement is beneficial for efficient delivery of drugs to veins and organs. The study also has applications in the polymer industry.

In chapter 4, effects of variable thermal conductivity on dusty fluid with an inhomogeneous distribution of solid particles have been investigated. The channel of flow is curved. As the density of solid particles increases, heat transference becomes slow. As thermal conductivity increases, heat transfer within the fluid becomes faster. The discussion of variable thermal conductivity is of great concern as many procedures in medical science and optimization of thermal energy storage systems performance requires accurate measurement of fluid's thermal conductivity.

In chapter 5, Newtonian dusty fluid propelling peristaltically through an asymmetric channel with both wall and thermal slip has been studied. Entropy generation analysis has also been carried out. Entropy generation rate grows as thermal slip enhances. The study of Entropy generation has vast implications in engineering for examining the performance of systems like power plants and refrigerators. Lower the entropy generation, the more efficient the system is. High entropy generation implies the system requires improvement.

In chapter 6, peristaltic second grade dusty fluid flowing through porous medium has been analyzed. Many biological structures, for instance lungs, kidneys, skin, bone marrow, and lymphatic systems are porous in nature. Filtration processes, water absorption in river beds and water transport through plant roots and stems are examples from geology. The porosity of the medium has significance effect on fluid velocity. As medium becomes more porous, fluid motion through medium becomes slow. This fact is helpful in improving the filtration process and controlling drug diffusion.

In chapter 7, effects of variable properties on viscous peristaltic fluid with particle suspension have been illustrated. Convective boundary conditions have also been incorporated. Variable viscosity and thermal conductivity are both responsible for slowing down the heat transfer through the fluid. Temperature profile declines due to an increase in the values of Biot numbers. This analysis is very productive for lubricant effectiveness in automobiles, accessing weather trends and cloud formation, cooling systems, and chemical reactors.

Thermal analysis of dusty viscous fluid with peristaltic movement through curved geometry have been discussed. This study can be extended to Non-Newtonian fluids. Thermal effects on few viscoelastic models have been studied in this dissertation while a vast class of viscoelastic fluids are left for future analysis. The current analysis further can be extended to other geometries like tubes, endoscopes, sheets etc.

# **Appendix**

### Chapter 2

$${\rm A1} = \frac{(h_2 + h_1) \left( -2\sqrt{2} + 2\sqrt{2} \left( 1 + {\rm F}_0 M^2 \beta \right) \cosh \left( \frac{(h_2 - h_1) M}{\sqrt{2}} \right) - M \left( {\rm F}_0 + 4\beta + 2{\rm F}_0 M^2 \beta^2 \right) \sinh \left( \frac{(h_2 - h_1) M}{\sqrt{2}} \right) \right)}{-4\sqrt{2} + 4\sqrt{2} (1 + (h_2 - h_1) M^2 \beta) \cosh \left( \frac{(h_2 - h_1) M}{\sqrt{2}} \right) - 2M (h_2 - h_1 + 4\beta + 2(h_2 - h_1) M^2 \beta^2) \sinh \left( \frac{(h_2 - h_1) M}{\sqrt{2}} \right)} \,,$$

$${\rm A2} = \frac{2\sqrt{2} - 2\sqrt{2}(1 + {\rm F}_0 M^2 \beta) \cosh \left( \frac{(h_2 - h_1) M}{\sqrt{2}} \right) + M({\rm F}_0 + 4\beta + 2{\rm F}_0 M^2 \beta^2) \sinh \left( \frac{(h_2 - h_1) M}{\sqrt{2}} \right)}{-2\sqrt{2} + 2\sqrt{2}(1 + (h_2 - h_1) M^2 \beta) \cosh \left( \frac{(h_2 - h_1) M}{\sqrt{2}} \right) + M(-h_2 + h_1 - 4\beta + 2(-h_2 + h_1) M^2 \beta^2) \sinh \left( \frac{(h_2 - h_1) M}{\sqrt{2}} \right)} \,,$$

$${\rm A3} = \frac{(F_0 - h_2 + h_1) \left(\sqrt{2}\cosh\left(\frac{h_2M}{\sqrt{2}}\right) - \sqrt{2}\cosh\left(\frac{h_1M}{\sqrt{2}}\right) - 2M\beta\left(\sinh\left(\frac{h_2M}{\sqrt{2}}\right) + \sinh\left(\frac{h_1M}{\sqrt{2}}\right)\right)\right)}{-2\sqrt{2} + 2\sqrt{2}(1 + (h_2 - h_1)M^2\beta)\cosh\left(\frac{(h_2 - h_1)M}{\sqrt{2}}\right) + M(-h_2 + h_1 - 4\beta + 2(-h_2 + h_1)M^2\beta^2)\sinh\left(\frac{(h_2 - h_1)M}{\sqrt{2}}\right)}\,,$$

$${\rm A4} = \frac{(F_0 - h_2 + h_1) \left(2 M \beta \left(\cosh \left(\frac{h_2 M}{\sqrt{2}}\right) + \cosh \left(\frac{h_1 M}{\sqrt{2}}\right)\right) + \sqrt{2} \left(-\sinh \left(\frac{h_2 M}{\sqrt{2}}\right) + \sinh \left(\frac{h_1 M}{\sqrt{2}}\right)\right)\right)}{-2 \sqrt{2} + 2 \sqrt{2} (1 + (h_2 - h_1) M^2 \beta) \cosh \left(\frac{(h_2 - h_1) M}{\sqrt{2}}\right) + M (-h_2 + h_1 - 4 \beta + 2 (-h_2 + h_1) M^2 \beta^2) \sinh \left(\frac{(h_2 - h_1) M}{\sqrt{2}}\right)},$$

$$C1 = \frac{\mathrm{E}_0(h_2 + h_1) + 2\mathrm{A3} \; h_1 \cosh\left(\frac{h_2 M}{\sqrt{2}}\right) + 2\mathrm{A4} h_1 \sinh\left(\frac{h_2 M}{\sqrt{2}}\right) - 2h_2\left(\mathrm{A3} \cosh\left(\frac{h_1 M}{\sqrt{2}}\right) + \mathrm{A4} \sinh\left(\frac{h_1 M}{\sqrt{2}}\right)\right)}{2(h_2 - h_1)} \; ,$$

$$\text{C2} = -\frac{\text{E}_0 + \text{A3} \cosh\left(\frac{h_2 M}{\sqrt{2}}\right) - \text{A3} \cosh\left(\frac{h_1 M}{\sqrt{2}}\right) + \text{A4} \sinh\left(\frac{h_2 M}{\sqrt{2}}\right) - \text{A4} \sinh\left(\frac{h_1 M}{\sqrt{2}}\right)}{h_2 - h_1} \,.$$

### Chapter 4

$$\begin{aligned} &\text{C1} = -\frac{1}{4(h_2 - h_1)^3(-h_2 + h_1 + 6\beta)^2(h_2 - h_1 + 2\varepsilon)} \bigg( 4(h_2 - h_1)^3(-h_2 + h_1 + 6\beta)^2(h_1 - \varepsilon) - Br(h_2 - h_1 + 2\varepsilon) \bigg( 3F_0^2(h_2 - h_1)^2(h_2 - h_1 + 8\varepsilon) + 2F_0 \bigg( h_2 h_1 \bigg( -h_2^4 B_1 + 4h_2^3 B_1(h_1 + 3\beta) + 4h_2 h_1 B_1(h_1 + 3\beta) \bigg) + 4h_2 h_1 B_1(h_1 + 4\beta) \bigg) \bigg) + (h_1 + 6\beta) - h_1^2 (-24 + B_1(h_1 + 6\beta)^2) - 6h_2^2 \bigg( -4 + B_1 \bigg( h_1^2 + 6h_1 \beta + 6\beta^2 \bigg) \bigg) \bigg) + (h_2 - h_1)^3 (-24 + B_1(-h_2 + h_1 + 6\beta)^2) \varepsilon \bigg) + 2(-h_2 + h_1) \bigg( h_2 h_1 \bigg( 12h_1^2 - E_0 h_2^3 B_1 - 3E_0 h_2 B_1(h_1 + 4\beta) \bigg) \bigg) \bigg) + (h_2 - h_1)^3 \bigg( -24 + B_1(-h_2 + h_1 + 6\beta)^2 \bigg) \varepsilon \bigg) + 2(-h_2 + h_1) \bigg( h_2 h_1 \bigg( 12h_1^2 - E_0 h_2^3 B_1 - 3E_0 h_2 B_1(h_1 + 4\beta) \bigg) \bigg) \bigg) + (h_2 - h_1)^3 \bigg( -24 + B_1(-h_2 + h_1 + 6\beta)^2 \bigg) \varepsilon \bigg) \bigg) + 2(-h_2 + h_1) \bigg( h_2 h_1 \bigg( 12h_1^2 - E_0 h_2^3 B_1 - 3E_0 h_2 B_1(h_1 + 4\beta) \bigg) \bigg) \bigg) \bigg) \bigg) \bigg) \bigg) \bigg) \bigg] \bigg( -\frac{h_1}{h_1} \bigg( -\frac{h_1}{h_1} \bigg) \bigg) \bigg) \bigg) \bigg( -\frac{h_1}{h_1} \bigg) \bigg( -\frac{h_1}{h_1} \bigg) \bigg) \bigg) \bigg( -\frac{h_1}{h_1} \bigg$$

$$\begin{split} &2\beta)(h_1+6\beta)+\mathrm{E}_0hB_1(h_1+6\beta)^2+3h_2^2\big(4+\mathrm{E}_0B_1(h_1+4\beta)\big)\big)+(h_2-h_1)^2\,\Big(12h_1+\mathrm{E}_0h_2^{\,2}B_1+\\ &\mathrm{E}_0B_1(h_1+6\beta)^2-2h_2\big(6+\mathrm{E}_0B_1(h_1+6\beta)\big)\big)\varepsilon\Big)\Big)\Big),\\ &C2=\frac{1}{2(h_2-h_1)^3(-h_2+h_1+6\beta)^2(h_2-h_1+2\varepsilon)}\bigg(2(h_2-h_1)^3(-h_2+h_1+6\beta)^2+Br(h_2+h_1)\bigg((h_2-h_1)^2(h_2-h_1)^3(-h_2+h_1+6\beta)^2+Br(h_2+h_1)\bigg)\bigg)\bigg)+Br(h_2+h_1)\bigg(12h_2^{\,2}+24h_2h_1+12h^2-\mathrm{E}_0h_2^{\,3}B_1+3\mathrm{E}_0h_2^{\,2}h_1B_1-3\mathrm{E}_0h_2h_1^{\,2}B_1+\mathrm{E}_0h_1^{\,3}B_1+\\ &12\mathrm{E}_0(h_2-h_1)^2B_1\beta+36\mathrm{E}_0(-h_2+h_1)B_1\beta^2\bigg)+\mathrm{FO}\bigg(h_2^{\,4}B_1-4h_2^{\,3}B_1(h_1+3\beta)-4h_2h_1\big(12+B_1(h_1+3\beta)(h_1+6\beta)\big)+h_1^{\,2}(-24+B_1(h_1+6\beta)^2)+6h_2^{\,2}\bigg(-4+B_1(h_1^{\,2}+6h_1\beta+B_1(h_1+6\beta)^2)\bigg)\bigg)\bigg)\bigg)\bigg(h_2-h_1+2\varepsilon)\bigg). \end{split}$$

## References

- [1] Lathern TW. Fluid motions in a peristaltic pump. M. Sc. Thesis, MIT, Cambridge, MA, (1966).
- [2] Yin, F., and Yuan Cheng Fung. "Peristaltic waves in circular cylindrical tubes." (1969) 579-87.
- [3] Shapiro AH, Jaffrin MY, Weinberg SL. Peristaltic pumping with long wavelengths at low Reynolds number. Journal of Fluid Mechanics. 37 (1969) 799-825.
- [4] Weinberg SL, Eckstein EC, Shapiro AH. An experimental study of peristaltic pumping. Journal of Fluid Mechanics. 49 (1971) 461-79.
- [5] Takabatake S, Ayukawa K, Mori A. Peristaltic pumping in circular cylindrical tubes: a numerical study of fluid transport and its efficiency. Journal of Fluid Mechanics. 193 (1988) 267-83.
- [6] Gupta BB, Seshadri V. Peristaltic pumping in non-uniform tubes. Journal of Biomechanics. 9 (1976) 105-9.
- [7] Brown TD, Hung TK. Computational and experimental investigations of two-dimensional nonlinear peristaltic flows. Journal of Fluid Mechanics. 83 (1977) 249-72.
- [8] Böhme G, Friedrich R. Peristaltic flow of viscoelastic liquids. Journal of Fluid Mechanics. 128 (1983) 109-22.
- [9] Pozrikidis C. A study of peristaltic flow. Journal of Fluid Mechanics. 180 (1987) 515-27.
- [10] Siddiqui AM, Schwarz WH. Peristaltic flow of a second-order fluid in tubes. Journal of Non-Newtonian Fluid Mechanics. 53 (1994) 257-84.
- [11] Mekheimer KS. Peristaltic flow of blood under effect of a magnetic field in a non-uniform channels. Applied Mathematics and Computation. 153 (2004) 763-77.

- [12] Tsui YY, Guo DC, Chen SH, Lin SW. Pumping flow in a channel with a peristaltic wall. Journal of Fluids Engineering. 136 (2014) 1-9.
- [13] Nadeem S, Akram S. Peristaltic flow of a Williamson fluid in an asymmetric channel.

  Communications in Nonlinear Science and Numerical Simulation. 15 (2010) 1705-16.
- [14] Javid K, Asghar Z, Saeed U, Waqas M. Porosity effects on the peristaltic flow of biological fluid in a complex wavy channel. Pramana. 96 (2022) 1-13.
- [15] Rani J, Hina S, Mustafa M. A novel formulation for MHD slip flow of elastico-viscous fluid induced by peristaltic waves with heat/mass transfer effects. Arabian Journal for Science and Engineering. 45 (2020) 9213-25.
- [16] Ellahi R, Hussain F. Simultaneous effects of MHD and partial slip on peristaltic flow of Jeffery fluid in a rectangular duct. Journal of Magnetism and Magnetic Materials. 393 (2015) 284-92.
- [17] Jagadesh V, Sreenadh S, Ajithkumar M, Lakshminarayana P, Sucharitha G. Investigation of dissipative heat transfer and peristaltic pumping on MHD Casson fluid flow in an inclined channel filled with porous medium. Numerical Heat Transfer, Part B: Fundamentals. (2023) 1-19.
- [18] Gafel HS. Significance of heat transfer on the peristaltic pump of blood fluid under the inclined magnetic field. Partial Differential Equations in Applied Mathematics. 8 (2023) 1-10.
- [19] Elmhedy Y, Abd-Alla AM, Abo-Dahab SM, Alharbi FM, Abdelhafez MA. Influence of inclined magnetic field and heat transfer on the peristaltic flow of Rabinowitsch fluid model in an inclined channel. Scientific Reports. 14 (2024) 1-15.

- [20] Rafiq M, Shaheen A, Trabelsi Y, Eldin SM, Khan MI, Suker DK. Impact of activation energy and variable properties on peristaltic flow through porous wall channel. Scientific Reports. 13 (2023) 1-19.
- [21] Abbas Z, Shakeel A, Rafiq MY, Khaliq S, Hasnain J, Nadeem A. Rheology of peristaltic flow in couple stress fluid in an inclined tube: Heat and mass transfer analysis. Advances in Mechanical Engineering. 14 (2022) 1-14.
- [22] Riaz A, Siddiqa A, Akram S, Nawaz T, Khan SU, Rehman SU. Mathematical modeling of thermal transfer in a symmetric peristaltic flow of a Newtonian fluid through a curved duct with entropy generation: a microfluidics application. International Journal of Modelling and Simulation. (2024) 1-7.
- [23] Abd-Alla AM, Abo-Dahab SM, Abdelhafez MA, Thabet EN. Effects of heat transfer and the endoscope on Jeffrey fluid peristaltic flow in tubes. Multidiscipline Modeling in Materials and Structures. 17 (2021) 895-914.
- [24] Nadeem S, Qadeer S, Akhtar S, Almutairi S, Fuzhang W. Mathematical model of convective heat transfer for peristaltic flow of Rabinowitsch fluid in a wavy rectangular duct with entropy generation. Physica Scripta. 97 (2022) 1-16.
- [25] Saffman PG. On the stability of laminar flow of a dusty gas. J. Fluid Mech. 13 (1962) 120-8.
- [26] Gupta RK, Gupta SC. Flow of a dusty gas through a channel with arbitrary time varying pressure gradient. Zeitschrift für angewandte Mathematik und Physik ZAMP. 27 (1976) 119-25.
- [27] Ghosh AK, Mitra DK. Flow of a dusty fluid through horizontal pipes. Revue Roumaine de Physique. 29 (1984) 631-46.

- [28] Dixit LA. Unsteady flow of a dusty viscous fluid through rectangular ducts. Indian Journal of Theoretical Physics. 28 (1980).
- [29] Kulshrestha PK, Puri P. Wave structure in oscillatory Couette flow of a dusty gas. Acta Mechanica. 46 (1983) 127-35.
- [30] Makinde OD, Chinyoka T. MHD transient flows and heat transfer of dusty fluid in a channel with variable physical properties and Navier slip condition. Computers & Mathematics with Applications. 60 (2010) 660-9.
- [31] Madhura KR, Swetha DS. Influence of volume fraction of dust particles on dusty fluid flow through porous rectangular channel. International Journal of Mathematics Trends and Technology-IJMTT. 50 (2017).261-75
- [32] Sivaraj R, Kumar BR. Unsteady MHD dusty viscoelastic fluid Couette flow in an irregular channel with varying mass diffusion. International Journal of Heat and Mass Transfer. 55 (2012) 3076-89.
- [33] Ali F, Bilal M, Gohar M, Khan I, Sheikh NA, Nisar KS. A report on fluctuating free convection flow of heat absorbing viscoelastic dusty fluid past in a horizontal channel with MHD effect. Scientific Reports. ;10 (2020) 1-15.
- [34] Mekheimer KS, El Shehawey EF, Elaw AM. Peristaltic motion of a particle-fluid suspension in a planar channel. International Journal of Theoretical Physics. 37 (1998) 2895-920.
- [35] Srinivasacharya D, Radhakrishnamacharya G, Srinivasulu CH. The Effects of Wall Properties on Peristaltic Transport of a Dusty Fluid. Turkish Journal of Engineering & Environmental Sciences. 32 (2008).357-65.

- [36] Eldesoky IM, El-Askary WA, El-Refaey AM, Ahmed MM. MHD Peristaltic Flow of Dusty Fluid through Flexible Channel under Slip Condition. In The International Conference on Mathematics and Engineering Physics 2016 (Vol. 8, No. International Conference on Mathematics and Engineering Physics (ICMEP-8), pp. 1-35). Military Technical College.
- [37] Ramesh K, Tripathi D, Bhatti MM, Khalique CM. Electro-osmotic flow of hydromagnetic dusty viscoelastic fluids in a microchannel propagated by peristalsis. Journal of Molecular Liquids. 314 (2020) 1-11.
- [38] Parthasarathy S, Arunachalam G, Vidhya M. Analysis on the effects of wall properties on MHD peristaltic flow of a dusty fluid through a porous medium. International Journal of Pure and Applied Mathematics. 102 (2015) 247-63.
- [39] Tariq H, Khan AA. Peristaltic flow of a dusty electrically conducting fluid through a porous medium in an endoscope. SN Applied Sciences. 2 (2020) 1-8.
- [40] Tariq H, Khan AA, Zaman A. Theoretical analysis of peristaltic viscous fluid with inhomogeneous dust particles. Arabian Journal for Science and Engineering. 46 (2021) 31-9.
- [41] Zeeshan A, Ijaz N, Bhatti MM, Mann AB. Mathematical study of peristaltic propulsion of solid–liquid multiphase flow with a biorheological fluid as the base fluid in a duct. Chinese Journal of Physics. 55 (2017) 1596-604.
- [42] Eldesoky IM, Abumandour RM, Kamel MH, Abdelwahab ET. The combined effects of wall properties and space porosity on MHD two-phase peristaltic slip transport through planar channels. International Journal of Applied and Computational Mathematics. 7 (2021) 1-37.
- [43] Abdelsalam SI, Vafai K. Particulate suspension effect on peristaltically induced unsteady pulsatile flow in a narrow artery: blood flow model. Mathematical biosciences. 283(2017) 91-105.

- [44] Dean WR. Fluid motion in a curved channel. Proceedings of the Royal Society A. Containing Papers of a Mathematical and Physical Character. 121(1928) 402-20.
- [45] Sato H, Kawai T, Fujita T & Okabe M. Two-dimensional peristaltic flow in curved channels, Transactions of the Japan Society of Mechanical Engineers (Part B). 643 (2000) 39-45.
- [46] Ali N, Sajid M, Abbas Z, Javed T. Non-Newtonian fluid flow induced by peristaltic waves in a curved channel. European Journal of Mechanics-B/Fluids. 29 (2010) 387-94.
- [47] Javid K, Ali N, Asghar Z. Rheological and magnetic effects on a fluid flow in a curved channel with different peristaltic wave profiles. Journal of the Brazilian Society of Mechanical Sciences and Engineering. 41 (2019) 1-14.
- [48] Ramanamurthy JV, Prasad KM, Narla VK. Unsteady peristaltic transport in curved channels. Physics of Fluids. 25 (2013).1-21
- [49] Abbasi A, Danish S, Farooq W, Khan MI, Akermi M, Hejazi HA. Peristaltic transport of viscoelastic fluid in curved ducts with ciliated walls. Physics of Fluids. 36 (2024).
- [50] Hina S, Mustafa M, Hayat T, Alotaibi ND. On peristaltic motion of pseudoplastic fluid in a curved channel with heat/mass transfer and wall properties. Applied Mathematics and Computation. 263 (2015) 378-91.
- [51] Hayat T, Farooq S, Alsaedi A. MHD peristaltic flow in a curved channel with convective condition. Journal of Mechanics. 33 (2017) 483-99.
- [52] Khan AA. Peristaltic movement of a dusty fluid in a curved configuration with mass transfer. Punjab University Journal of Mathematics. 53 (2021) 55-71.
- [53] Rashed ZZ, Ahmed SE. Peristaltic flow of dusty nanofluids in curved channels. Comput. Mater. Continua. 66 (2021) 1012-26.

- [54] Ahmed R, Ali N, Khan SU, Rashad AM, Nabwey HA, Tlili I. Novel microstructural features on heat and mass transfer in peristaltic flow through a curved channel. Frontiers in Physics. 8 (2020) 1-13.
- [55] Narla VK, Prasad KM, Ramana Murthy JV. Second-law analysis of the peristaltic flow of an incompressible viscous fluid in a curved channel. Journal of Engineering Physics and Thermophysics. 89 (2016) 441-8.
- [56] Narla VK, Tripathi D, Bég OA, Kadir A. Modeling transient magnetohydrodynamic peristaltic pumping of electroconductive viscoelastic fluids through a deformable curved channel. Journal of Engineering Mathematics. 111 (2018) 127-43.
- [57] Javed M, Hayat T. Effects of heat transfer on MHD peristaltic transport of dusty fluid in a flexible channel. In2017 14th international Bhurban conference on applied sciences and technology (IBCAST) 2017 (pp. 539-550). IEEE.
- [58] Sivaraj R, Kumar BR. Chemically reacting dusty viscoelastic fluid flow in an irregular channel with convective boundary. Ain shams engineering journal. 4 (2013) 93-101.
- [59] Bhatti MM, Zeeshan A, Ijaz N, Bég OA, Kadir A. Mathematical modelling of nonlinear thermal radiation effects on EMHD peristaltic pumping of viscoelastic dusty fluid through a porous medium duct. Engineering science and technology, an international journal. 20(2017) 1129-39.
- [60] Kalpana G, Saleem S. Heat transfer of magnetohydrodynamic stratified dusty fluid flow through an inclined irregular porous channel. Nanomaterials. 12 (2022) 1-13.
- [61] Elmhedy Y, Abd-Alla AM, Abo-Dahab SM, Alharbi FM, Abdelhafez MA. Influence of inclined magnetic field and heat transfer on the peristaltic flow of Rabinowitsch fluid model in an inclined channel. Scientific Reports. 14 (2024) 1-35.

- [62] Zeeshan A, Ijaz N, Bhatti MM. Flow analysis of particulate suspension on an asymmetric peristaltic motion in a curved configuration with heat and mass transfer. Mechanics & Industry. 19 (2018) 1-11.
- [63] Riaz A, Khan SU, Zeeshan A, Khan SU, Hassan M, Muhammad T. Thermal analysis of peristaltic flow of nanosized particles within a curved channel with second-order partial slip and porous medium. Journal of Thermal Analysis and Calorimetry. 143 (2021) 1997-2009.
- [64] Tariq H, Khan AA, Zaman A. Peristaltically wavy motion on dusty Walter's B fluid with inclined magnetic field and heat transfer. Arabian Journal for Science and Engineering. 44 (2019) 7799-808.
- [65] Hayat T, Zahir H, Tanveer A, Alsaedi A. Soret and Dufour effects on MHD peristaltic transport of Jeffrey fluid in a curved channel with convective boundary conditions. PLoS One. 12 (2017) 1-50.
- [66] Sinha A, Shit GC, Ranjit NK. Peristaltic transport of MHD flow and heat transfer in an asymmetric channel: Effects of variable viscosity, velocity-slip and temperature jump. Alexandria Engineering Journal. 54 (2015) 691-704.
- [67] Hayat T, Ali N. Effect of variable viscosity on the peristaltic transport of a Newtonian fluid in an asymmetric channel. Applied Mathematical Modelling. 32 (2008) 761-74.
- [68] Khan AA, Ellahi R, Usman M. The effects of variable viscosity on the peristaltic flow of non-Newtonian fluid through a porous medium in an inclined channel with slip boundary conditions. Journal of Porous media. 16 (2013).59-67
- [69] Akbar Y, Abbasi FM. Impact of variable viscosity on peristaltic motion with entropy generation. International Communications in Heat and Mass Transfer. 118(2020) 1-8.

- [70] Tanveer A, Ashraf MB, Masood M. Entropy analysis of peristaltic flow over curved channel under the impact of MHD and convective conditions. Numerical Heat Transfer, Part B: Fundamentals. 85(2024) 45-57.
- [71] Abbasi FM, Hayat T, Ahmad B. Numerical analysis for peristaltic transport of Carreau-Yasuda fluid with variable thermal conductivity and convective conditions. Journal of Central South University. 22(2015) 4467-75.
- [72] Vaidya H, Rajashekhar C, Manjunatha G, Prasad KV, Makinde OD, Vajravelu K. Heat and mass transfer analysis of MHD peristaltic flow through a complaint porous channel with variable thermal conductivity. Physica Scripta. 95 (2020) 1-11.
- [73] Mekheimer KS, Abd Elmaboud Y. Simultaneous effects of variable viscosity and thermal conductivity on peristaltic flow in a vertical asymmetric channel. Canadian Journal of Physics. 92 (2014) 1541-55.
- [74] Manjunatha G, Rajashekhar C, Vaidya H, Prasad KV, Vajravelu K. Impact of heat and mass transfer on the peristaltic mechanism of Jeffery fluid in a non-uniform porous channel with variable viscosity and thermal conductivity. Journal of Thermal Analysis and Calorimetry. 139 (2020) 1213-28.
- [75] Khan WA, Farooq S, Kadry S, Hanif M, Iftikhar FJ, Abbas SZ. Variable characteristics of viscosity and thermal conductivity in peristalsis of magneto-Carreau nanoliquid with heat transfer irreversibilities. Computer Methods and Programs in Biomedicine. 190 (2020) 1-9.
- [76] Bibi F, Hayat T, Farooq S, Khan AA, Alsaedi A. Entropy generation analysis in peristaltic motion of Sisko material with variable viscosity and thermal conductivity. Journal of Thermal Analysis and Calorimetry. 143 (2021) 363-75.

- [77] Bhatti MM, Zeeshan A. Analytic study of heat transfer with variable viscosity on solid particle motion in dusty Jeffery fluid. Modern Physics Letters B. 30 (2016) 1-13.
- [78] Swetha DS, Madhura KR. Mathematical modelling on peristaltic motion and temperature distribution of dusty Jeffrey fluid under the influence of variable viscosity. International Journal of Ambient Energy. 44 (2023) 2034-46.
- [79] Kalpana G, Madhura KR. Computational study on heat transfer of MHD dusty fluid flow under variable viscosity and variable pressure down an inclined irregular porous channel. Int. J. Emerg. Tech. Adv. Eng. 7 (2017) 358-69.
- [80] Hussain Q, Hayat T, Asghar S, Alsaadi F. Heat and mass transfer analysis in variable viscosity peristaltic flow with hall current and ion-slip. Journal of Mechanics in Medicine and Biology. 16 (2016) 1-27.
- [81] Hussain Q, Asghar S, Hayat T, Alsaedi A. Heat transfer analysis in peristaltic flow of MHD Jeffrey fluid with variable thermal conductivity. Applied Mathematics and Mechanics. 36 (2015) 499-516.
- [82] Al-Aridhee AA, Al-Khafajy DG. Influence of varying temperature and concentration on Mhd peristaltic transport for jeffrey fluid with variable viscosity through porous channel.

  Journal of Al-Qadisiyah for Computer Science and Mathematics. 11 (2019) 38-49.
- [83] Noreen S, Malik A, Rashidi MM. Peristaltic flow of shear thinning fluid via temperature-dependent viscosity and thermal conductivity. Communications in Theoretical Physics. 71 (2019) 367-76.
- [84] Hayat T, Khan AA, Bibi F, Alsaedi A. Entropy minimization for magneto peristaltic transport of Sutterby materials subject to temperature dependent thermal conductivity and non-

- linear thermal radiation. International Communications in Heat and Mass Transfer. 122 (2021) 1-13.
- [85] Vaidya H, Prasad KV, Khan MI, Mebarek-Oudina F, Tlili I, Rajashekhar C, Elattar S, Khan MI, Al-Gamdi SG. Combined effects of chemical reaction and variable thermal conductivity on MHD peristaltic flow of Phan-Thien-Tanner liquid through inclined channel. Case Studies in Thermal Engineering. 36 (2022) 1-14.
- [86] Konch J, Hazarika GC. Effects of variable viscosity and thermal conductivity on mhd free convection flow of dusty fluid along a vertical stretching sheet with heat generation. International Research Journal of Engineering and Technology. 3 (2016) 1029-38.
- [87] Konch J, Hazarika G. Effects of variable viscosity and variable thermal conductivity on hydromagnetic dusty fluid flow due to a rotating disk. Frontiers in Heat and Mass Transfer (FHMT). 8 (2017) 1-10.
- [88] Srinivas S, Kothandapani M. Peristaltic transport in an asymmetric channel with heat transfer—a note. International Communication in Heat and Mass Transfer. 35 (2008) 514-22.
- [89] Mehmood UO, Mustapha N, Shafie S. Nonlinear peristaltic flow of Walter's B fluid in an asymmetric channel with heat transfer and chemical reactions. Thermal Science. 18 (2014) 1095-107.
- [90] Kothandapani M, Srinivas S. Non-linear peristaltic transport of a Newtonian fluid in an inclined asymmetric channel through a porous medium. Physics Letters A. 372 (2008) 1265-76.